SEQUENCE STRATIGRAPHY AND RESERVOIR ANALYSIS OF THE UPPER KEARNY FORMATION (MORROWAN SERIES, LOWER PENNSYLVANIAN SYSTEM) WITHIN THREE KANSAS FIELDS

by

K.L. Luchtel

Kansas Geological Survey
Open-file Report 99-31

SEQUENCE STRATIGRAPHY AND RESERVOIR ANALYSIS OF THE UPPER KEARNY FORMATION (MORROWAN SERIES, LOWER PENNSYLVANIAN SYSTEM) WITHIN THREE KANSAS FIELDS

by

Kristie L. Luchtel
B. S., Oklahoma State University, 1996

Submitted to the Department of
Geology and the Faculty of the
Graduate School of the University of
Kansas in partial fulfillment of the
requirements for the degree of
Master of Science.

Dr. Timothy Carr, Chairman

Dr. Anthony W. Walton

Dr. Don Steeples

For the Department

August 11, 1999
Date thesis accepted

ACKNOWLEDGEMENTS

This thesis is dedicated in the memory and honor of my beloved Grandfather John A. Swenson, whose love, guidance, teaching, and encouragement allowed me to accomplish my goals.

Above all others, I praise God for giving me the opportunities, strength, and knowledge to achieve the goals that he has laid out before me and to continue on my life path that he has chosen. I thank God for restoring the health of my Sister Mistie, for keeping my Mother, Carol with me, and for giving me a loving Father, Bill. I would like to express my love and gratitude to my family for standing beside me through all the stress and confusion, and for making me the person I am today.

I wish to express my deepest appreciation to Dr. Tim Carr who provided me ultimate support as my advisor and an incredible opportunity to be a member of the Kansas Geological Survey Petroleum Section. I also thank Drs. Don Steeples and Anthony Walton for their advice, critiques, and encouragement in both the classroom and in the editing process of this thesis.

Special gratitude is due to Mr. Abdulrahman M. I. Alissa who gave me the ability to laugh and enjoy my life while working 24-hour days. Without his camaraderie, helpful ideas, and assistance this thesis would not have been as enjoyable or accomplished in a timely manner.

I would like to express a warm thank you to all the staff of the Kansas Geological Survey for their scientific knowledge and insight, especially Drs. Lynn Watney, Evan Franseen, David Newell and John Doveton, Bill Guy, and Alan Byrnes.

A special thank you to Mr. Peter Coffin of Anadarko Petroleum Company who provided support, knowledge, and the core used in this study.

TABLE OF CONTENTS

LIST OF FIGURES

LIST OF TABLES

ABSTRACT

Successful secondary recovery projects in Morrowan sandstone hydrocarbon reservoirs have spurred activity to further investigate the potential in the upper Morrowan fields of southwestern Kansas. This study defines the sequence-stratigraphic framework, depositional environments, and reservoir characterization of the upper Kearny Formation (Morrowan Series, Lower Pennsylvanian System), in the Santa Fe Trail, Cimarron Valley, and Stirrup oil and gas fields, Hugoton Embayment, Morton County, Kansas. The study demonstrates the importance of sequence-stratigraphic concepts and the incised-valley depositional model for the prediction of lithologic successions occurring in response to fluctuations of relative sea-level as well as sediment supply.

Upper Morrowan reservoir rocks were subdivided into nine lithofacies and three lithofacies assemblages (marine, estuarine, and fluvial). Lithofacies assemblages, as observed in cores, were correlated with wireline-log responses to extend the lithofacies interpretations beyond the limited core control. The upper Morrowan siliciclastic succession consists of two sequences that were deposited within two incised valleys. The incised valleys developed as a result of major relative falls in sea-level. During subsequent rise in sea-level the incised valleys filled with fluvial and estuarine lithofacies (transgressive systems tract). With continued sea-level rise and landward shift of sediment sources, the study area became a starved margin setting (highstand systems tract) characterized by marine shale, mudstone, and limestone. Chronostratigraphic cross-sections and sandstone isopach and isoporosity maps demonstrate that the estuarine lithofacies assemblage and the thickest reservoir sandstones are concentrated adjacent to a fault along the western margin of the study area. The observations support the hypothesis that deposition of upper Morrowan incised-valley fills were influenced by both glacial eustacy and local and regional tectonics.

Reservoir quality is influenced by the grain sizes of depositional lithofacies. Five types of sandstones within the incised-valley fills are potential reservoirs. Secondary porosity predominants in all potential reservoir lithofacies. The coarse-grained fluvial lithofacies as compared to the fine-grained estuarine lithofacies form reservoir intervals that have higher production rates, are more laterally continuous, contain less detrital mud and clay, retain more primary and secondary porosity, have lower bulk volume water and water saturations, and have higher permeabilities.

CHAPTER ONE

INTRODUCTION

Upper Morrowan sandstones are productive of oil and gas over a large area of southwestern Kansas, southeastern Colorado, and northwestern Oklahoma (Emery, 1985; Wheeler et al., 1990; Al-Shaieb et al., 1995; Andrews, 1997; Schoeling and Fox, 1998). In 1951, Morton County was the site of the first significant Morrowan discoveries in southwestern Kansas (Swanson, 1979). Excellent reservoirs consisting of highly porous and permeable sandstones encased in impermeable shales and mudstones (stratigraphic traps), coupled with relatively large reserves, shallow drilling depths (less than 6,000 ft), and low drilling costs make upper Morrowan valley-fill sandstones attractive exploration targets (Davis, 1963; Clark, 1987; Sonnenberg et al., 1990; Wheeler et al., 1990). Continued exploration and development and the potential for application of enhanced-oil recovery technologies (e.g., carbon-dioxide flooding) require a better understanding of upper Morrowan stratigraphy and facies relationships to improve success rates and to optimize hydrocarbon recovery.

The purpose of this investigation is to (1) describe and classify lithofacies from four cores into lithofacies assemblages based on objective criteria (e.g., grain size, sedimentary structures, and ichnofauna), (2) develop criteria for recognizing lithofacies in wireline logs, (3) combine core analyses with wireline-log data and cross-sections to build a sequence-stratigraphic framework, (4) utilize the sequence-

stratigraphic framework to build a depositional model for the area, and (5) apply petrophysical data derived from cores and wireline-logs to define the reservoir characteristics for each lithofacies (e.g., lateral continuity, porosity, permeability, water saturation, and bulk volume water).

Study Area

The Hugoton Embayment of southwestern Kansas is the deepest Paleozoic basin in Kansas and contains nearly 9,500 ft (2,900 m) of sedimentary strata (Merriam, 1963). The upper Morrowan is a southward-thickening unit ranging from 250 to 500 ft (75–150 m) thick and occurs at depth intervals ranging from approximately 4,400 to 6,000 ft (1300–1900 m) (Merriam, 1963; Zeller, 1968; Swanson, 1979; Franz, 1985b).

This study pertains to the sequence stratigraphy and reservoir characterization of the upper Kearny Formation (Morrowan Series, Pennsylvanian System) within the Santa Fe Trail, Cimarron Valley, and Stirrup fields (sec. 32, 33, 34, 35, T32S, R40W; sec. 2-12, 17-20, T33S, R40W; and sec. 11, 12, 13, T33S, R41W, T31S-T32S, R41W-R40W, respectively), Hugoton Embayment, Morton County, southwestern Kansas (Figure 1.1). The fields were discovered in 1963, 1975, and 1987, respectively, extend along the boundary of one township, lie parallel to one another, and have reported oil and gas production from upper Morrowan reservoirs (Figure 1.1).

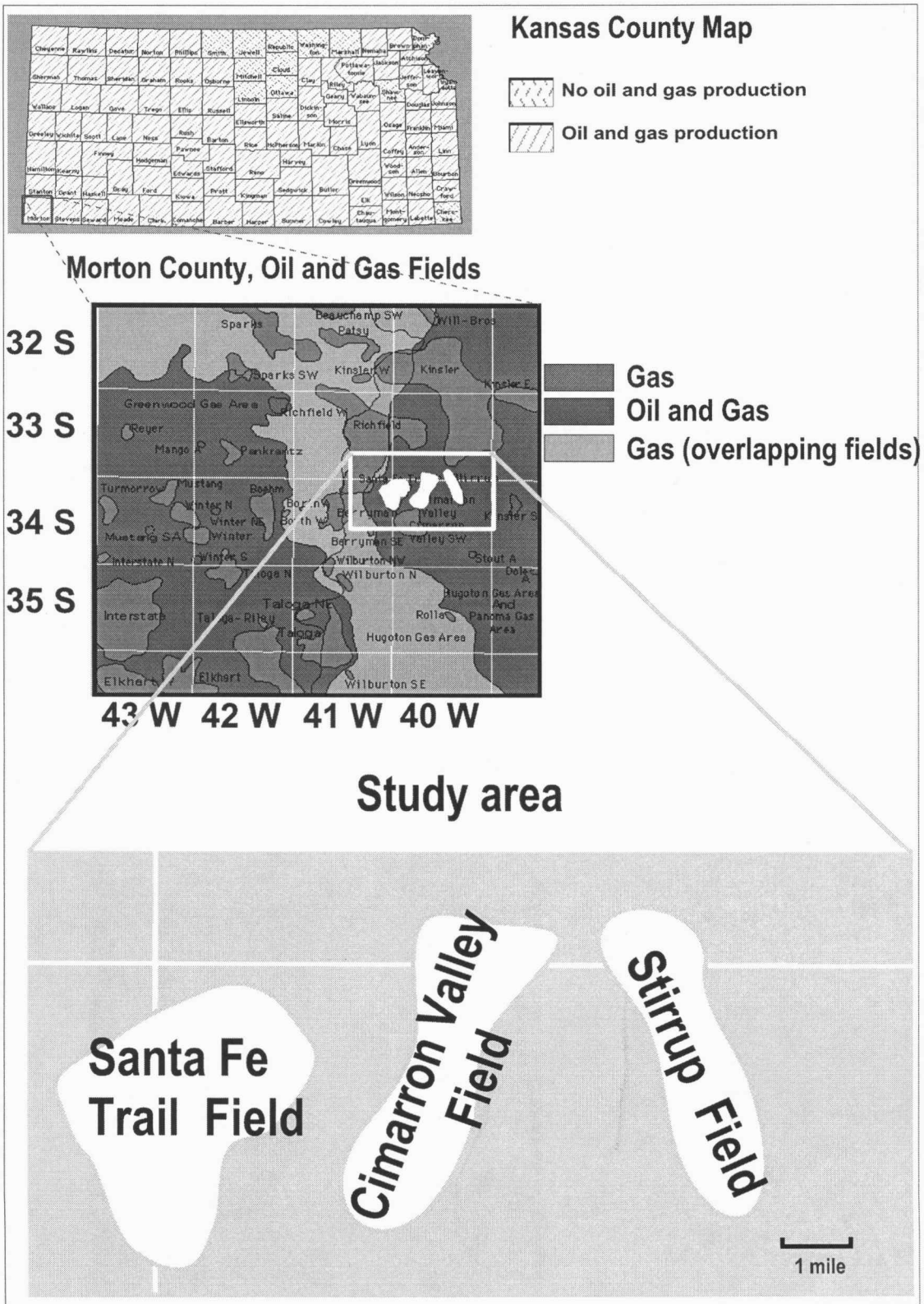

Figure 1.1 Location of study area in southwestern Kansas (modified from Digital Petroleum Atlas, 1997).

Previous Investigations

The economics of upper Morrowan reservoirs have made them primary drilling targets in southwestern Kansas, northwestern Oklahoma, and southeastern Colorado (Krystinik and Blakeney, 1990; Wheeler et al., 1990; Al-Shaieb et al., 1995). Different stratigraphic intervals within the Morrowan have previously been assigned informal names and letters designating the producing sandstones (Swanson, 1979; Franz, 1985b). Hammuda (1973) discussed the effects of paleostructures and the pre-Pennsylvanian unconformity on Morrowan depositional history.

There have been several interpretations of the depositional environments of Morrowan reservoirs including deltas, carbonate platforms, fluvial point bars, transgressive fluvial-channel fills, stream-mouth bar deposits, and incised-valley fills (Swanson, 1979; Franz, 1985a; Clark, 1987; Rader, 1990). In the panhandle of Oklahoma, just south of the study area, Arro (1965) interpreted some of the upper Morrowan sandstone reservoirs as beach and shallow-marine bar deposits. Benton (1971) established that the upper Morrowan sandstone in the Postle Field (T5N-R13ECM, Texas County, Oklahoma) was deposited within a fluvial system that drained the eroded Morrowan paleotopography. Swanson (1979) published a regional paper that suggested coastal-plain fluvial to deltaic processes for deposition of the upper Morrowan strata within the Anadarko Basin (Wheeler et al., 1990). Emery (1985) believed that upper Morrowan reservoirs were deposited in estuarine, tidal-flat, beach, and offshore bar environments. Sutterlin and Hastings (1986) interpreted upper Morrowan sandstones in Clark County, Kansas, as being

predominantly tidal estuarine deposits, in contrast to the inferred predominantly fluvial character of the sandy portion of Morrowan fills. Sonnenberg (1985), Emery and Sutterlin (1986), Krystinik et al. (1987), Wheeler et al. (1990), Sonnenberg et al. (1990), and Krystinik and Blakeney (1990) have interpreted the areas of southeastern and eastern Colorado as well as southwestern Kansas as incised-valley deposits. Subsequent studies by Krystinik and Blakeney (1990), Sonnenberg et al. (1990), and Wheeler et al. (1990) described valley-fill reservoirs in eastern Colorado and western Kansas, where at least seven episodes of incision and valley fill have occurred. Morrowan sandstones of Morton and Stevens counties, Kansas, are thought to be composed of delta-front and high-energy shoreface deposits (Sonnenberg et al., 1990; Wheeler et al., 1990). Al-Shaieb et al. (1995) and Puckette et al. (1996) have also described northern Anadarko shelf regions of the Oklahoma Panhandle as being incised-valley environments. Within the Morrowan strata, Wheeler et al (1990) recognized 12 commonly occurring facies based on grain size, and sedimentary and biogenic structures.

Significance of Study

Upper Morrowan sandstone reservoirs in southwestern Kansas produce oil and gas from narrow ~1.5–5-mile-wide (2.41–8.05 km), elongate, sinuous, and highly productive stratigraphic and structural-stratigraphic traps (Krystinik and Blakeney, 1990). The producing intervals are clean, porous, and highly permeable sandstones that range from 2 to 30 ft thick (0.6–9 m).

Discoveries of Morrowan reservoirs on the Las Animas Arch, Colorado, and in nearby areas spurred further exploration activity in southwestern Kansas (Shirley, 1985). In addition, carbon-dioxide flooding projects have been highly successful in Morrowan reservoirs of the Postle unit of Texas County, Oklahoma, directly south of the study area (Schoeling and Fox, 1998). The need to assess the potential for increasing oil recovery using carbon-dioxide flooding has increased the requirement for an improved understanding of Morrowan reservoir geometry and lateral continuity of facies (Schoeling and Fox, 1998). The study focuses on selected upper Morrowan reservoirs and delineates their petrophysical properties and lateral continuity.

Methodology

Four cored wells (two in Stirrup Field and two in Cimarron Valley Field) were analyzed for sedimentary structures, grain size, ichnofauna, and grain types to establish the lithofacies and infer the depositional environments. Upper Morrowan sandstone bodies were classified into depositional facies based on the presence and absence of sedimentary structures, as developed by Nichols et al. (1991), Dalrymple et al. (1992), Miall (1992; 1996), Allen and Posamentier (1993), Zaitlin et al. (1994), and Reading and Collinson (1996). Geologists' reports and logs, and dipmeter logs were used to supplement lithological descriptions in the identification and determination of depositional environments. Core analyses were combined with data from 76 digitized wireline-log suites in LAS format (Canadian Well Logging Society's LAS Committee, 1993). The log suites consisted of gamma-ray, density

(Dphi) and neutron (Nphi) porosity, bulk-density, spontaneous-potential, photoelectric, and resistivity curves. Wells within the study area are located one-quarter mile or less from each other. Upper Morrowan sandstone isopach and isoporosity maps were constructed with the aid of wireline-logs. Petrophysical analyses were applied to wells without core to extend the limited core data throughout the three fields. Wireline-log data were used to build seven cross-sections in order to display the sequence-stratigraphic framework for the study area. Cores, wireline logs, isopach and isoporosity maps, and seven chronostratigraphic cross-sections provided information for a depositional model of the upper Morrow in the Santa Fe Trail, Cimarron Valley, and Stirrup fields.

Analysis of twenty-five thin sections from two cores, three porosity and permeability core-plug studies, Pickett plots, and data derived from wireline logs helped determine the relationship of different lithofacies within the sandstone reservoirs in terms of porosity, permeability, water saturation, and bulk volume water. Core-plug analyses and wireline logs were used to find porosity values for the upper Morrowan lithofacies within the study area. The porosity values for the different lithofacies were mapped to define the lateral continuity of the reservoirs.

CHAPTER TWO

STRATIGRAPHY AND TECTONICS

Geologic Setting

The Hugoton Embayment, located in southwestern Kansas and southeastern Colorado, is an asymmetrical southward-thickening basin that has an overall northwest–southeast trend into the Anadarko Basin (Rader, 1987; Sonnenberg, 1990; Youle, 1992; Figure 2.1). The Hugoton Embayment is a northern extension of the Paleozoic Anadarko Basin and has been referred to as the Anadarko or Dodge City Shelf (Merriam, 1963; Rader, 1987). The embayment formed in the late Cambrian through Ordovician time and received its thickest accumulation of sediment during the late Mississippian, Pennsylvanian, and Early Permian. The Hugoton Embayment was tectonically inactive by the Mesozoic (Merriam, 1963).

At the beginning of the Mississippian Period, tectonic activity in the midcontinent was at a minimum. By the Osagian Stage, rapid subsidence began in the Anadarko Basin and Hugoton Embayment and is attributed to the North American and the South American plates colliding (Craig and Varnes, 1979; Sonnenberg et al., 1990). During this time, differential uplift began to occur in Kansas along major structural features such as the Nemaha and the Central Kansas Uplifts (Brown, 1995). During the Mississippian, several uplift and subsidence events occurred with continued differential downwarping of the Hugoton Embayment. During the early late Mississippian (Meremecian Stage), the craton was uplifted and extensive erosion

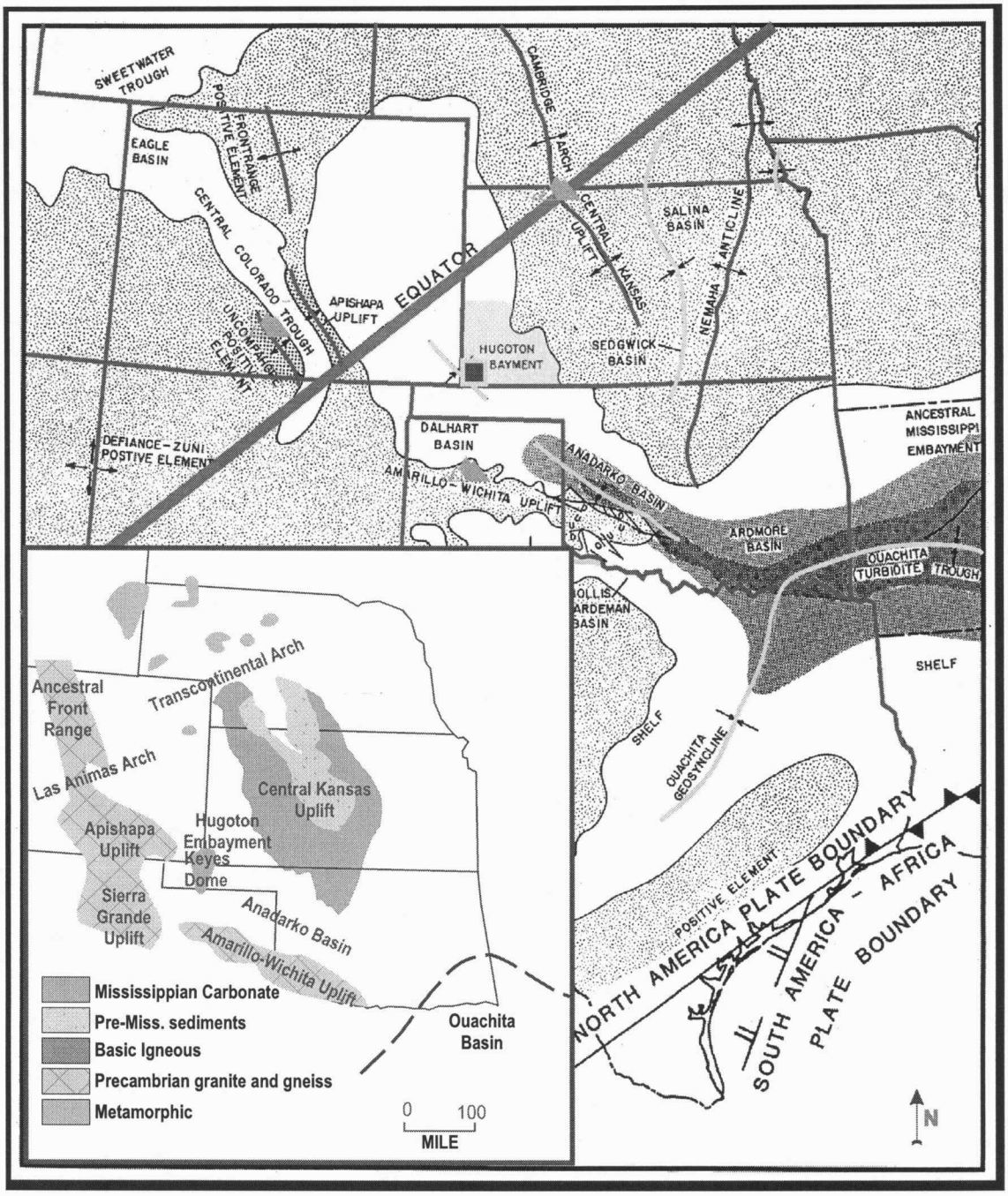

Figure 2.1 Paleogeographic and source area maps of the Lower Pennsylvanian. The Hugoton Embayment is located just south of the paleo-equator (modified from Sonnenberg et al., 1990; Wheeler et al., 1990).

occurred on the shelf as the seas withdrew from the Hugoton Embayment (Frezon and Dixon, 1975). Near the end of the Mississippian (Chesteran Stage), the Hugoton Embayment began receiving detrital sediments from the Apishapa Uplift and Las Animas Arch, which served as sediment source areas from the west (Rader, 1987; Montgomery and Morrison, 1999).

Early Pennsylvanian Tectonics

In the Early Pennsylvanian Morrowan Stage, tectonic conditions in Kansas were quiescent. Relative sea-level fluctuations were of high frequency and were glacio-eustatically controlled (Bowen et al., 1993). During this time, relative sea level is thought to have been at a eustatic lowstand and later became more erratic, with seven glacially induced eustatic sea-level fluctuations (Ross and Ross, 1985; Figure 2.2). Regionally extensive unconformities related to sea-level fluctuations were developed within upper Morrowan strata in the Hugoton Embayment.

Morrowan valley-fill systems in southwestern Kansas formed along the flank of an intracratonic basin. Regional gradients in the Hugoton Embayment during the upper Morrowan have been estimated at less than 0.5 to 1 degree and range between 1 ft/mi to 35 ft/mi (0.3–6.6 m/km; Swanson, 1979; Bolyard, 1990; Al-Shaieb et al., 1995). Upper Morrowan incised valleys with lateral slopes ranging from 0.5 to 5 degrees are relatively distinct structures in the nearly flat terrain of the Hugoton Embayment.

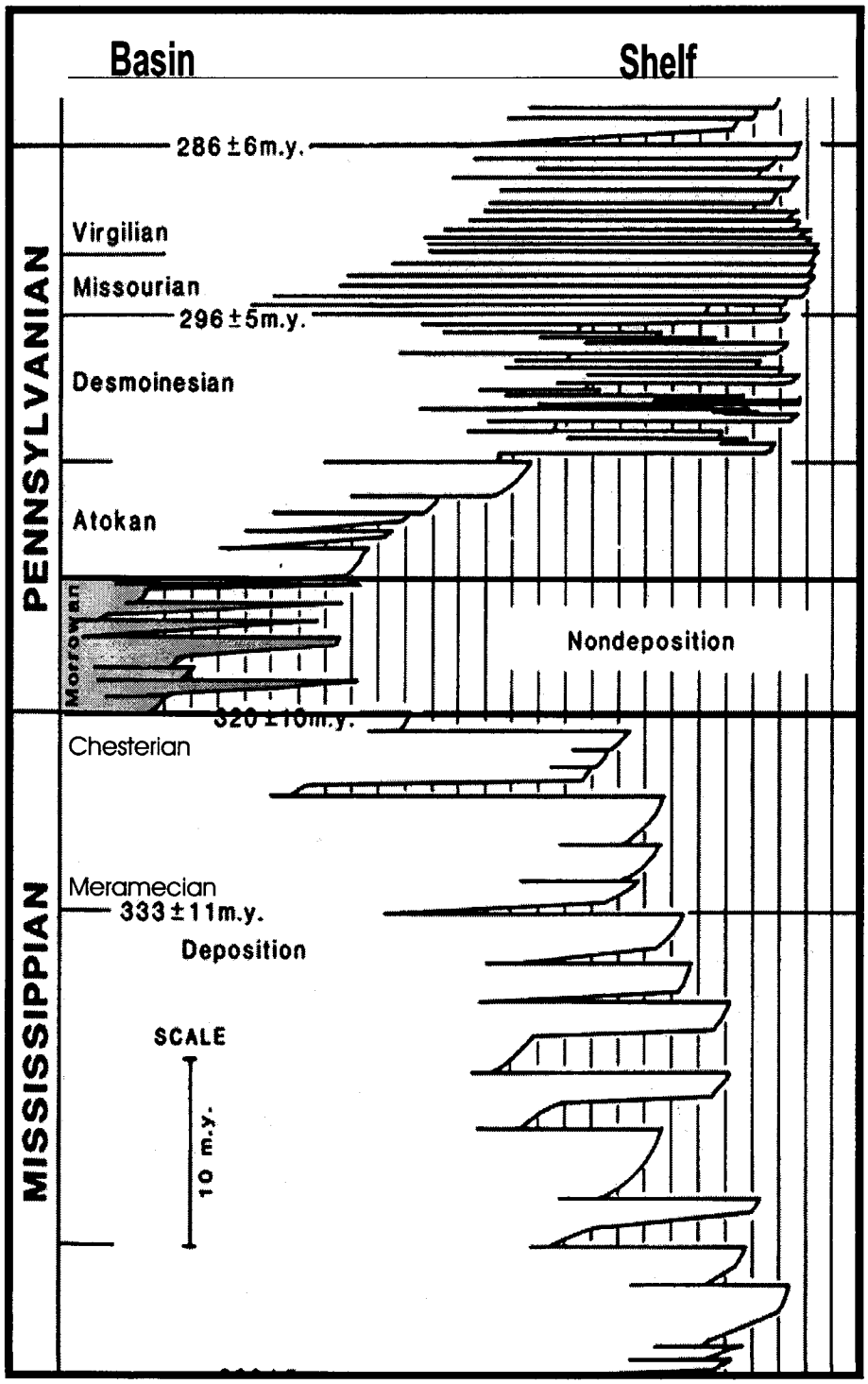

Figure 2.2 Coastal onlap curves for the Mississippian and Pennsylvanian times (modifided from Ross and Ross, 1985).

Regional Stratigraphy

The Kearny Formation (Morrowan Stage, Lower Pennsylvanian System) of southwestern Kansas, southeastern Colorado, and northwestern Oklahoma contains the rocks that lie immediately below the Gray Group or the Thirteen-Finger limestone (Pennsylvanian, Atokan) and immediately above the Mississippian Chester and Shore Airport Formations (Merriam, 1963; Zeller, 1968; Wheeler et al., 1990; Youle, 1992; Abegg, 1994; Figure 2.3). Morrowan strata in southwestern Kansas are unconformable with both the underlying Mississippian and the overlying Pennsylvanian Atokan rocks (Merriam, 1963; Zeller, 1968; Wheeler et al., 1990). Youle (1992) described complex interfingering of Atokan strata with facies equivalents to Morrowan rocks. The Kearny Formation is informally subdivided at the top of a more resistive calcareous sandstone and is described as the upper and lower Morrow members (Swanson, 1979; Rascoe and Adler, 1983; Abegg, 1994). The informal upper and lower Morrow terminology will be used throughout this study. The upper Morrow contains predominantly siliciclastic sediments consisting of black marine shales, thin carbonaceous shales, and elongate, discontinuous, medium- to coarse-grained sandstones (Swanson, 1979; Franz, 1985b; Sonnenberg, 1990). The upper Morrow sandstones have occasionally been referred to as the Purdy sandstones (Sonnenberg, 1990; Al-Shaieb et al., 1995).

The type locality for the Morrow is near the town of Morrow in Washington County, northwestern Arkansas (Adams, 1904). The upper Morrowan rocks are present only in the subsurface within the study area (Zeller, 1968). A type log for the

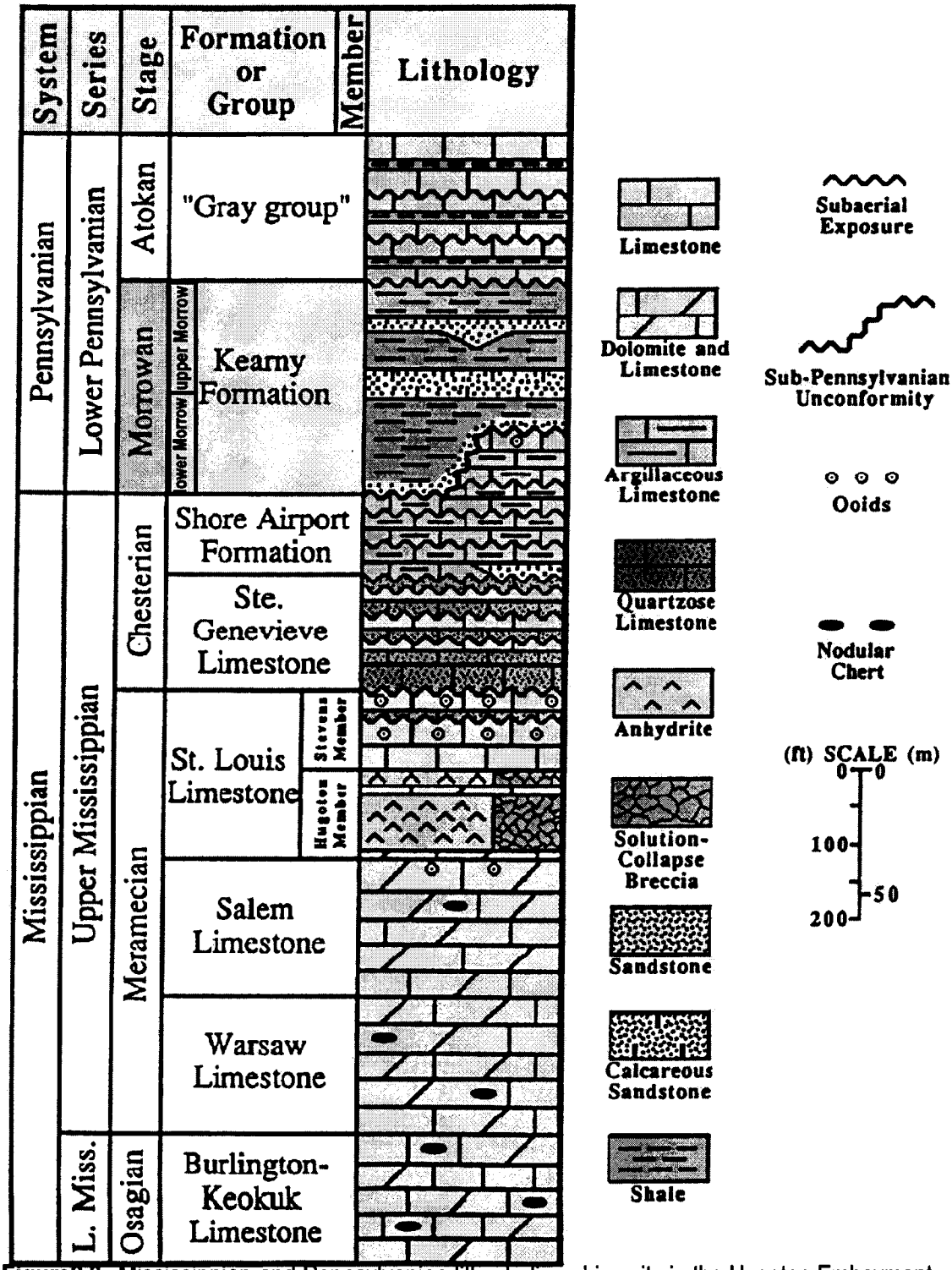

Figure2.3 Mississippian and Pennsylvanian lithostratigraphic units in the Hugoton Embayment. The Kearny Formation is informally subdivided into the lower and upper Morrow (modified from Abegg, 1994).

Santa Fe Trail, Cimarron Valley, and Stirrup fields is illustrated in Figure 2.4. Youle (1992) shows that the Morrowan (Kearny Formation) thins toward the north, northeast, and east in the Hugoton Embayment and pinches out toward the Central Kansas Uplift.

Climate in the Early Pennsylvanian

During the early Pennsylvanian, the equator was almost directly over the study area (5 degrees north; Krystinik and Blakeney, 1990; Figure 2.1). The resulting climate of the midcontinent was semiarid to humid (Schopf, 1975). Broad, shallow, cratonic seas and land areas having record plant growth covered much of the midcontinent area (Krystinik and Blakeney, 1990; Al-Shaieb et al., 1995).

Source Areas

Sediment distribution during the upper Morrowan time was influenced by the broad, low-relief shelf physiography, rapid glacio-eustatic sea-level fluctuations, low subsidence rates, and low rates of sediment supply (Sonnenberg, 1990; Figure 2.1). Several factors, including the climate and relief of the source areas, affected the grain size and distribution of sediment in the study area. Higher relief source areas had faster rates of erosion than lower relief areas, and were less likely to experience extensive weathering of the sediment prior to transport. Areas of low relief experienced weathering and soil development prior to sediment transport (Rader, 1987).

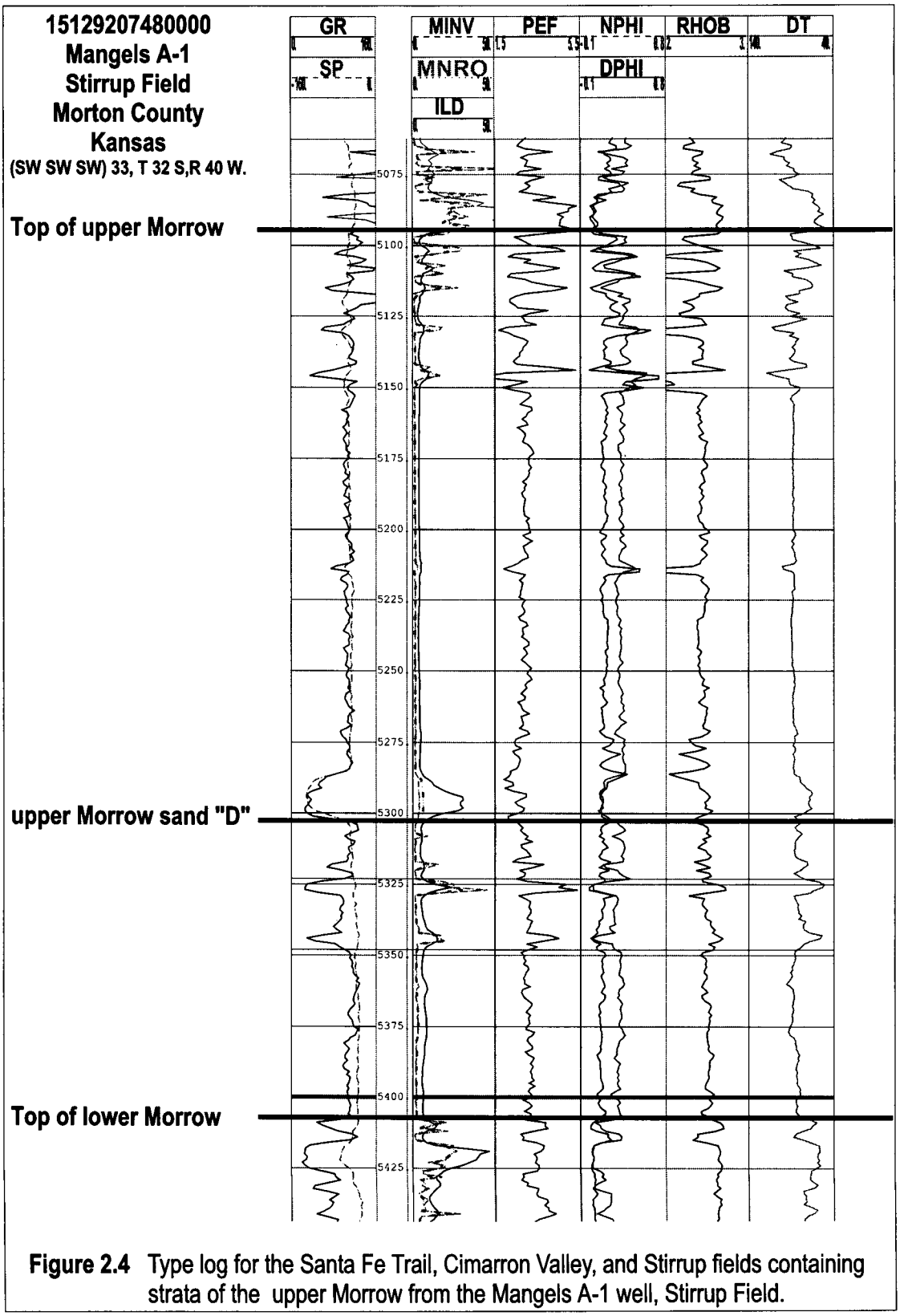

Figure 2.4 Type log for the Santa Fe Trail, Cimarron Valley, and Stirrup fields containing strata of the upper Morrow from the Mangels A-1 well, Stirrup Field.

Although a majority of the North American craton was exposed in the early Pennsylvanian, the Hugoton Embayment remained a downwarped area that continued to receive detrital sediments. The rivers that deposited upper Morrowan sandstones emanated from several paleotopographic highs that included the Transcontinental Arch to the north, to a lesser degree from the Central Kansas Uplift and Pratt Anticline to the east, the Amarillo-Wichita Uplift to the south, the Keyes Dome and Sierra-Apishapa-Grande Uplift to the southwest, and the Las Animas Arch to the west (Merriam, 1963; Swanson, 1979; DeVoto, 1980; Clark, 1987; Rader, 1987; Sonnenberg et al., 1990; Youle, 1992; Figure 2.2). These rivers flowed predominately southeastward towards the deeper part of the Anadarko Basin and were subjected to episodic discharge fluctuations (Krystinik and Blakeney, 1990; Figure 2.1).

Local Structure

A near-vertical, Mississippian age (?) fault divides the Santa Fe Trail and Cimarron Valley fields on the western margin of the study area (Figure 2.5). This fault was observed on wireline-log cross-sections and verified by three-dimensional seismic data (Peter Coffin, Anadarko Petroleum Company, pers. comm., 1998,). Upper Morrowan oil and gas production occurs on both the up-dip (western) and the down-dip (eastern) side of the fault.

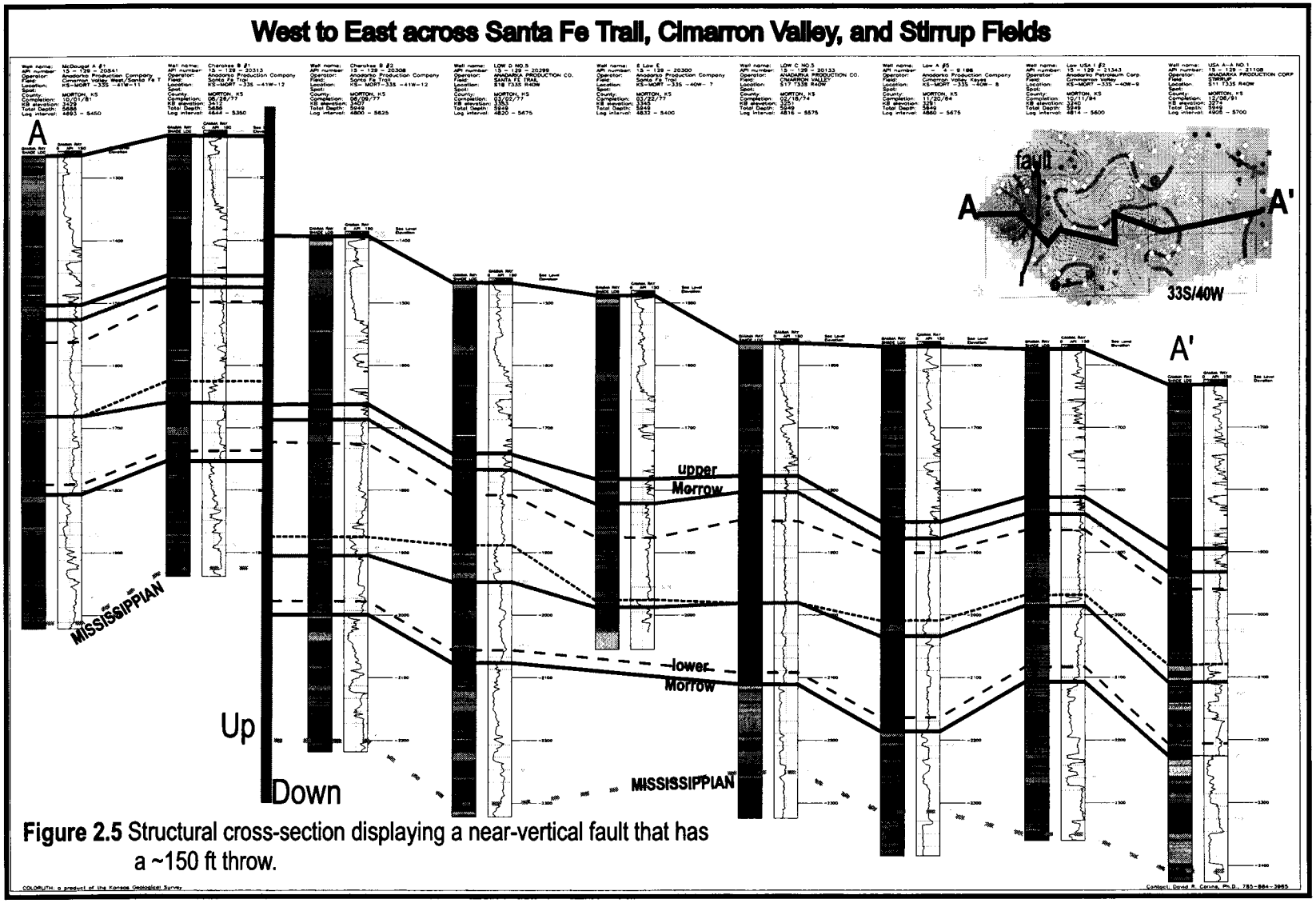

Figure 2.5 Structural cross-section displaying a near-vertical fault that has a ~150 ft throw.

CHAPTER THREE

CORE DESCRIPTIONS

Introduction

Upper Morrowan strata within the study area are predominantly siliciclastic. One hundred seventy-six feet (52.80 m) of upper Morrowan reservoir rock were recovered from four cores in the study area (Table 3.1; Figure 3.1). The cores were subdivided into nine lithofacies and grouped into three assemblages based on objective criteria consisting of grain size, sedimentary structures, lithoclasts, bioclasts, and ichnofauna (Table 3.2). In general, the lithofacies assemblages show a vertical transition from marine into fluvial and estuarine depositional environments.

Core	Field	Well location	Cored interval (ft)	Recovered core (ft)
Tucker F3	Santa Fe Trail	C-SW, SW/4, 6-33S-40W	5,352–5,397	45
Low G1	Santa Fe Trail	C-SE, NW/4, 6-33S-40W	5,357–5,395 5,364–5,410	37 25
Myers B2	Stirrup	C, N/2, SE/4, SE/4, 33-32S-40W	5,261–5,299	38
USA I2	Stirrup	NW/4, NE/4, SW/4, 3-33S-40W	5,244–5,275	31

Table 3.1 Information regarding the four cored intervals.

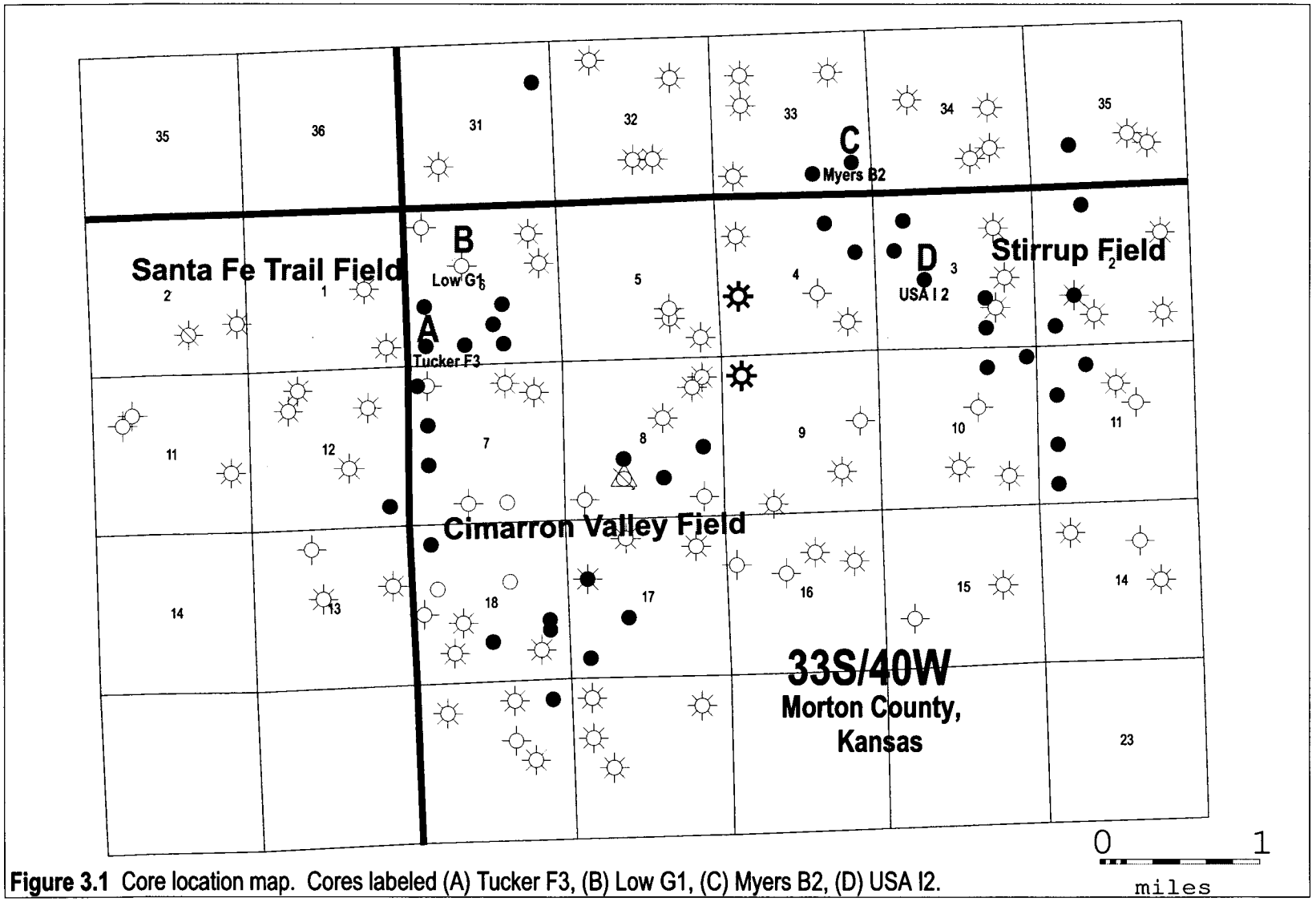

Figure 3.1 Core location map. Cores labeled (A) Tucker F3, (B) Low G1, (C) Myers B2, (D) USA I2.

Lithofacies		Description	Depositional Environment
Marine	One	Black, calcareous, micaceous, fossiliferous, thinly laminated mudstones. May grade upward into non-fossiliferous, black fissile shales	Low-energy, anoxic, offshore shelf setting that underwent a continual increase in water depth
	One B (1-B)	Light-gray, glauconitic, massive, calcite-cemented, echinoderm-rich wackestone to packstone	Moderately-high energy, nearshore open shelf
	One C (1-C)	Tan to olive, well-sorted, bioclastic, glauconitic, calcite-cemented, cross-bedded, medium- to coarse-grained quartz sandstone	High-energy, shallow marine setting, such as an upper shoreface
Fluvial	Two	Light-gray, matrix-supported, mudclast conglomerate	Nonmarine channel lag deposited in a high-current energy river
	Three	Light-gray, fine- to coarse-grained sandstone that grades upward into shale and mudstone	Migrating interchannel bars to sheet sands of a braided river
	Four	Light-gray to tan, low- to high-angle trough to tabular cross-bedded, coarse- to very coarse-grained conglomeratic sandstone	Stacked fluvial channel deposits from a high-energy (braided) river system located relatively close to the source area
	Five	Light-gray to tan, low-angle cross-bedded, medium- to coarse-grained sandstone	Stacked channel sandstones deposited in a braided river
Estuarine	Six	Light-gray, matrix-supported, medium-grained conglomerate interbedded with dark gray, slightly bioturbated, fine- to very fine-grained sandstone	Moderately low-energy, tidally influenced upper estuary that experienced high-energy surges of coarser-grained fluvial material
	Seven	Light-gray, fine- to very fine-grained quartz sandstone interbedded with black mudstones	Low-energy, slightly restricted, and tidally influenced mid-estuary

Table 3.2 Summary table of lithofacies and their depositional environments.

Assemblage of Marine Lithofacies

Lithofacies One

Lithofacies One consists of black, calcareous, micaceous, fossiliferous, thinly laminated mudstones that grade upward into nonfossiliferous, black, fissile shales. Lithofacies One is present at the base of the Tucker F3 (5,282.1–5,397 ft), the Myers B2 (5,294.3–5,300 ft), and the Low G1 (5,394.5–5,395 ft) cores. Locally discontinuous, light-gray sandy siltstone laminae and bioclast-rich, coarse-grained, calcite-cemented, conglomeratic sandstone lenses are present (figures 3.2A and 3.2B). Subangular to subrounded quartz and feldspar grains, echinoderms, gastropods, and brachiopods are the dominant clasts within the conglomeratic sandstone lenses (Figure 3.2B). Glauconite and pyrite nodules are locally present. Lithofacies One is rarely bioturbated, with only a few occurrences of *Planolites* sp. ichnofauna taxa. Lithofacies One has a sharp erosional contact with the overlying coarser-grained Lithofacies One-B, Two, and Four (figures 3.2C and 3.2D). An underlying contact for Lithofacies One was not observed within the cores.

The abundance of echinoderms, gastropods, and brachiopods in association with glauconite and pyrite suggests a marine environment (Krystinik and Blakeney, 1990). Slightly bioturbated mudstones that grade upward into non-bioturbated, non-fossiliferous, black, fissile shales indicate a slow sedimentation rate under increasingly anoxic bottom-water conditions. The low abundance and low diversity of ichnofauna taxa within black, organic-rich shales support an anoxic to low-

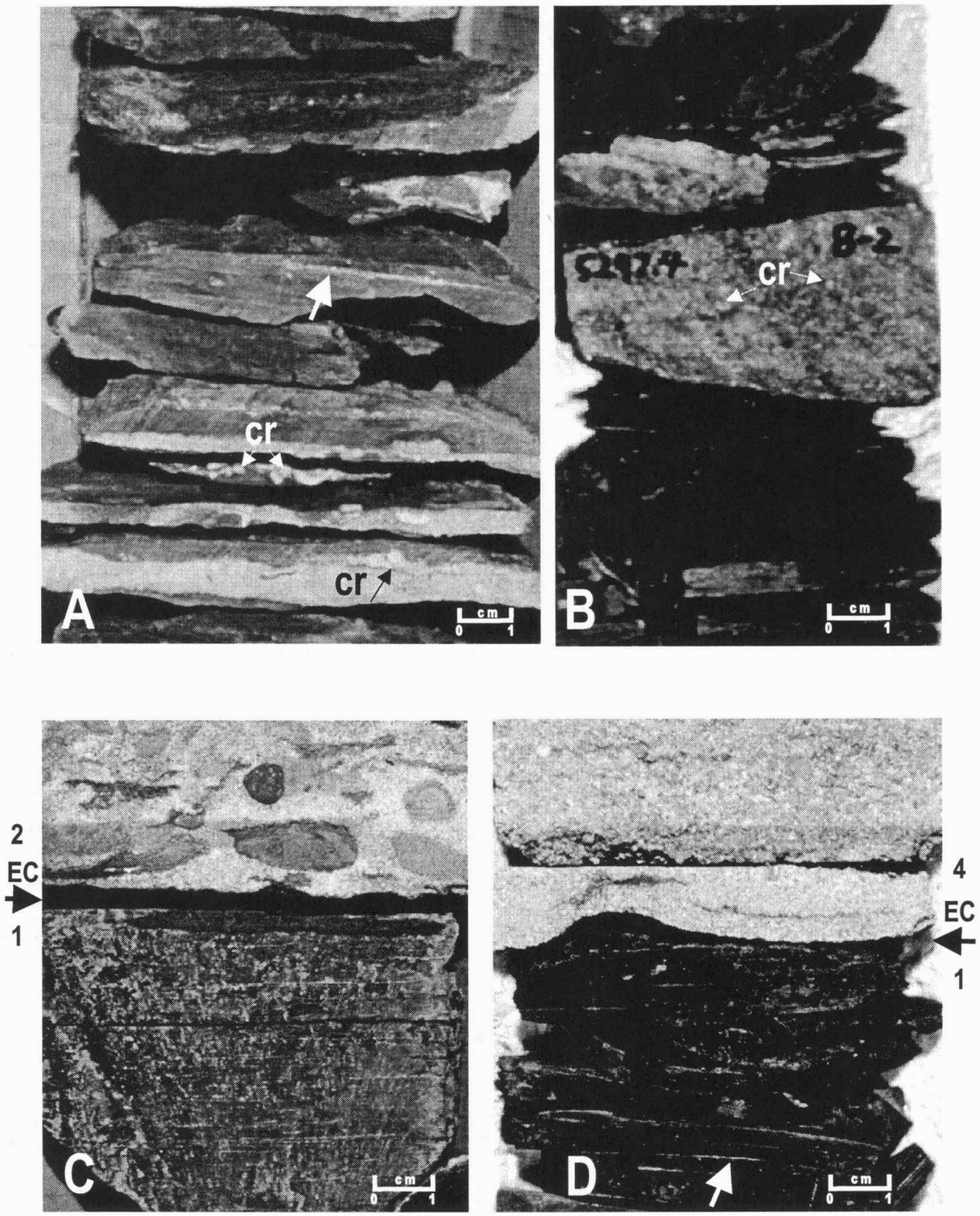

Figure 3.2 Lithofacies One
(A) and **(B)** Lithofacies One is dark black, fossiliferous, thinly laminated mudstones and fissile shales with discontinuous siltstone and thin beds of bioclastic-rich (cr-crinoid) conglomeratic sandstone lenses. **(C)** Sharp erosional contact (EC) of Lithofacies One with overlying Lithofacies Two. **(D)** Sharp erosional contact of Lithofacies One with overlying Lithofacies Four. Discontinuous siltstone laminae (white arrow) are locally present.

oxygenated setting (Tarbuck and Lutgens, 1990; Pemberton and MacEachern, 1992). Thinly laminated mudstone interbedded with sandy siltstone laminae indicate periodic fluctuations in current energy and sediment supply (Barclay, 1988). Locally present, thin, bioclastic-rich conglomeratic sandstone lenses suggest episodic, high-energy events such as storm or surge deposits derived from the upper shelf (Barclay, 1988; figures 3.2A and 3.2B).

Wheeler et al. (1990) identified a similar lithofacies in southeast Colorado as facies #1, an offshore marine environment that ranges from the inner to the outer shelf. South of the study area, on the northwestern shelf of the Anadarko basin, a comparable lithofacies was described as fossiliferous marine shale representing shelf muds deposited during maximum marine transgressions (Al-Shaieb et al., 1995). Shallow-marine shales that are analogous to Lithofacies One dominate most of the upper Morrowan strata (Krystinik and Blakeney, 1990; Bowen et al., 1993). Based on stratigraphic position, marine bioclasts, and sedimentary features, Lithofacies One is interpreted as a marine mudstone to shale deposited in a low-energy, anoxic, offshore shelf setting that underwent a continual increase in water depth.

Lithofacies One-B

Lithofacies One-B (1-B) is a light-gray, glauconitic, massive, calcite-cemented, echinoderm-rich wackestone to packstone (Dunham, 1962). Lithofacies One-B is present only in the Low G1 core (5,393.2–5,394.5 ft).

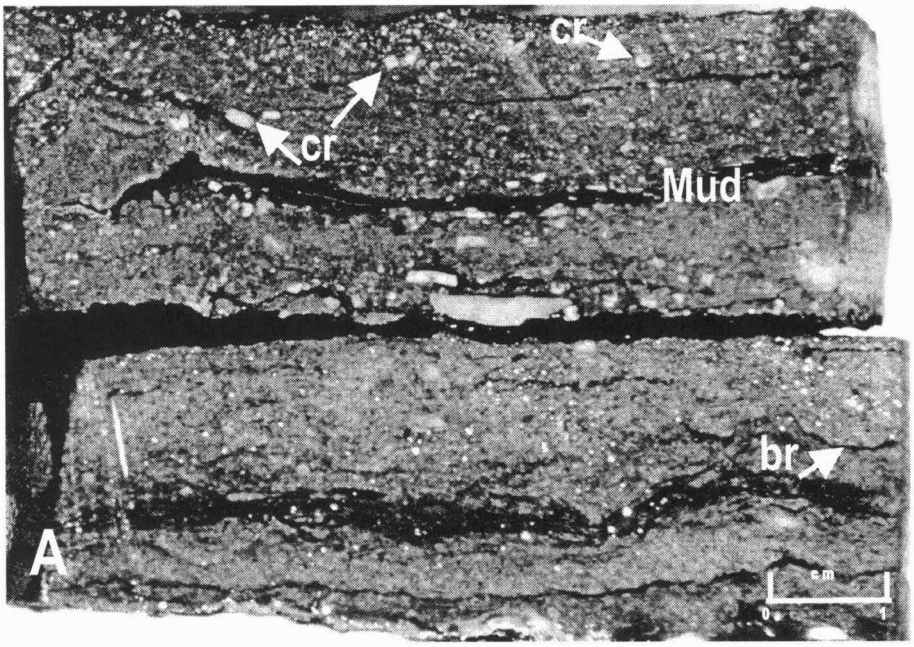

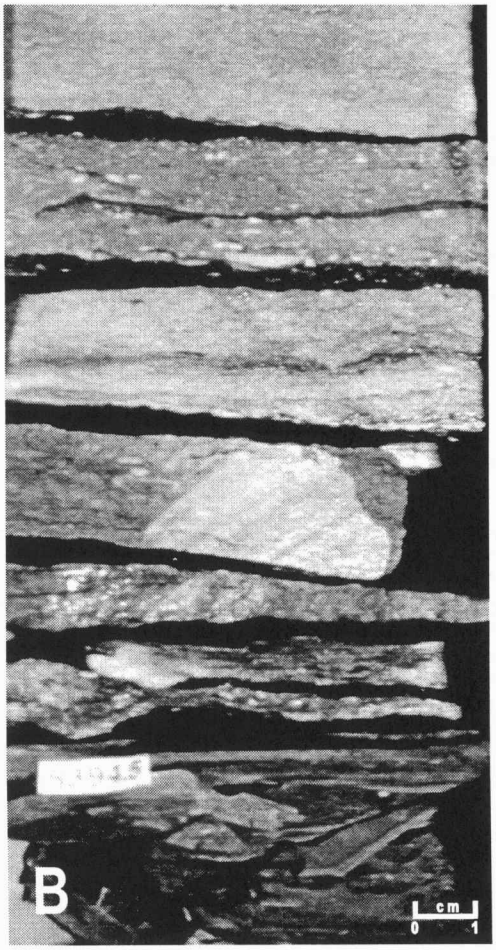

Lithofacies One-C
← EC
Lithofacies One-B

Figure 3.3 Lithofacies One-B

(A) Marine, crinoid-rich wackestone to packstone with discontinuous mud laminae (Mud). Crinoids (cr) and brachiopods (br) are the dominant bioclasts.

(B) Sharp erosional contacts (EC) of Lithofacies One-B with the underlying Lithofacies One and with the overlying Lithofacies One-C.

Lithofacies One-B
← EC
Lithofacies One

The texture of lithofacies One-B varies from a wackestone to a packstone with echinoderm, bivalve, and brachiopod fragments as the main bioclasts (Figure 3.3A). Locally present are planar and wavy laminae and thin beds of argillaceous shale and mudstone along with rare pyrite nodules (Figure 3.3A). Lithofacies One-B has a sharp erosional contact with both the underlying Lithofacies One and with the overlying Lithofacies One-C (Figure 3.3B).

The presence of glauconite, pyrite, and an abundance of echinoderm, bivalve, and brachiopod fragments in Lithofacies One-B suggests an open marine environment (Heckel, 1972). Wavy laminae of shale and mudstone interbedded with wackestone and packstone intervals indicate a fluctuation in current energy and sediment supply (Wilson and Jordan, 1983). A similar lithofacies was described as facies #2 and was interpreted as a shallow marine, open-shelf deposit (Wheeler et al., 1990). Based on high mud content, abundance of bioclasts, and stratigraphic position with the underlying offshore marine shale (Lithofacies One), Lithofacies One-B is interpreted to have been deposited in a moderately high-energy, nearshore open-shelf setting.

Lithofacies One-C

Lithofacies One-C is a tan to olive, well-sorted, bioclastic, glauconitic, calcite-cemented, cross-bedded, medium- to coarse-grained quartz sandstone (Figure 3.3A). Lithofacies One-C was observed only in the Low G1 core (5,392.1–5,393.2 ft).

Bioclasts (50–80%), dominated by echinoderms with minor brachiopod, bivalve, and gastropod fragments, and quartz (20–50%) are the main constituents of

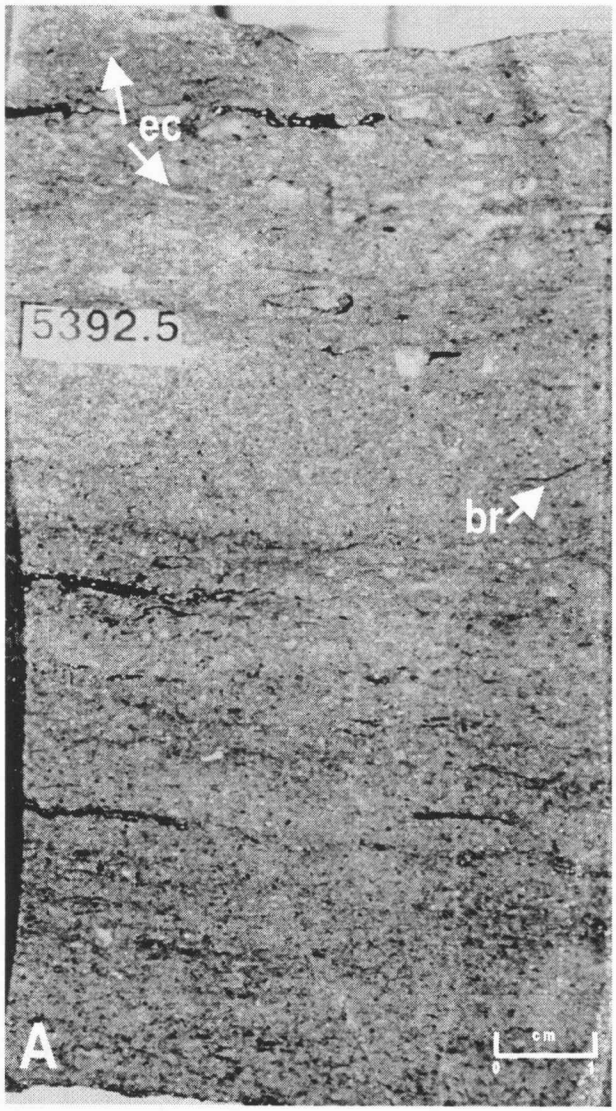

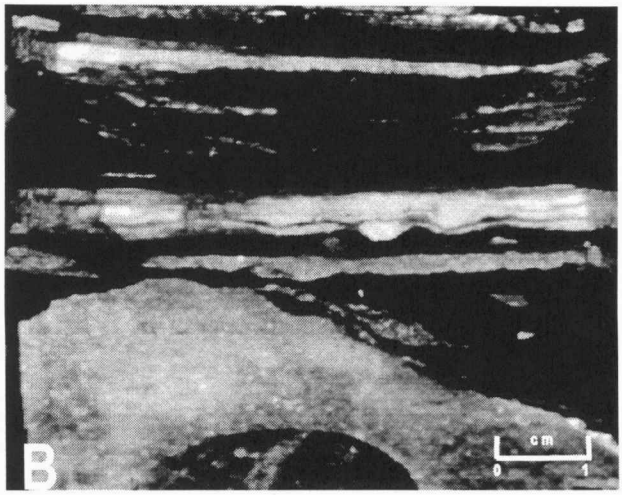

Lithofacies Seven

EC

Lithofacies One-C

Figure 3.4 Lithofacies One-C

(A) Well-sorted, bioclastic, glauconitic, calcite-cemented, cross-bedded, coarse- to medium-grained quartz sandstone. Lithofacies One-C has series of normal-graded intervals and an abundance of echinoderms (ec) and brachiopods (br).

(B) Lithofacies One-C has a sharp erosional contact (EC) with the overlying Lithofacies Seven.

Lithofacies One-C (Figure 3.4A). Low-angle, planar cross-beds were observed throughout Lithofacies One-C (Figure 3.4A). The cross-beds display a series of normally-graded intervals ranging from 1 to 3 cm in thickness in an overall fining upward succession. Locally present are discontinuous mud laminae and a few scattered glauconite grains. Lithofacies One-C has a sharp erosional contact with both the underlying Lithofacies One-B and the overlying Lithofacies Seven (figures 3.3B and 3.4B).

Glauconite, calcite cement, and an abundance of bioclasts (echinoderms, brachiopods, bivalves, and gastropods) indicate a normal marine environment (Heckel, 1972; Scholle, 1979; Wilson and Jordan, 1983). The well-sorted nature, low-angle cross-bedding, and low mud content, along with an absence of mud drapes, suggest a high-energy environment. Large-scale cross-bedding, fining upward trends from medium- to coarse-grained sandstone, and rare mud laminae indicate a migration of underwater dunes in a shallow, upper shoreface environment (Embry and Podruski, 1988; Andrews, 1997).

Lithofacies One-C resembles lithofacies F and facies #5 described by Franz (1985b) and Wheeler et al. (1990), respectively. Franz (1985b) interpreted lithofacies F as an estuary to tidal flat deposit, whereas Wheeler et al. (1990) interpreted facies #5 as an upper shoreface to tidal channel deposit. Kasino and Davies (1979) interpreted similar facies found within the upper Morrow of Cimarron County, Oklahoma, as sandy limestones deposited in tidal flats. Based on low-angle cross-beds, lack of mud, abundance of bioclasts, and well-sorted grains, Lithofacies One-C

is interpreted to have been deposited in a high-energy, shallow marine setting, such as an upper shoreface environment.

Assemblage of Fluvial Lithofacies

Lithofacies Two

Lithofacies Two is represented by a light-gray, matrix-supported, mudclast conglomerate. This lithofacies is present in cores from the Tucker F3 (5,381.8–5,382.1 ft) and the Low G1 (5,390.4–5,391 ft).

Lithofacies Two has a matrix that is light-gray, angular to subangular, poorly to moderately sorted, submature, medium-grained subarkose to sublitharenite (Folk, 1951, 1974). The matrix is composed primarily of quartz, microcline, sodium plagioclase, and rock fragments. In addition, the matrix has trace amounts of glauconite and limonite. Matrix-supported conglomerate lacks both internal bedding and clast imbrication. Mudclasts, composed of mud and shale, are poorly sorted, rounded to subrounded, lenticular, and iron-oxide stained. A majority of the clasts are "rolled mudballs" that range from 1.5 to 6 cm in diameter with an average of 2 cm (figures 3.5A and 3.5B). Bioclasts and ichnofauna were not observed in Lithofacies Two. Lithofacies Two has a gradational contact with the overlying Lithofacies Four and Lithofacies Three and a sharp erosional contact with the underlying Lithofacies One and Lithofacies Seven (figures 3.2C and 3.5B).

Lack of imbrication of the mudclasts and the lack of bioturbation indicate rapid bedload deposition (Shultz, 1984; Raddysh, 1988). Rapid bedload

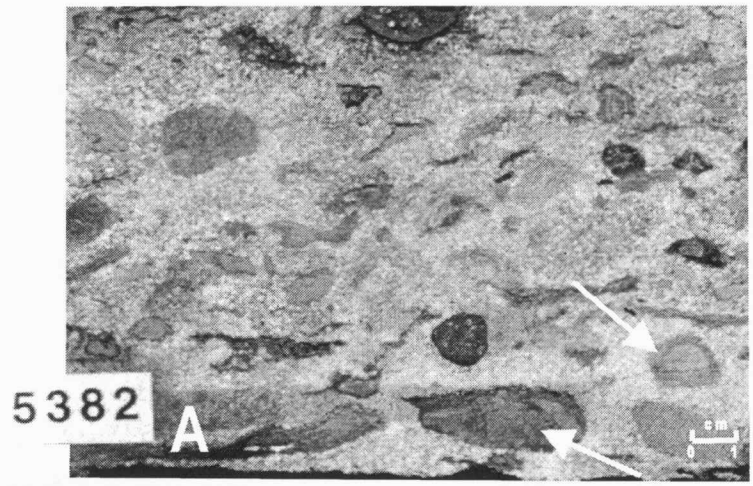

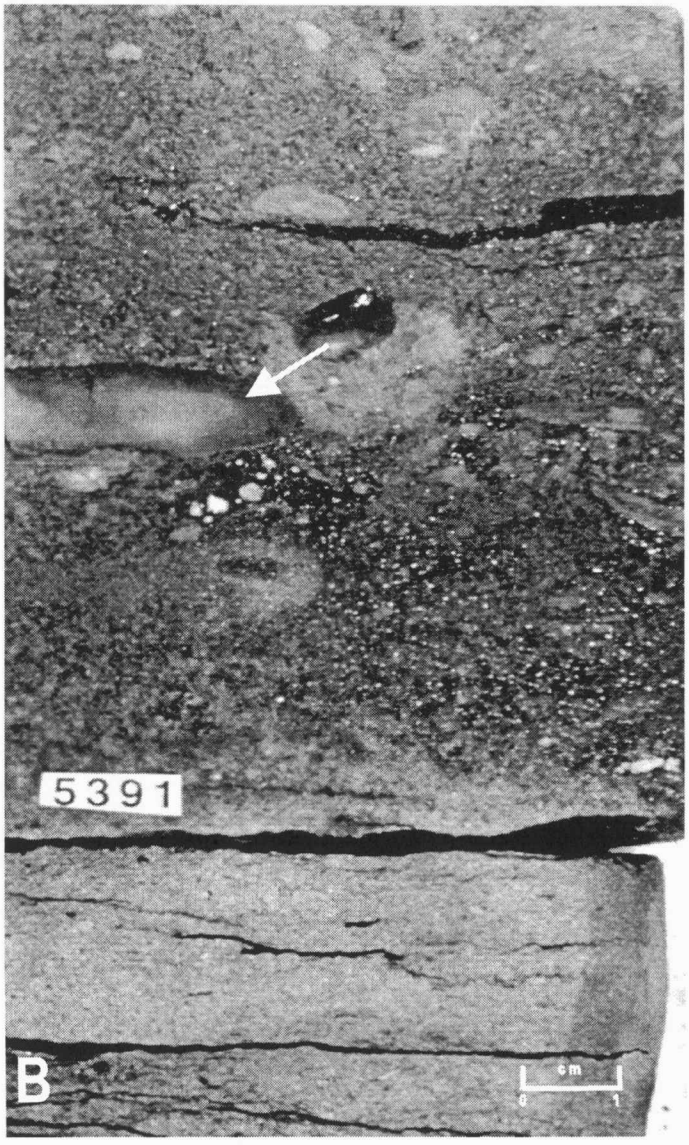

Figure 3.5 Lithofacies Two

(A) Light-gray, matrix-supported, mudclast conglomerate. Dark colors within the mudclasts are due to iron-oxide staining.

(B) Sharp erosional contact (EC) with the underlying Lithofacies Seven. Mudclasts are composed of circular laminae that have iron-oxide stains (white arrows).

Lithofacies Two
← EC
Lithofacies Seven

deposition is supported by the presence of subangular feldspar and quartz grains, which indicate a short distance of transportation. The erosional contact with the underlying deep-water lithofacies (Lithofacies One) along with the presence of limonite and iron-oxide staining indicate scouring and filling processes under subaerial conditions. Subaerial conditions are further supported by a lack of bioturbation and by an absence of marine fauna. Mudclasts similar to those observed in Lithofacies Two are associated with erosional surfaces related to channel migration (Al-Shaieb et al., 1995; Collinson, 1996). The rip-up clasts could have been scoured from the underlying strata of marine shale or from the surrounding channel floors and banks.

Lithofacies Two is comparable to Morrowan facies #7, as defined by Wheeler et al. (1990). Facies #7 was interpreted as a fluvial channel deposit of a braided stream, channel-bottom lag, or lower point-bar setting. In the northwestern shelf of the Anadarko Basin, Al-Shaieb et al. (1995) and Puckette et al. (1996) interpreted a similar lithofacies of the upper Morrowan as a channel lag deposit. Franz (1985b) interpreted this unit of the Low G1 core as lithofacies B, a fluvial channel-lag deposit. On the basis of sharp contacts with the underlying Lithofacies One, abundance of rip-up clasts, iron-oxide staining, and lack of bioclasts, Lithofacies Two is interpreted as channel lag that has been deposited in a nonmarine, high-current-energy, fluvial environment. The landward shift in lithofacies from marine (Lithofacies One) to fluvial, the evidence of a subaerial exposure (iron-oxide staining), and the sharp erosional truncation with the underlying Lithofacies One are interpreted to be the

result of a relative fall in sea-level and evidence for a sequence boundary (Figure 3.2C).

Lithofacies Three

Lithofacies Three is a light-gray, fine- to coarse-grained sandstone that grades upward into shale and mudstone. Lithofacies Three is present in cores from the USA I2 (5,246.6–5,247 ft; 5,260.4–5,262.4 ft; and 5,272.1–5,275 ft), the Low G1 (5,372.2–5,377 ft), and the Tucker F3 (5,363.4–5,364 ft; 5,369.9–5,370.7 ft; 5,373.5–5,374.5 ft; and 5,376.7–5,379.2 ft).

Throughout the unit, Lithofacies Three has low-angle planar to small-scale trough cross-beds; however, near the top of the unit, Lithofacies Three has a sharp contact with laminae and beds of organic-rich laminated shale, mudstone, and coal (figures 3.6A and 3.6B). Lithofacies Three consists of fining upward sandstone intervals (~18–70 cm thick) that are 0composed of angular to subangular quartz, microcline, sodium plagioclase, and ro0ck fragments. The sandstones are submature and range from quartzarenites or subarkoses to sublitharenites (Folk, 1951, 1974). Lithofacies Three contains siderite, kaolinite, muscovite, stylolitic shale, lignite coal fragments, and coal laminae with minor plant remnants (figures 3.6B and 3.6C). Quartz overgrowths and calcite and dolomite cement are common within the sandstone intervals. Black, thinly laminated, organic-rich shales, mudstones, and coals (~2 mm–6 cm thick) with locally present discontinuous siltstone laminae abruptly overlie the sandstone intervals (Figure 3.6A). Marine

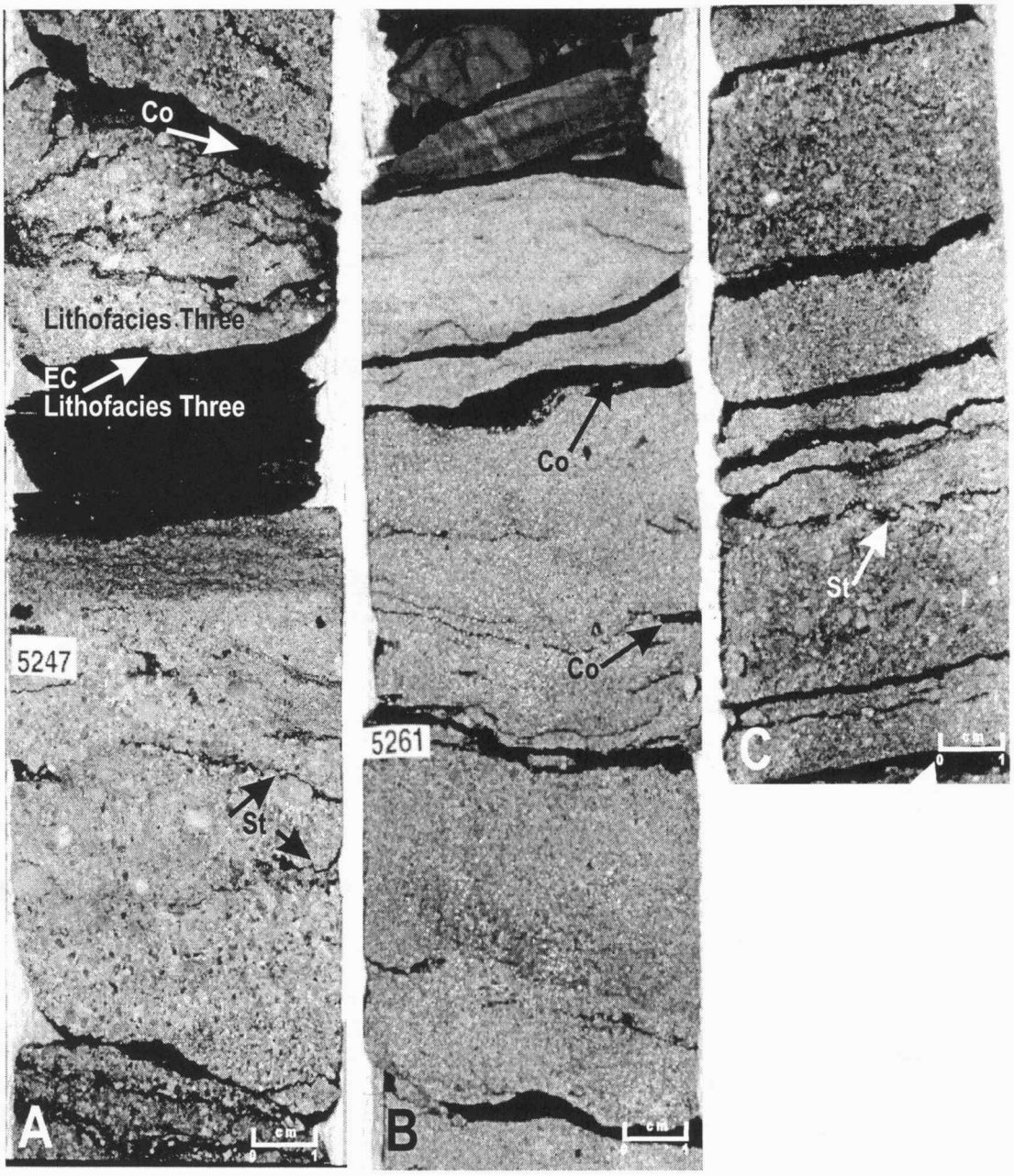

Figure 3.6 Lithofacies Three

(A) Fine- to coarse-grained, nonmarine sandstone that grades upward into planar shale and mudstone thin beds. Lithofacies Three contains stylolitic contacts (St) and coal laminae (Co). There is an erosional contact (EC) between two successions of Lithofacies Three.

(B) Sandstone of Lithofacies Three showing an upward increase in abundance of coal.

(C) There are low-angle and small-scale trough cross-beds as well as stylolitic contacts throughout Lithofacies Three.

bioclasts and ichnofauna were not observed in Lithofacies Three. Lithofacies Three has a sharp erosional contact with the overlying Lithofacies One, Two, Three, and Four and a gradational contact with the underlying Lithofacies Four and Lithofacies Six.

Absence of marine bioclasts and ichnofauna suggest a nonmarine environment (Wightman et al., 1987; Pemberton and MacEachern, 1992; Collinson, 1996). The nonmarine interpretation is supported by the presence of lignite flakes, clasts, and laminae observed throughout the lithofacies (Diessel, 1992; Nemec, 1992). Lithofacies Three is dominated by subangular to angular, moderately sorted, submature quartz and feldspar grains that suggest sediment deposition was relatively close to the source. Studies of the upper Morrowan in the Interstate Field, southwest Kansas, have interpreted the very coarse nature of a lithofacies as indicative of a nearby source area for the sediments (Sonnenberg, 1990). Normally-graded intervals, current ripples, trough cross-beds, and abrupt vertical changes of sandstone bodies into shale units indicate periodic fluctuations in sediment load, flow discharge, and capacity (Barclay, 1988; Miall, 1996).

Micaceous mudstones are commonly restricted in extent and are interpreted as the remnants of a weak current setting within the tops of midchannel islands or channel units (Collinson, 1996) or the deposits within standing pools of water during low-stage channel abandonment within sandy braided sediments (Alberta, 1987; Miall, 1996). The fining-upward intervals of Lithofacies Three resemble braided fluvial deposits of the Devonian Battery Point Formation, Quebec, Canada, and the

sandflat deposits of the South Saskatchewan River, Canada (Cant and Walker, 1976, 1978). Based on fining upward intervals, coarse and angular grains, lack of both bioclasts and ichnofauna, and sedimentary structures, Lithofacies Three is interpreted to have been deposited in migrating interchannel bars (channel abandonments) to sheet sands of a possibly braided river.

Lithofacies Four

Lithofacies Four is a light-gray to tan, low- to high-angle trough to tabular cross-bedded, coarse- to very coarse-grained conglomeratic sandstone (Figure 3.7A). Lithofacies Four is present in the USA I2 (5,244–5,246.6 ft; 5,247–5,260.4 ft; 5,262.4–5,271.3 ft; and 5,271.8–5,272.1 ft), the Tucker F3 (5,364–5,369.9 ft; 5,370.7–5,373.5 ft; 5,374.5–5,376.7 ft; and 5,379.2–5,381.8 ft), the Myers B2 (5,261–5,265.5 ft; 5,265.8–5,268.3 ft; 5,270.1–5,287.5 ft; and 5,291.5–5,294.3 ft), and the Low G1 (5,377–5,390.4 ft) cores. Lithofacies Four is the dominant observed lithofacies composing 42.6% of the recovered cores.

Lithofacies Four consists of subangular to angular, moderately sorted quartz, sodium plagioclase, microcline, and rock fragments. The sandstone intervals are submature and classified as quartzarenites to subarkoses (Folk, 1951, 1974). Normally-graded intervals ranging from ~2.5 to ~25 cm in thickness that fine into medium-grained sandstones were observed throughout the lithofacies (figures 3.7A and 3.7B). These fining-upward intervals are highlighted by color variations in cement (quartz overgrowths and dolomite) and kaolinite mud content

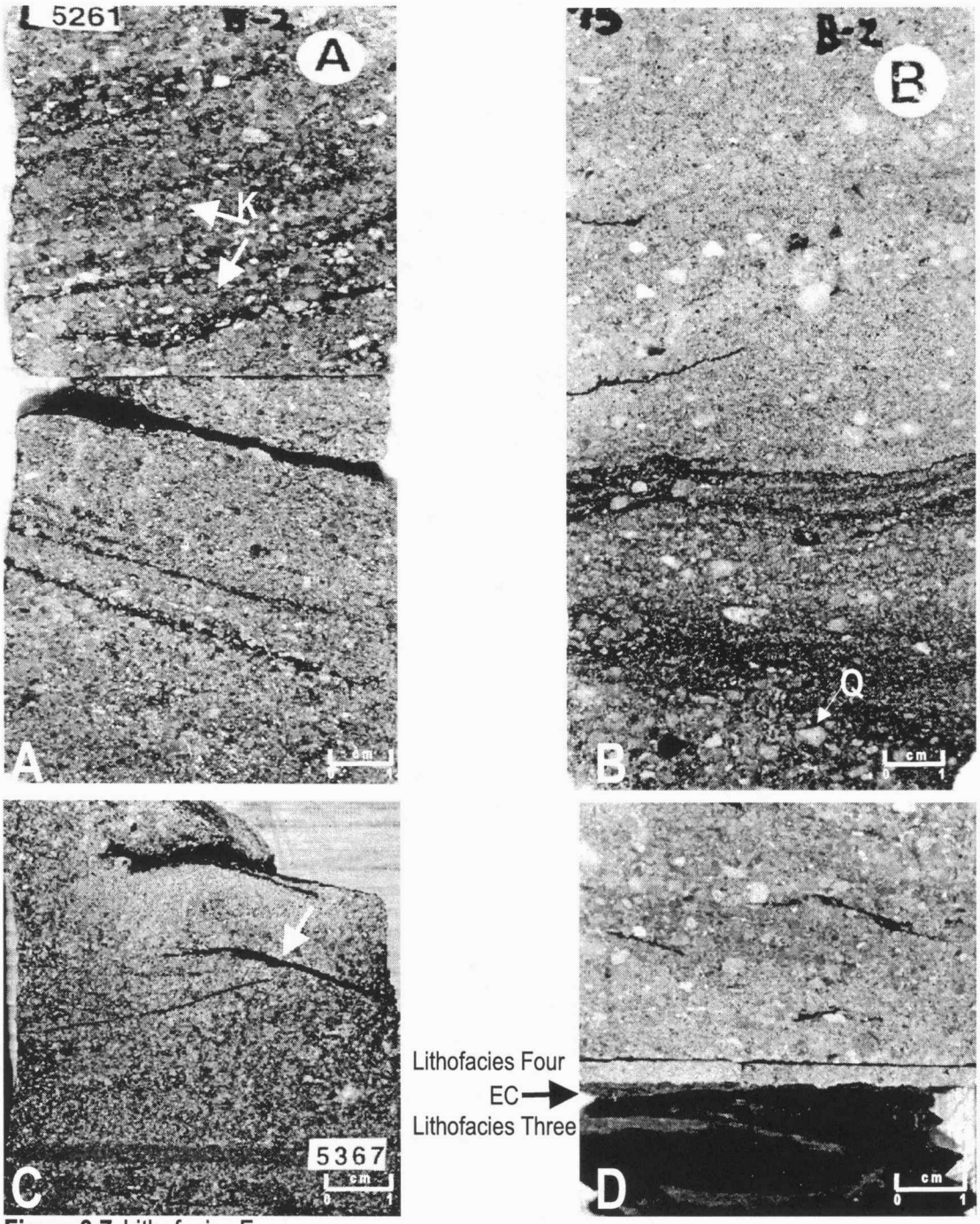

Figure 3.7 Lithofacies Four

(A) Lithofacies Four is a light-gray to tan, low- to high-angle trough to tabular cross-bedded, coarse- to very coarse-grained conglomeratic sandstone. Lithofacies Four contains fining upward intervals and feldspar lithoclasts (K). **(B)** Normally-graded intervals and very-coarse-grained, subangular to angular lithoclasts (Quartz- Q) are present throughout Lithofacies Four. **(C)** Sandstones have reactivation surfaces in trough cross-beds. **(D)** Lithofacies Four has local mud laminae and shows a sharp erosional contact (EC) with the underlying Lithofacies Three.

(figures 3.7A and 3.7B). Locally present are reactivation surfaces (Figure 3.7C), shale laminae (generally associated with stylolites), scour surfaces, mudclasts, mica, and rare pyrite and siderite nodules. With the exception of the base of the USA I2 core, where a few echinoderm and bivalve fragments were detected, bioturbation and marine fauna were not observed in Lithofacies Four. Lithofacies Four has sharp erosional contacts with the underlying Lithofacies One and Lithofacies Two (Figure 3.2D) and sharp and gradational contacts with both the overlying and the underlying Lithofacies Three and Lithofacies Five (Figure 3.7D).

The lack of *in situ* bioclasts and bioturbation and the presence of feldspar lithoclasts suggest a nonmarine environment (Collinson, 1996; Miall, 1996). As observed from the wireline-log dipmeters, the cross-bedding structures in Lithofacies Four show a dominant southeast uni-directional flow (Figure 3.8). The observed dipmeter patterns suggest a high-energy, river environment (Barclay, 1988; Schlumberger, 1989). The interpreted fluvial, high-energy environment is supported by the absence of shale and by the presence of trough and planar cross-beds and ripple structures. The fining upward beds that were observed within Lithofacies Four are interpreted as the products of periodic waning of current energy.

Repetition of trough and planar cross-bedding within Lithofacies Four suggests bar migration in a braided stream system (Walker and Cant, 1978). In Morrowan sandstone facies, braided assemblages have been interpreted based on massive to cross-stratified, coarse to very coarse-grained and pebbly sandstone with common mud clasts (Krystinik and Blakeney, 1990). Lithofacies Four resembles

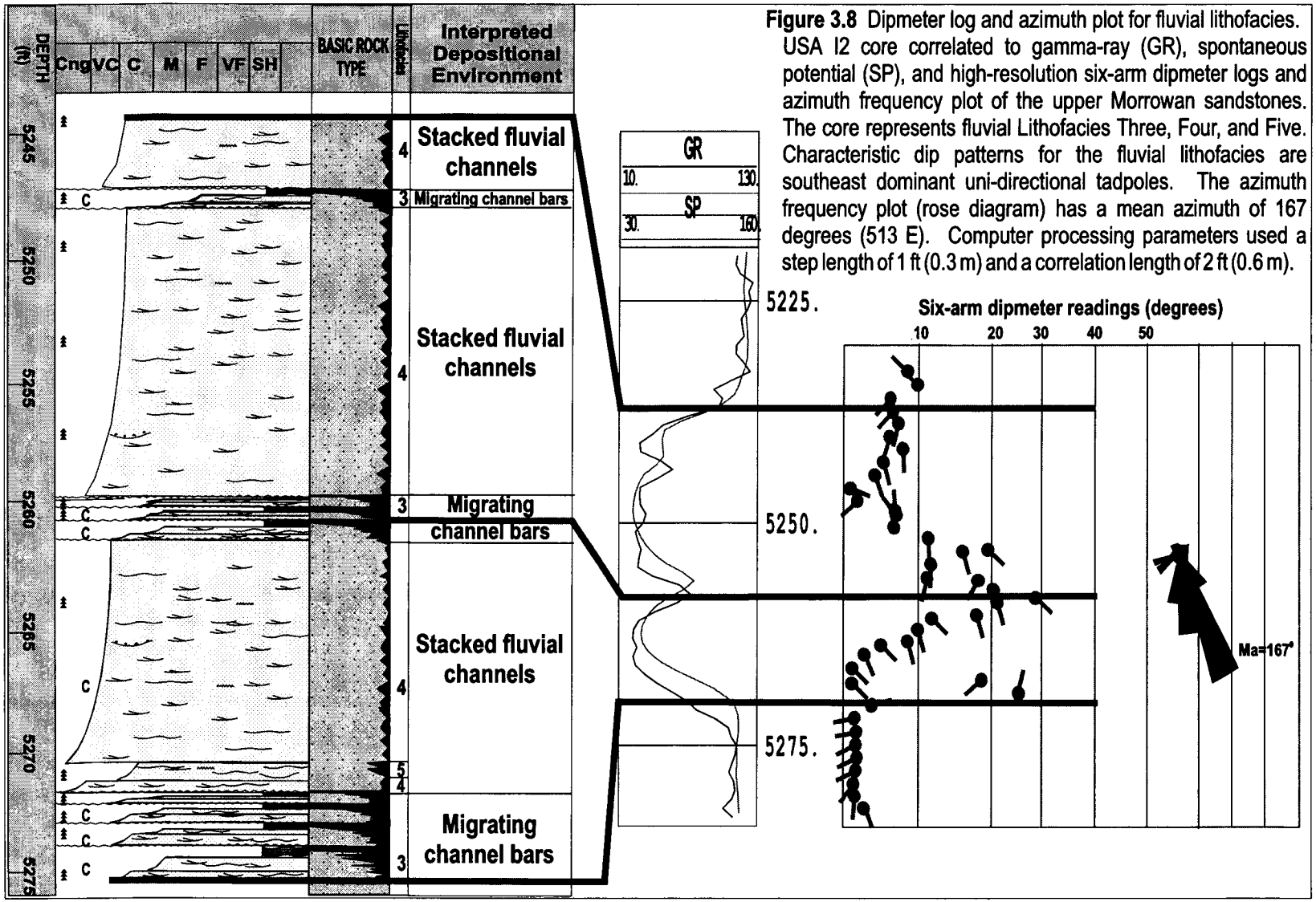

Figure 3.8 Dipmeter log and azimuth plot for fluvial lithofacies. USA I2 core correlated to gamma-ray (GR), spontaneous potential (SP), and high-resolution six-arm dipmeter logs and azimuth frequency plot of the upper Morrowan sandstones. The core represents fluvial Lithofacies Three, Four, and Five. Characteristic dip patterns for the fluvial lithofacies are southeast dominant uni-directional tadpoles. The azimuth frequency plot (rose diagram) has a mean azimuth of 167 degrees (513 E). Computer processing parameters used a step length of 1 ft (0.3 m) and a correlation length of 2 ft (0.6 m).

Wheeler et al.'s (1990) facies #8, which was interpreted as fluvial channel deposits. Al-Shaieb et al. (1995) and Puckette et al. (1996) identified similar lithofacies in the northern Anadarko shelf as fluvial sandstones deposited by high-energy braided streams. Based on uni-directional dipmeter readings; angularity of the very coarse grained sands; low- to high-angle trough and planar cross-beds; presence of coal; and submaturity of the sandstones, Lithofacies Four is interpreted as stacked fluvial sandstones that have been deposited in a high-energy (braided) river system located relatively close to the source area. In the Myers B2 core, Lithofacies Four has a sharp erosional contact and a landward shift in lithofacies from marine to fluvial with the underlying Lithofacies One (Figure 3.2D). Therefore, the contact that separates Lithofacies One from Lithofacies Four is interpreted to be a sequence boundary that resulted from a relative fall in sea-level.

Lithofacies Five

Lithofacies Five is a light-gray to tan, low-angle cross-bedded, medium- to coarse-grained sandstone. Lithofacies Five was observed in cores from the Myers B2 (5,265.5–5,265.8 ft; 5,268.3–5,270.1 ft; and 5,287.5–5,291.5 ft), the Low G1 (5,369.2–5,372.2 ft), the USA I2 (5,271.3–5,271.8 ft), and the Tucker F3 (5,362.9–5,363.4 ft and 5,376.7–5,379.2 ft). Moderately sorted, subangular to angular quartz, microcline, sodium plagioclase, and rock fragments are the main constituents of Lithofacies Five. Lithofacies Five is submature and is classified as a quartzarenite to

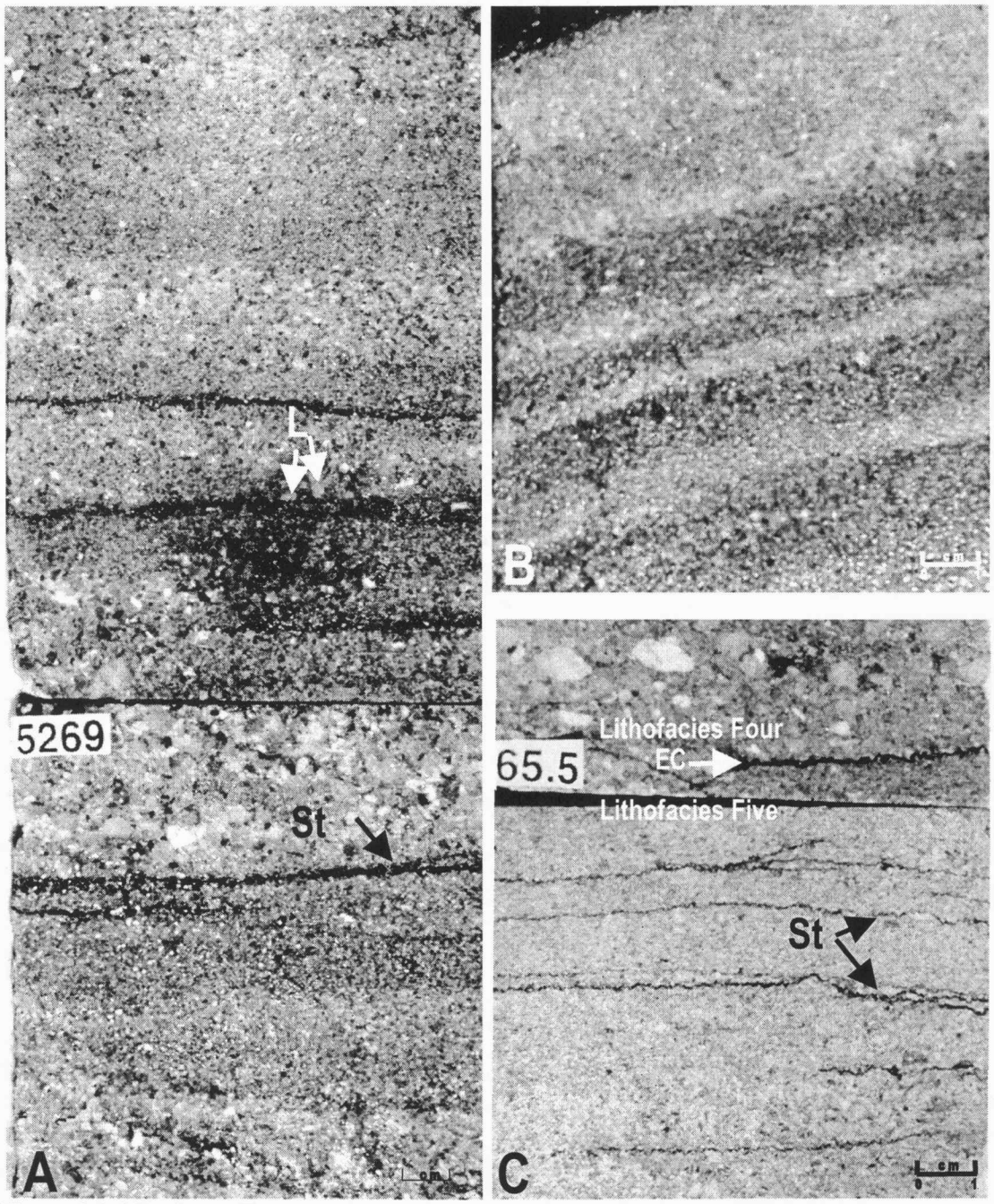

Figure 3.9 Lithofacies Five

(A) Lithofacies Five is a light-gray to tan, low-angle cross-bedded, medium- to coarse-grained sandstone. Lithofacies Five contains series of normally-graded successions based with coarse lithoclasts (L) and capped by mud, coal laminae, and stylolitic contacts (St). **(B)** Medium-angle, planar cross-beds with fining upward intervals (1-3 cm) characterize Lithofacies Five. There are color variations in the sandstones due to differences in mineral and cement concentrations. **(C)** Lithofacies Five has low to horizontal planar cross-beds within fining upward intervals capped by sylolitic contacts and a sharp erosional contact with overlying Lithofacies Four.

sublitharenite or subarkose (Folk, 1951, 1974). Quartz overgrowths and dolomite are the dominant cements for this lithofacies. Lithofacies Five is composed of a series of normally-graded successions ranging from ~1 to ~4 cm in thickness (figures 3.9A and 3.9B). Commonly, these normally-graded intervals have erosive bases floored with coarse-grained lithoclasts and are capped by fine- to medium-grained sandstones with stylolitic shales, mud, or lignite laminae (~1–3 mm thick; figures 3.9A and 3.9B). Mica, siderite, kaolinite, and limonite minerals are locally present in Lithofacies Five. Marine bioclasts and ichnofauna were not observed. Lithofacies Five has sharp erosional surfaces with both the underlying and the overlying Lithofacies Four and Lithofacies Three and has a gradational contact with the overlying Lithofacies Seven (Figure 3.9C).

An absence of both bioclasts and ichnofauna and the presence of siderite suggest a nonmarine environment (Folk, 1951, 1974; Pemberton and MacEachern, 1992). The nonmarine interpretation is supported by the presence of localized, thin coal laminae that are characteristic of active braidplain regimes (Collinson, 1996). The submaturity and moderately sorted nature along with subangular to angular grains indicate deposition close to the source areas (Sonnenberg, 1990).

Lithofacies Five resembles Wheeler et al.'s (1990) facies #6, which was interpreted as either fluvial or estuarine deposits. Based on uni-directional dipmeter readings; coarse-grained sandstones, stratigraphic relationships with the other lithofacies; lack of marine bioclasts and ichnofauna; abundance of coal; and other

sedimentary structures, Lithofacies Five is interpreted to have been deposited as stacked channel sandstones in a fluvial (braided) river environment.

Assemblage of Estuarine Lithofacies

Lithofacies Six

Lithofacies Six is a light-gray, matrix-supported, medium-grained conglomerate interbedded with dark gray, slightly bioturbated, fine- to very fine-grained sandstone (Figure 3.10). This lithofacies is present in the Tucker F3 (5,357.1–5,362.9 ft) and Low G1 (5,366.5–5,368.5 ft) cores.

The conglomerate intervals are composed of subangular to subrounded, poorly sorted mudclasts and quartz and feldspar lithoclasts (2–5 mm in diameter) in a fine-grained sand matrix (Figure 3.10A). Micaceous shales are commonly interbedded within the conglomerate intervals. Absence of marine fauna and a low diversity and low abundance of *Skolithos* ichnofauna taxa (*Planolites* sp. and *Palaeophycus* sp.) characterize Lithofacies Six (figures 3.10C and 3.10D). Coal streaks (Figure 3.10C); herringbone cross-beds (Figure 3.10B); discontinuous shale laminae; climbing ripples; wavy, flaser, and heterolithic bedding; and burrows are present within the silty, fine-grained sandstone intervals. The fine-grained sandstone intervals are classified as quartzarenites to subarkoses (Folk, 1951, 1974).

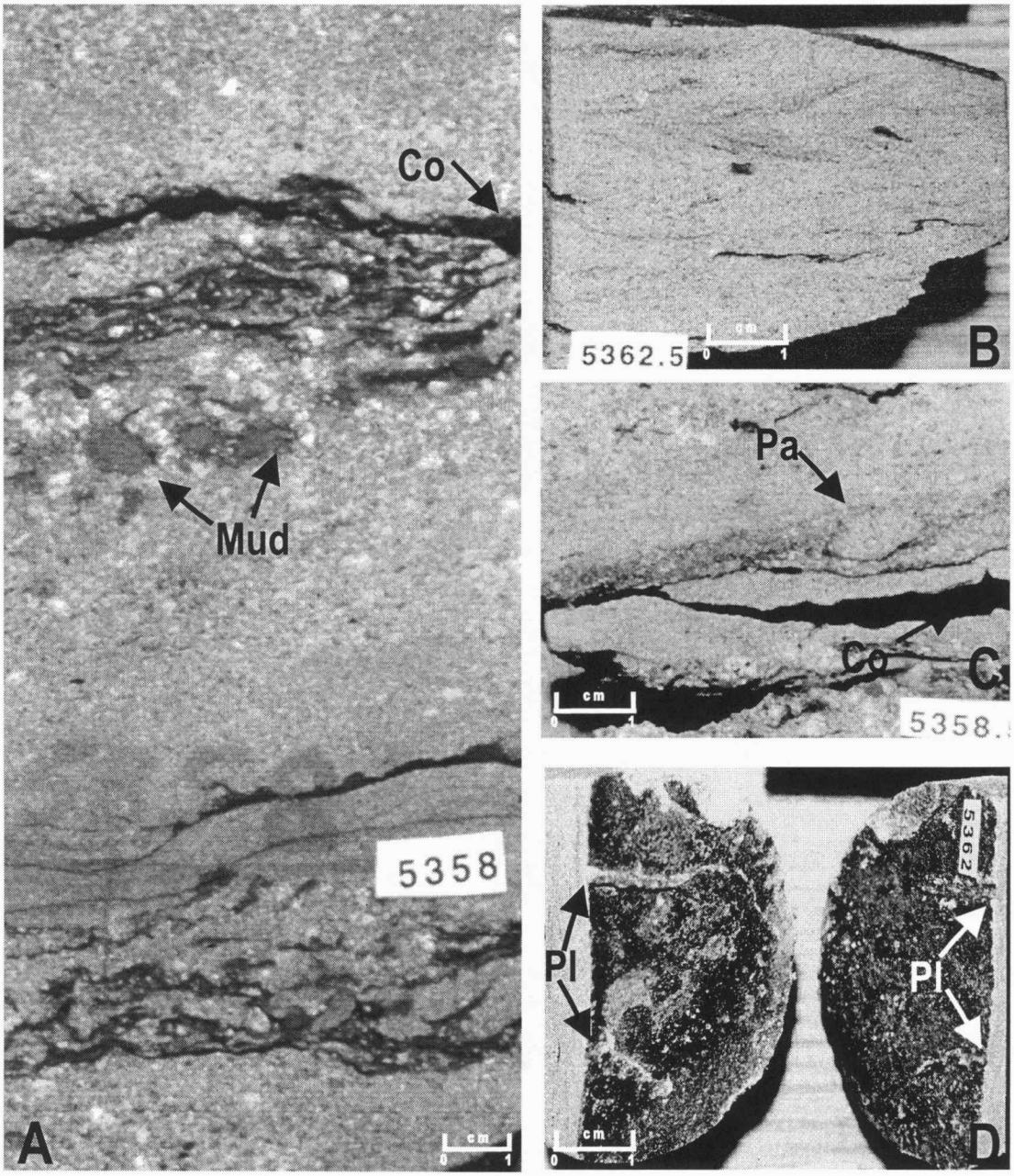

Figure 3.10 Lithofacies Six

(A) Lithofacies Six is light-gray, matrix-supported, medium-grained conglomerates interbedded with dark gray, slightly-bioturbated, fine- to very fine-grained sandstones. Conglomerates are composed of subangular to subrounded lithoclasts and mudclasts (Mud) and contain mud and coal laminae (Co). **(B)** Herringbone cross-beds are common in Lithofacies Six. **(C)** *Palaeophycus* (Pa) ichnofossils are found in fine-grained sandstone. Lithofacies Six contains wavy bedding and coal laminae. **(D)** The fine-grained sandstones of Lithofacies Six display a full-relief *Planolites* (Pl) ichnofossil preserved on bedding plain of core (black on bottom, white on top).

Lithofacies Six has a gradational contact with the underlying Lithofacies Four, Five, and Seven and with the overlying Lithofacies Seven.

The absence of observed marine bioclasts, hummocky cross-stratification, or extensive bioturbation suggest that Lithofacies Six was not deposited under fully marine conditions. The low abundance, low diversity, and small sizes of ichnofauna taxa along with a lack of body fossils suggest a marine-influenced or a stressed (brackish) shallow water environment (Frey and Howard, 1975, 1980, 1985; Barnes, 1984; Ekdale et al., 1987; Wightman et al., 1987; Barclay, 1988; Beynon et al., 1988; Pemberton and MacEachern, 1992). Herringbone structures observed within the sandstone intervals suggest a tidally influenced environment. The tidally influenced environment is supported by wireline-log dipmeters (Figure 3.11). The dipmeter tadpoles show a bi-directional northwest–southeast flow (Schlumberger, 1989). Conglomerate beds containing mud rip-up clasts alternating with fine-grained sandstones suggest either fluctuations in discharge (Steel and Thompson, 1983) or surge deposits due to seasonal variations (Allen, 1992; Miall, 1996).

Franz (1985 a,b) interpreted this succession of the Low G1 core to represent deposits from an estuary or tidal channel that were reworked in its upper part. Based on stratigraphic position, herringbone structures, and low diversity and small sizes of ichnofauna, Lithofacies Six is interpreted to have been deposited in a moderately low-energy, tidally influenced upper estuary environment that experienced high-energy surges of coarser-grained fluvial material.

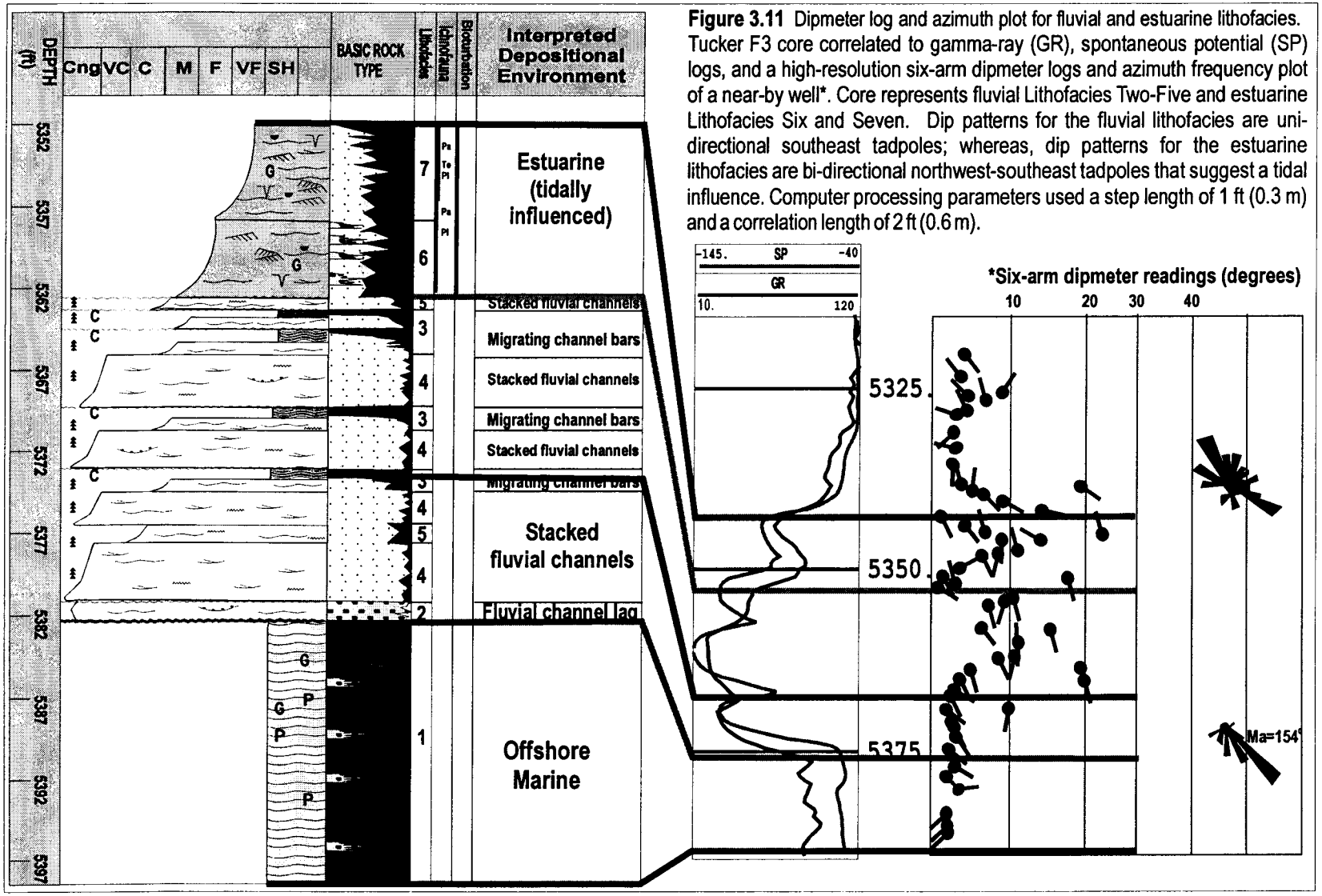

Figure 3.11 Dipmeter log and azimuth plot for fluvial and estuarine lithofacies. Tucker F3 core correlated to gamma-ray (GR), spontaneous potential (SP) logs, and a high-resolution six-arm dipmeter logs and azimuth frequency plot of a near-by well*. Core represents fluvial Lithofacies Two-Five and estuarine Lithofacies Six and Seven. Dip patterns for the fluvial lithofacies are uni-directional southeast tadpoles; whereas, dip patterns for the estuarine lithofacies are bi-directional northwest-southeast tadpoles that suggest a tidal influence. Computer processing parameters used a step length of 1 ft (0.3 m) and a correlation length of 2 ft (0.6 m).

Lithofacies Seven

Lithofacies Seven is a light-gray, fine- to very fine-grained quartz sandstone interbedded with black mudstones (figures 3.12A and 3.12B). Lithofacies Seven is present in cores from the Tucker F3 (5,357.1–5,352 ft) and the Low G1 (5,357–5,366.5 ft; 5,368.5–5,369.2 ft; and 5,391–5,392.1 ft).

Alternating very fine-grained sandstone and mudstone laminae, mud drapes, climbing ripples, and wavy, ripple, lenticular, and flaser bedding are observed throughout Lithofacies Seven. Lithofacies Seven is an immature, very fine- to fine-grained subarkose that is micaceous (0–1.8%), glauconitic (0–0.1%), and shale clast-bearing (0–5%). Lithofacies Seven contains quartz, microcline (0–15%), pyritized wood fragments, and coal flakes in a silty, micaceous clay detrital matrix. Locally present are soft-sediment deformation features and bioturbated sandstones (figures 3.12A and 3.12B). Marine body fossils are not present, but a moderate diversity and abundance of ichnofauna taxa are observed in the bioturbated, wavy, and ripple-bedded, fine-grained sandstones and shale intervals. The ichnofauna assemblage includes vertical escape structures (fugichnia), small *Planolites* sp., *Monocraterion* sp., *Palaeophycus* sp., *Bergaueria* sp., and *Teichichnus* sp. (figures 3.12B, 3.12C, and 3.12D). Lithofacies Seven has a gradational contact with the underlying Lithofacies Six and a sharp erosional contact with both the underlying Lithofacies One-C (Figure 3.4B) and the overlying Lithofacies Two.

Lenticular and wavy beds, starved ripples, mud drapes, herringbone structures, and intervals of heterolithic strata consisting of laminated mudstone

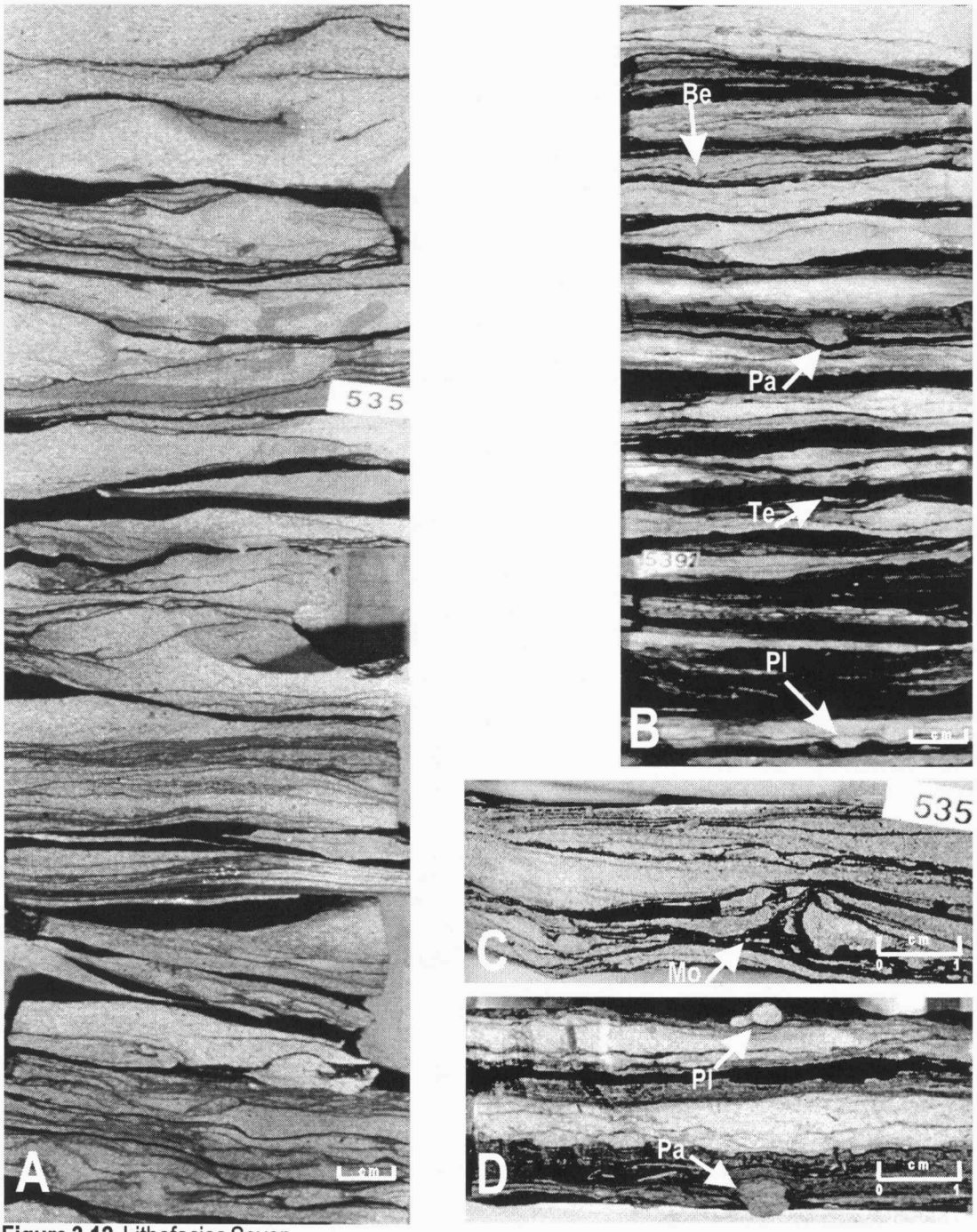

Figure 3.12 Lithofacies Seven

(A) Lithofacies Seven is a light-gray, fine- to very fine-grained quartz sandstone interbedded with black mudstones. There are alternating sandstones and mud laminae, wavy, ripple, and flaser bedding, and bioturbation. **(B)** Trace fossils developed in wavy and ripple-bedded fine sandstones and mudstones. *Planolites* (Pl), *Palaeophycus* (Pa), *Bergueria* (Be), and *Teichichnus* (Te) ichnofauna reflects an estuarine (brackish) setting. **(C)** *Monocraterion* (Mo) is present within the fine-grained sandstone. **(D)** *Planolites* (Pl) and *Palaeophycus* (Pa) ichnofauna taxa are in wavy shale laminae.

alternating with very fine-grained sandstone suggest a tidally influenced estuarine setting (Pettijohn et al., 1973; Thomas et al., 1987; Dalrymple, 1992; Zaitlin et al., 1994). A tidally influenced environment is supported by a bi-directional northwest–southeast flow as was observed from the wireline-log dipmeters (Figure 3.11; Schlumberger, 1989). Lack of marine fauna and a moderate diversity and moderate abundance of small-sized ichnofauna suggest a stressed (brackish) water environment (Pemberton and Frey, 1982; Wightman et al., 1987; Barclay, 1988; Beynon et al., 1988; Pemberton and MacEachern, 1992). The ichnofauna are either depauperate *Cruziana* or *Skolithos* taxa consisting of feeding structures formed by deposit feeders or dwelling structures constructed by suspension feeders. Similar ichnofauna assemblages develop under low-energy, stressful, brackish water conditions (Barnes, 1984; Beynon et al., 1988; Pemberton and MacEachern, 1992).

Interbedded sandstone and mudstone intervals represent an alternation between a slow current carrying fine-grained sand and a very slow current carrying mud (Tillman and Martinson, 1984; Strobl, 1988). The variation in current energy is consistent with the bioturbated sandy intervals that represent longer periods of sand deposition. Climbing ripples suggest a significant introduction of sediment during high flow conditions (McKee, 1965; Jopling and Walker, 1968). Lenticular to flaser bedding located stratigraphically above coarser-grained lithofacies (Lithofacies Three, Four, and Five) suggest the gradual abandonment of a fluvial channel setting and transition to an estuarine environment (Stear, 1985; Alberta, 1987; Tornqvist, 1993; Collinson, 1996).

Lithofacies Seven is similar to estuarine and possible tidal flat deposits described in upper Morrow lithologies in Cimarron County, Oklahoma (Kasino and Davies, 1979). Deposits of tidal estuarine point bars in the fluvial–estuarine transition zone of the Gironde Estuary, France, contain fine- to medium-grained (fining upward), rippled sand units with flaser bedding and sand–mud alternations (Allen, 1992). Franz (1985b) defined Lithofacies Seven of the Low G1 core as lithofacies D and interpreted it as shallow marine, low and variable flow, nearshore deposits. Wheeler et al. (1990) described Morrowan facies #4 as intertidal, nearshore marine to estuarine deposits. Based on stratigraphic position; dipmeter readings; heterolithic strata; lenticular and flaser bedding; and a moderate diversity and abundance of small-sized ichnofauna, Lithofacies Seven is interpreted to have been deposited in a low-energy, slightly restricted, tidally influenced, mid-estuary environment.

CHAPTER FOUR

WIRELINE-LOG RESPONSES OF LITHOFACIES ASSEMBLAGES

Introduction

From the cored intervals of the Tucker F3, Low G1, Myers B2, and USA I2, the upper Morrow successions were classified into three assemblages of lithofacies: marine, fluvial, and estuarine. The lithofacies assemblages were integrated with their wireline-log responses to extend the lithofacies interpretations beyond the limited core control. Seven stratigraphic cross-sections show the result of the integrated core and log interpretations. The cross-sections were used to establish a sequence-stratigraphic framework and depositional model throughout the Santa Fe Trail, Cimarron Valley, and Stirrup fields (Appendix A).

The objective of this chapter is to characterize the wireline-log responses of the marine, fluvial, and estuarine lithofacies assemblages. Responses of eight wireline-log tools were determined for each of the lithofacies assemblages by using wireline-log data from the four cored and additional wells as summarized in Table 4.1 and described in detail below.

Lithofacies assemblage	PEF (E/B)	GR (API)	SP (mV)	Caliper	SGRD RES (ohm-m)	Nphi/ Dphi (g/cc)	Rhob (g/cc)	Sonic (μs/ft)
Marine (Lithofacies One)	3.0–3.3	105–130	$^{+}30$–$^{+}65$	Washed out	3–7	N>D	2.45–2.6	85–120
Fluvial (Lithofacies Two, Three, Four, and Five)	1.8–2.4	25–40	$^{-}30$–$^{-}65$	Mudcake	15–75	N<D	2.4–2.55	65–80
Estuarine (Lithofacies Six and Seven)	2.6–3	60–80	0–$^{-}35$	Mudcake	6–15	N<D	2.4–2.45	75–85

Table 4.1 Summary of characteristic log responses for upper Morrow lithofacies assemblages in study area.

Wireline-Log Data

Well logging is the *in situ* measurement of the petrophysical properties of subsurface lithological units (Schlumberger, 1989). Wireline-log data from 76 wells in the study area (spaced at approximately one-quarter mile [400 m]) were digitized (Figure 4.1). Seven chronostratigraphic wireline-log correlations were constructed as shown in Appendix A. Correlation and mapping of the lithofacies across the study area used a minimum of four log curves per well that included photoelectric index (PEF), gamma ray (GR), spontaneous potential (SP), caliper, neutron and density porosity (Nphi and Dphi), bulk-density (Rhob), resistivity (short-normal, deep induction, shallow guard, etc.), and sonic ($\Delta\tau$). Not all of the described curves are available for all wells or cores used in this study or used in the cross-sections.

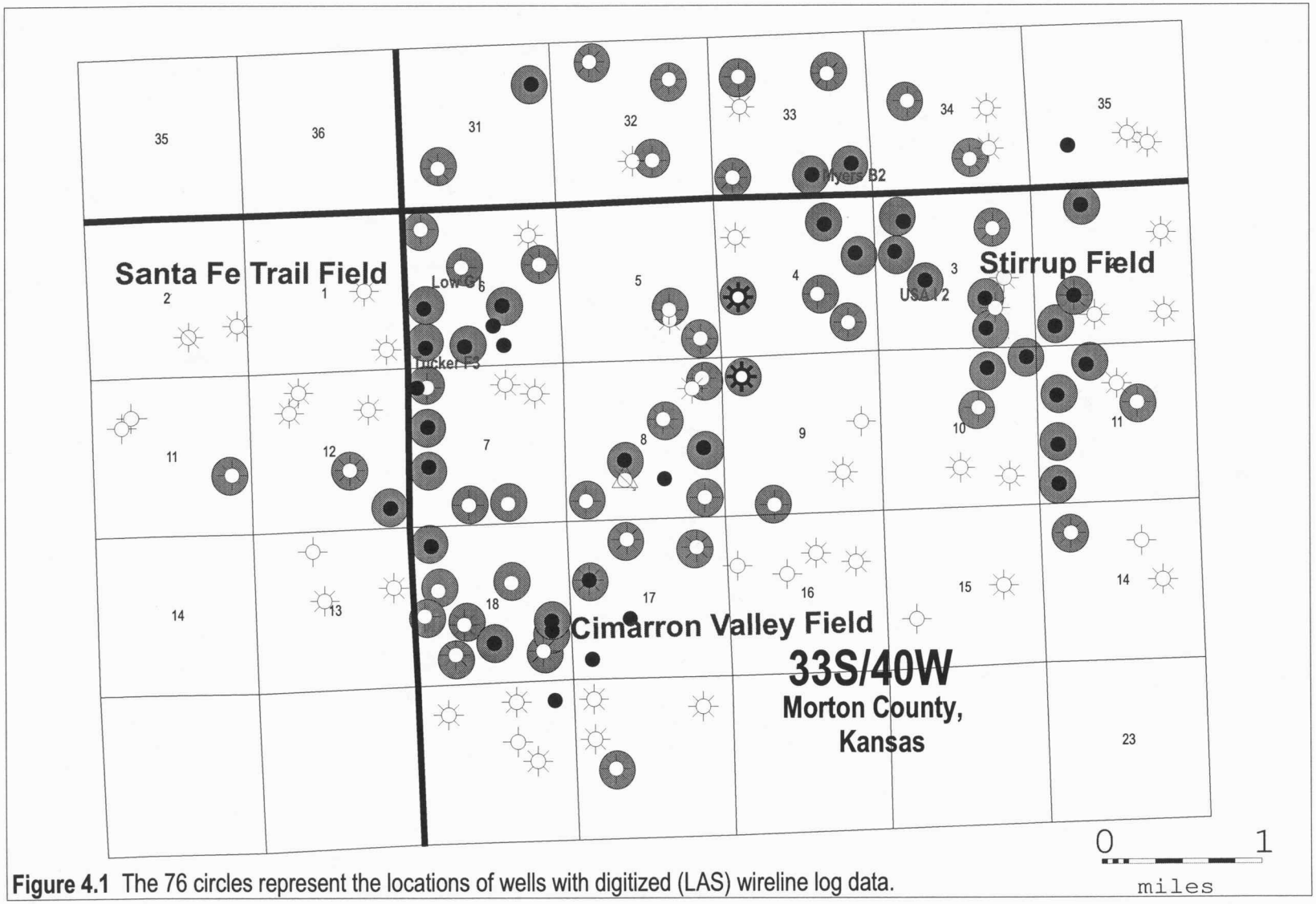

Figure 4.1 The 76 circles represent the locations of wells with digitized (LAS) wireline log data.

Photoelectric log

The photoelectric index (PEF) log records the amount of absorption of low-energy gamma rays of a formation in barns per electron on a 0–10 scale (Doveton, 1998). The recorded PEF value is a direct function of the aggregate atomic numbers of the elements in the formation (Doveton, 1994). The strong influence of the atomic numbers and the slight response to fluid or gas content make the PEF log a sensitive indicator of mineralogy (Doveton, 1998). Lithologies can be accurately differentiated when the PEF log is combined with the neutron and density porosity logs (Doveton, 1994, 1998).

Gamma-Ray log

The gamma-ray (GR) log records the natural gamma radiation (radioactivity) occurring in the borehole and is usually expressed in terms of API units (Schlumberger, 1989; Doveton, 1998). The gamma-ray tool acts as a "Geiger counter" measuring the amount of the principal gamma-radiating elements (potassium, thorium, and uranium) found in sediments (Doveton, 1998). Potassium, thorium, and uranium are usually associated with shales and muds; therefore, the gamma-ray curve reflects the amount of shales and muds in the formations (Phillips Petroleum, 1989). In evaluating typical sedimentary sequences, the gamma-ray log is used both for the definition of bed boundaries between shales and sandstones or carbonates and in evaluating the shale content of shaly units (Doveton, 1998).

Spontaneous potential log

The spontaneous potential (SP) log records variations in naturally occurring potentials in a borehole in millivolts (Phillips Petroleum, 1989). The SP measures the electrical potential produced by the interaction of formation water, conductive drilling fluid, and certain ion-selective rocks (Schlumberger, 1989). The magnitude of SP curve deflection is controlled by the difference in salinity between the formation water and the mud filtrate (Doveton, 1994, 1998). If the formation salinity is greater than the mud filtrate, the SP is expected to deflect to the left, called a negative potential (Doveton, 1998). A positive potential is created when the SP deflects to the right because the salinity of the formation water is lower than that of the mud filtrate (Schlumberger, 1989). The deflection in SP (negative or positive) is a response to the permeability of ion flow and will normally correlate with hydraulic permeability (Doveton, 1994). Generally, the SP log is used for determining sand and shales, finding Rw values (formation resistivity), and distinguishing between permeable and non-permeable zones (Phillips Petroleum, 1989; Doveton, 1998).

Caliper log

The caliper log records the diameter of the borehole (Phillips Petroleum, 1989). The caliper tool moves along the borehole wall and measures the borehole diameter to monitor for areas of thickness or buildup on the walls (mudcake) and for areas of expanded borehole diameter (washout). Mudcake buildup on the borehole wall is evidence that the formation has the ability to move liquids and possesses

permeability and porosity (Phillips Petroleum, 1989). An area of washout indicates less permeable strata (e.g., shales, mudstones, unconsolidated sands, salts, etc.; Phillips Petroleum, 1989).

Resistivity logs (short normal and shallow guard)

Resistivity logs record the opposition to the flow of electric current offered by a material of unit length and unit cross-sectional area in ohm-meters (Doveton, 1998). The resistivity tool consists of two types of electrodes; current electrodes, which emit electrical current into the formation, and potential electrodes, which measure the electrical potential across the formation (Phillips Petroleum, 1989; Schlumberger, 1989). The further the electrodes are placed apart, the further the depth of investigation but the poorer the vertical resolution (Phillips Petroleum, 1989). Formation water will conduct electricity depending on the temperature and the amount of salt in the water (Phillips Petroleum, 1989). Salt water conducts electricity very well, whereas fresh water or hydrocarbon does not conduct electricity well. Formation resistivity depends on the amount and type of water in the pore spaces plus the amount of hydrocarbons in the formation (Phillips Petroleum, 1989). An increase in porosity will decrease the resistivity, while a decrease in porosity will increase the resistivity (Doveton, 1998).

Density log

The density log (Dphi) records the electron density in grams per cubic centimeter of the elements making up the formation by recording the number of Compton-scattering collisions made by gamma rays emitted from a calibrated radioactive source (Phillips Petroleum, 1989; Schlumberger, 1989; Doveton, 1998). Electron density is dependent on the density of the rock matrix, the porosity of the rock, and the density of the pore fluids (Phillips Petroleum, 1989). Density logs are primarily used as porosity logs; however, they can be used to estimate oil yields from oil shales, evaluate shaley sands, and recognize complex lithologies when corrected for specific lithology matrices (Doveton, 1994, 1998).

The bulk-density log (Rhob) records the sum of the densities of the formations multiplied by their proportions in grams per cubic centimeter (Doveton, 1994, 1998). The bulk-density depends on the density of the pore fluid and the density of the matrix material. The bulk-density log aids in the recognition of certain lithologies and minerals (e.g., coals, salt beds) that have appreciable density contrasts with typical sandstones, carbonates, and shales (Doveton, 1994, 1998).

Neutron log

Neutron logs (Nphi) are used primarily to delineate porous formations and determine their porosity by responding to the amount of hydrogen nuclei present in the formations (Phillips Petroleum, 1989). The neutron tool records in grams per cubic centimeter and operates by radiating high-energy neutrons into the borehole

walls from a calibrated source (Doveton, 1998). The neutrons that are emitted into the formations lose energy by colliding with atoms of nearly the same size (hydrogen). Therefore, the higher the content of hydrogen atoms (e.g., water, hydrocarbons) in a formation, the lower the neutron log value will be (Schlumberger, 1989; Doveton, 1998). When combined with the density or resistivity logs, the neutron log can be used to evaluate porosity values, identify lithology, and detect gas zones (Phillips Petroleum, 1989).

Sonic log

The sonic log records the time ($\Delta\tau$) required for a compressional elastic wave to traverse 1 ft of formation (Phillips Petroleum, 1989). The tool operates by producing low ultrasonic acoustic waves with a transmitting transducer (Doveton, 1998). The first signal, which is the first compressional wave, to reach the receiving transducer triggers the recording of the interval transit time ($\Delta\tau$), measured in microseconds per foot (Doveton, 1998). The velocity of the compressional wave is dependent on both the density and the elasticity of the rock matrix (Schlumberger, 1989). When calibrated to a velocity of a known lithology, a sonic log can be used as a porosity log (Phillips Petroleum, 1989).

Wireline-Log Data Tied to Core

The four cores in the study area (Tucker F3, Low G1, Myers B2, and USA I2) were grouped into marine, fluvial, and estuarine lithofacies assemblages and were correlated to their particular log suites (figures 4.2–4.6). The marine lithofacies assemblage includes Lithofacies One, One-B, and One-C as defined from the cores of the Tucker F3, Low G1, and Myers B2. The fluvial lithofacies assemblage corresponds with Lithofacies Two, Three, Four, and Five as observed in cores from the Tucker F3, Low G1, Myers B2, and USA I2. The estuarine lithofacies assemblage correlates with Lithofacies Six and Seven from the Tucker F3 and Low G1 cores. Each lithofacies assemblage exhibits distinguishing log characteristics, as shown on cross-section C–C' and on each individual core and wireline-log correlation (Table 4.1; figures 4.3–4.6; Appendix A, Figure C–C'). Because of the lateral variations and the shifting of lithologies and mineral compositions, wireline signatures differed slightly from well to well.

Responses of wireline logs to the marine lithofacies assemblage

The marine lithofacies assemblage reflects the lithological and physical properties that correspond to Lithofacies One, One-B, and One-C as defined in cores from the Tucker F3, Low G1, and Myers B2 (figures 4.3–4.5). The marine lithofacies assemblages are located stratigraphically both beneath the coarser-grained fluvial lithofacies (Lithofacies Two, Three, Four, and Five) and above the finer-grained estuarine facies (Lithofacies Six and Seven) as displayed in figures 4.3–4.5.

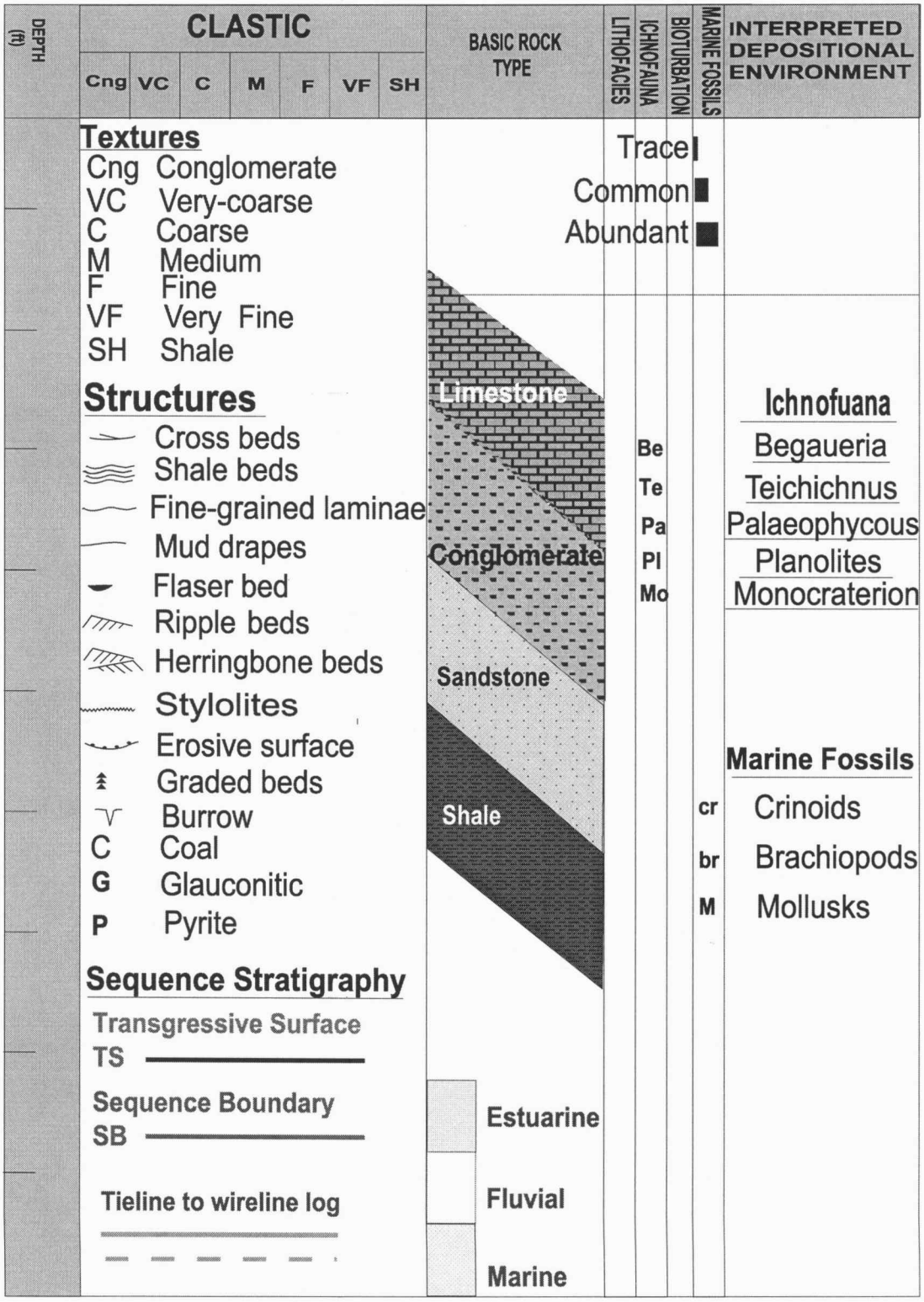

Figure 4.2 Legend for stratigraphic columns (figures 4.3-4.6) of cores tied to wireline logs.

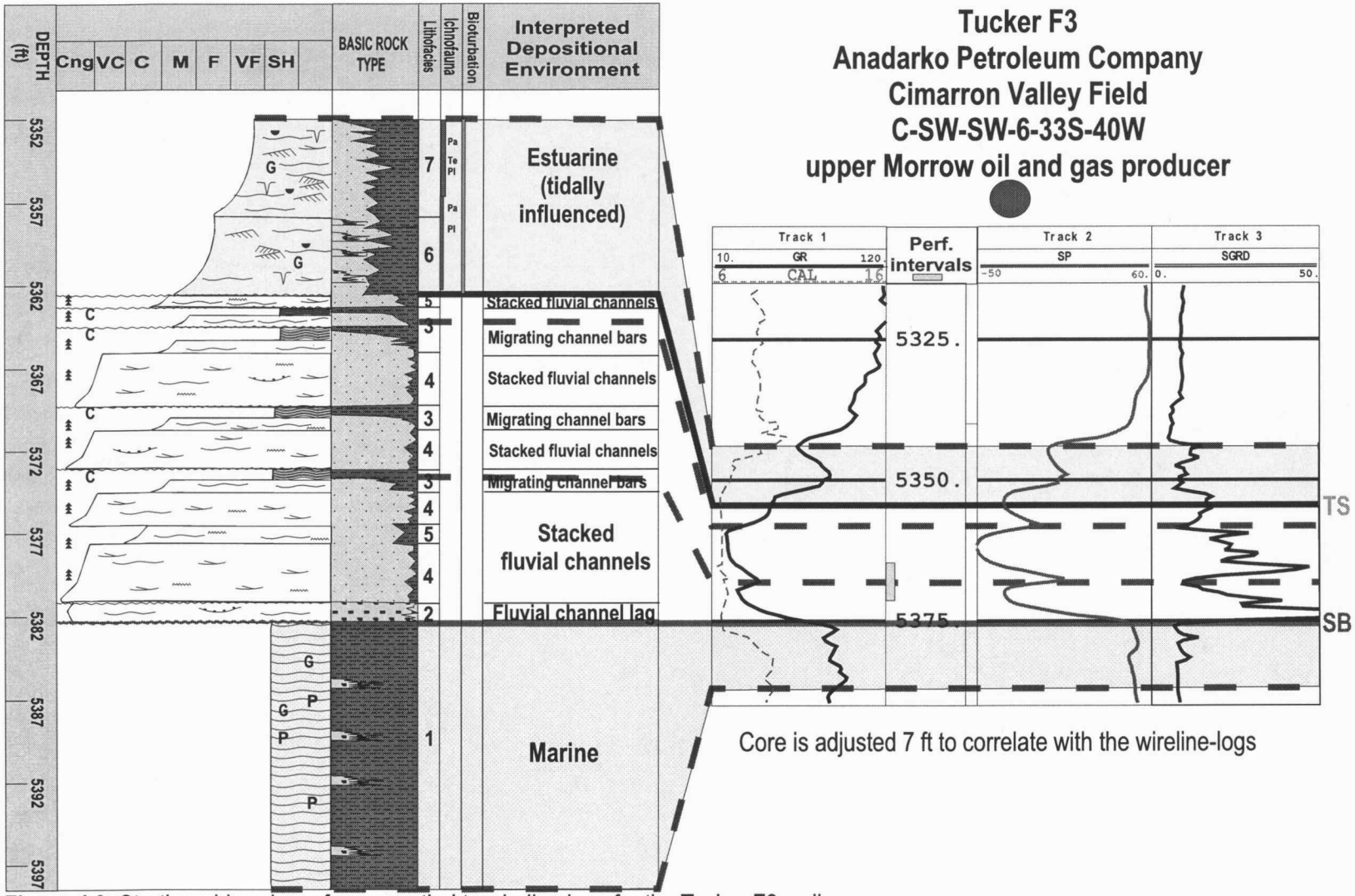

Figure 4.3 Stratigraphic column from core tied to wireline logs for the Tucker F3 well.

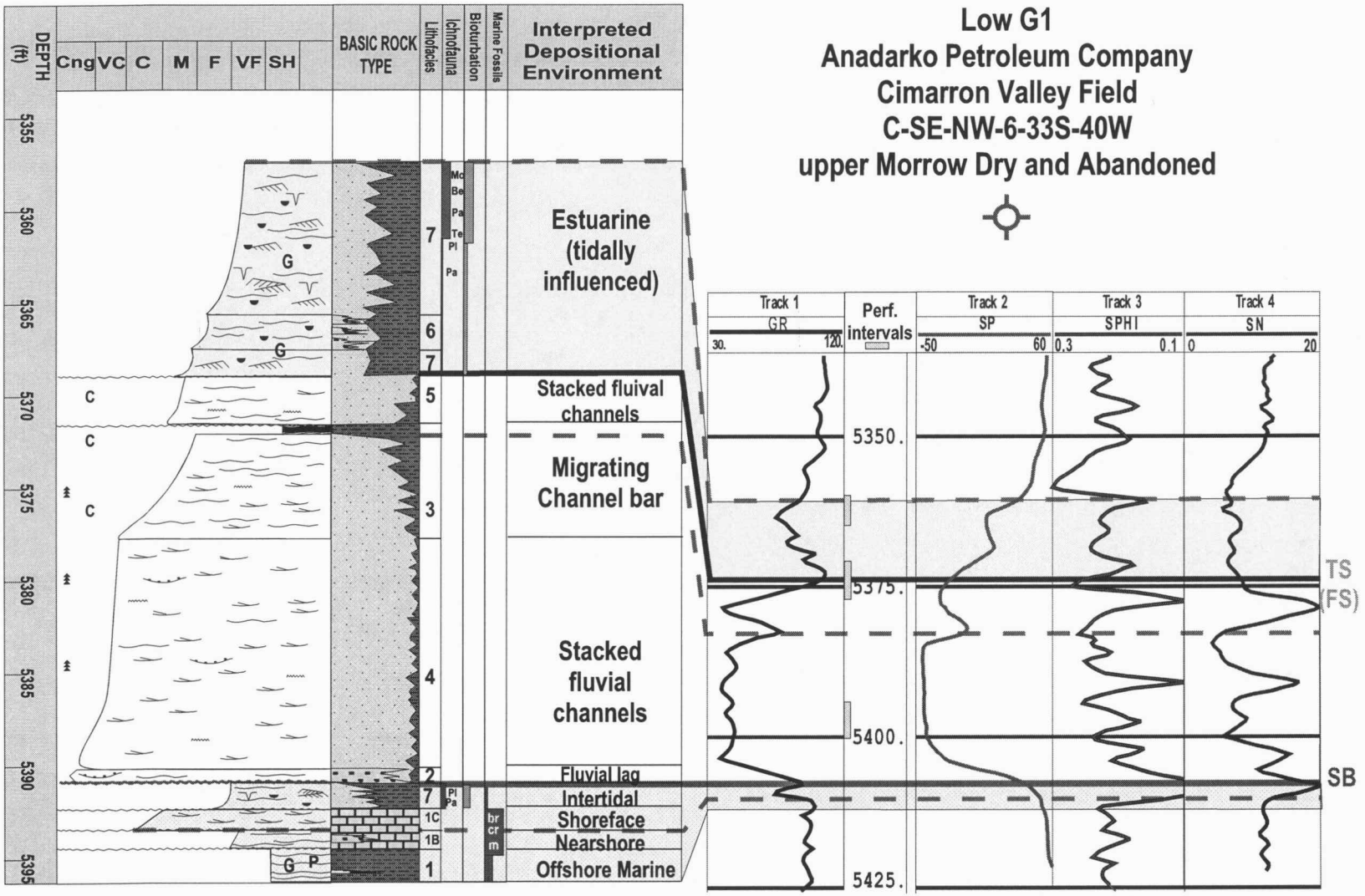

Figure 4.4 Stratigraphic column from core tied to wireline logs for the Low G1 well. Core is adjusted 16.4 ft to correlate with wireline logs.

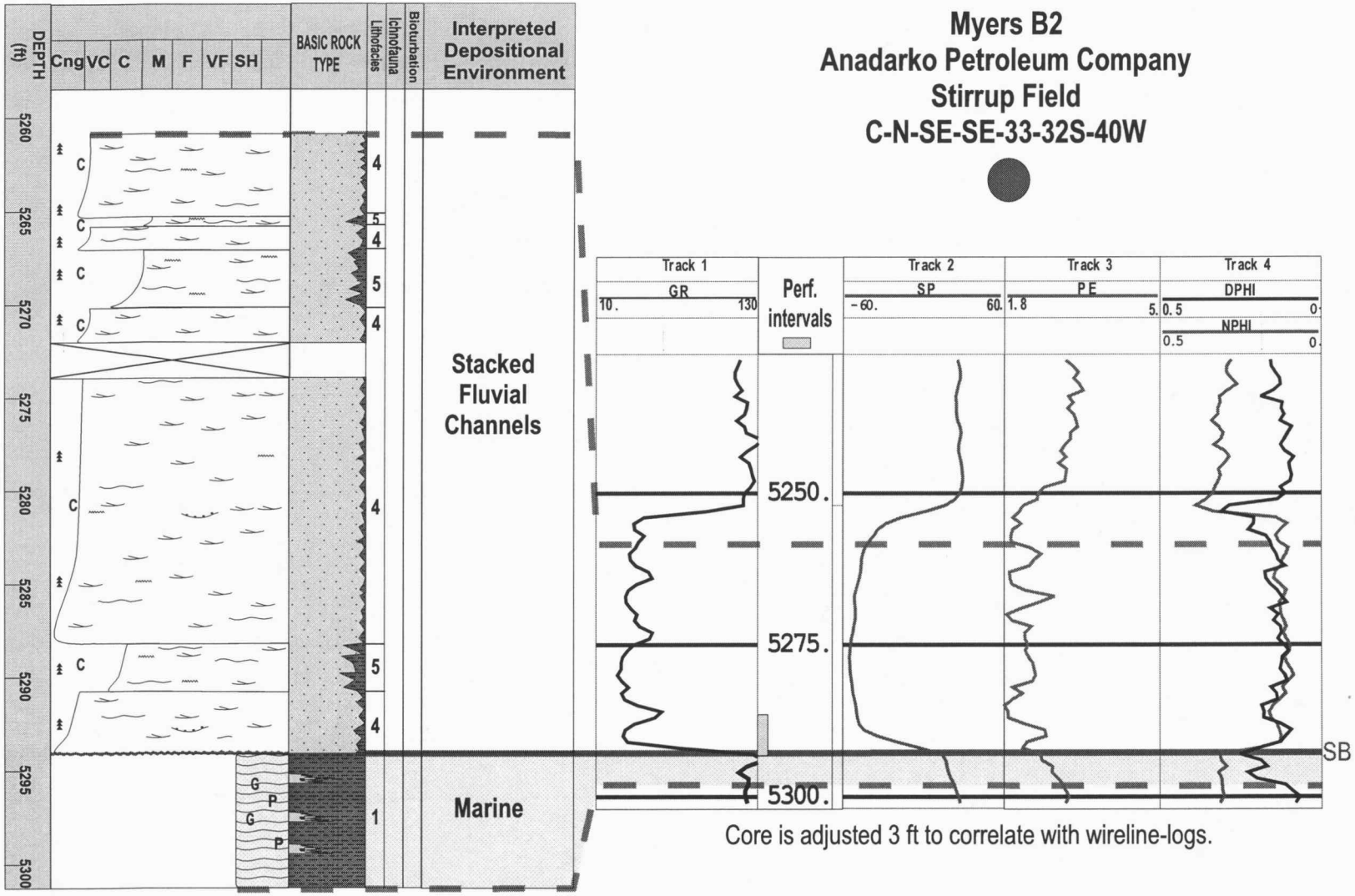

Figure 4.5 Stratigraphic column from core tied to wireline logs for the Myers B2 well.

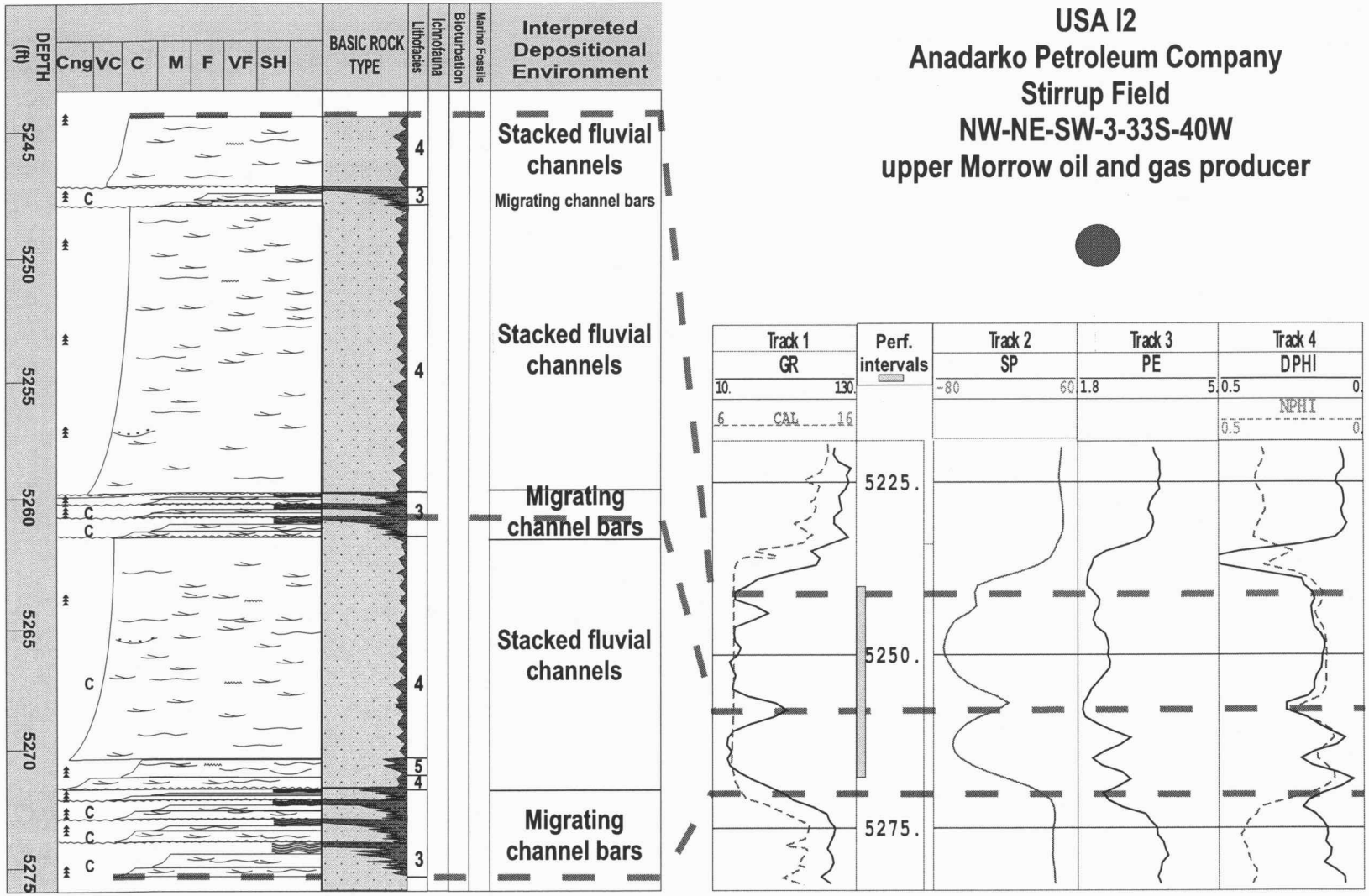

Figure 4.6 Stratigraphic column from core tied to wireline logs from the USA I2 well. Core is adjusted 6 ft to correlate with wireline logs.

Lithofacies One (marine shales and mudstones) has distinct responses on the wireline-log curves (Table 4.1). The neutron and density porosity curves (Nphi, Dphi) exhibit wide separation, with the Nphi deflecting far to the left of the Dphi curve (e.g., Myers B2, 5,294.3–5,300 ft; Figure 4.5). This wide separation suggests a shale lithology (Schlumberger, 1989). The PEF curve displays values that range from 3 to 3.3 B/E, which reflects an illite mineralogy that characterizes the black fissile shales and mudstones observed in core (e.g., Myers B2, 5,294.3–5,300 ft; Figure 4.5; Doveton, 1998). A representative log response to Lithofacies One is a washed-out caliper curve, which indicates a shale or mudstone lithology (e.g., Tucker F3, 5,375–5,390 ft; Figure 4.3).

The marine lithofacies assemblages have gamma-ray signatures (GR) that display high values (105–130 API), spontaneous potential logs (SP) that have positive values (+30–65 mV), bulk-density logs with moderately high values (2.45–2.6 g/cc), sonic logs with relatively high velocities (85–120 μs/ft), and resistivity curves (short-normal, shallow guard) that display relatively low values (3–7 ohm/m; figures 4.3–4.5). Lithofacies One-B and One-C (outer shelf and upper shoreface, respectively) produce a log response that has a sharp deflection to the left on the gamma ray (~75 API) and a sharp deflection to the right (~25 ohm/m) on the resistivity curves (e.g., Low G1, 5,392.1–5,394.5 ft; Figure 4.4).

Responses of wireline logs to the fluvial lithofacies assemblage

The fluvial lithofacies assemblage reflects the lithological characters of Lithofacies Two (channel lag), Three (migrating channel bars), Four (stacked fluvial bars), and Five (stacked fluvial bars), as defined from the Tucker F3, Low G1, Myers B2, and USA I2 cores (figures 4.3–4.6).

Wireline-log signatures that characterize the fluvial assemblage include the PEF curve, which displays values ranging from 1.8 to 2.4 B/E, reflecting the quartz-rich fluvial sandstone lithofacies with carbonate cement (Doveton, 1986, 1998). The Nphi and Dphi porosity curves occasionally overlie each other, with the density curve deflecting to the left of the neutron curve, suggesting quartz sandstone lithologies (e.g., USA I2, 5,244–5,272 ft; Figure 4.6; Schlumberger, 1989). The lack of separation between the Nphi and Dphi curves could be generated by the high amount of calcite and dolomite cement within the sandstones (Doveton, 1994). The bulk-density values for the fluvial assemblage were relatively low (2.4–2.55 g/cc) and indicate a sandstone lithology with a slight mud content (Doveton, 1998). Caliper logs exhibit mud or filter cake, indicating that the fluvial assemblages are porous and permeable (e.g., Tucker F3, 5,356–5,375 ft and USA I2, 5,244–5,272 ft; figures 4.3 and 4.6). As a unit, the fluvial assemblage has blocky gamma-ray shapes with low values that range from 25 to 40 API (e.g., Myers B2, 5,252–5,295 ft; Figure 4.5). The low gamma-ray values reflect the relatively clean sandstones with low mud content (Phillips Petroleum, 1989; Doveton, 1998). Sonic porosity values range from 65 to 80 μs/ft, suggesting a quartz-rich composition (Doveton, 1998).

The fluvial lithofacies assemblage has spontaneous potential curves that are bell to cylindrical in shape and have values that range from –30 to –65 mV (e.g., Low G1, 5,375–5,392 ft; Figure 4.4). Strata within Lithofacies Three display sharp fluctuations on the wireline logs, as shown in figures 4.3, 4.4, and 4.6. Thinly laminated, nonmarine mudstones that cap Lithofacies Three produce a sharp deflection to the right on both the gamma-ray (~45–65 API) and the SP (~0 mV) logs (e.g., USA I2, 5,260–5,262 ft; 5,272–5,275 ft; Figure 4.6). Lithofacies Five displays slight fluctuations to the right on the gamma ray (~45 API) due to an increased mud and silt content as compared with the cleaner sandstones of Lithofacies Four (e.g., Myers B2, 5,268.3–5,270.1 ft; Figure 4.5).

Responses of wireline logs to the estuarine lithofacies assemblage

Wireline-log responses of the estuarine lithofacies assemblage reflects lithological properties of Lithofacies Six and Seven, as observed in the Tucker F3 and Low G1 cores (figures 4.3 and 4.4). These lithofacies represent fine-grained deposits from a tidally influenced estuary. The estuarine assemblage exhibits an erosional contact or flooding surface (transgressive surface) in core. The flooding surface is represented by a sharp contrast in the wireline-log signatures as compared with the underlying fluvial lithofacies (e.g., Low G1 contact at 5,374 ft and Tucker F3 contact at 5,355 ft; figures 4.3 and 4.4).

Lithofacies Six and Seven have PEF values of 2.6 to 3 B/E, which suggests a mineralogy composed of quartz with an abundance of kaolinite and smectite clays

(Doveton, 1998). The caliper log exhibits mudcake buildup on the borehole walls, indicating that the sandstones of the estuarine assemblage are porous and have the ability to transmit fluids (e.g., Tucker F3, 5,345–5,355 ft; Figure 4.3). Egg to funnel-shaped, low-valued, spontaneous potential (0–-35 mV) curves are interpreted as representing a decrease in permeability and an increase in mud content within the estuarine lithofacies assemblage as compared with the fluvial lithofacies assemblage (e.g., Tucker F3, 5,340–5,350 ft; Figure 4.3). The neutron log falls to the left of the density log with an occasional overlap, reflecting a sandstone lithology with carbonate cement (Doveton, 1998). Moderately low resistivity (6–15 ohm-m) values from the shallow guard and short-normal logs characterize the fine-grained, high mud-content sandstones (e.g., Tucker F3, 5,345–5,355 ft; figures 4.3). Gamma-ray values of 60–80 API, bulk-density values of 2.4–2.45 g/cc, and interval transit velocities of 75–85 μs/ft reflect a notable mud and shale increase in the quartz-rich, estuarine sandstones as compared with the wireline responses of the underlying cleaner sandstones of the fluvial lithofacies assemblage (e.g., Low G1, 5,373–5,362 ft; Figure 4.4; Doveton, 1998).

CHAPTER FIVE

SEQUENCE STRATIGRAPHY AND DEPOSITIONAL MODEL

Introduction

This chapter examines the sequence stratigraphy and depositional environments within the upper Morrowan incised-valley fills that comprise the Santa Fe Trail, Cimarron Valley, and Stirrup fields of southwestern Kansas. Sequence-stratigraphic concepts were used to understand the lithologic successions that occurred in response to fluctuations of relative sea-level as well as sediment supply. Seven chronostratigraphic cross-sections were integrated with sedimentary structures (core), geologists' reports and logs, sandstone isopach maps, and wireline-log data to develop a sequence-stratigraphic framework and to construct a depositional model for the study area (Figure 5.1; Appendix A).

In the study area, the upper Morrowan successions are represented by two sequences, a lower and an upper sequence. Lithological (core) data, wireline logs (including lithological cyberlook logs [e.g., USA H-1]), and geologists' reports and logs (e.g., Lemon Trust 1-31, USA I2, Myers B2, and Government C2) were used for defining the lower sequence (Figure 5.1). However, only wireline-log data and geologists' reports and logs were available for the upper sequence. Seismic data were not available for this study. The study area experienced at least two major fluctuations in relative sea-level. The falls in sea-level resulted in subaerial exposure

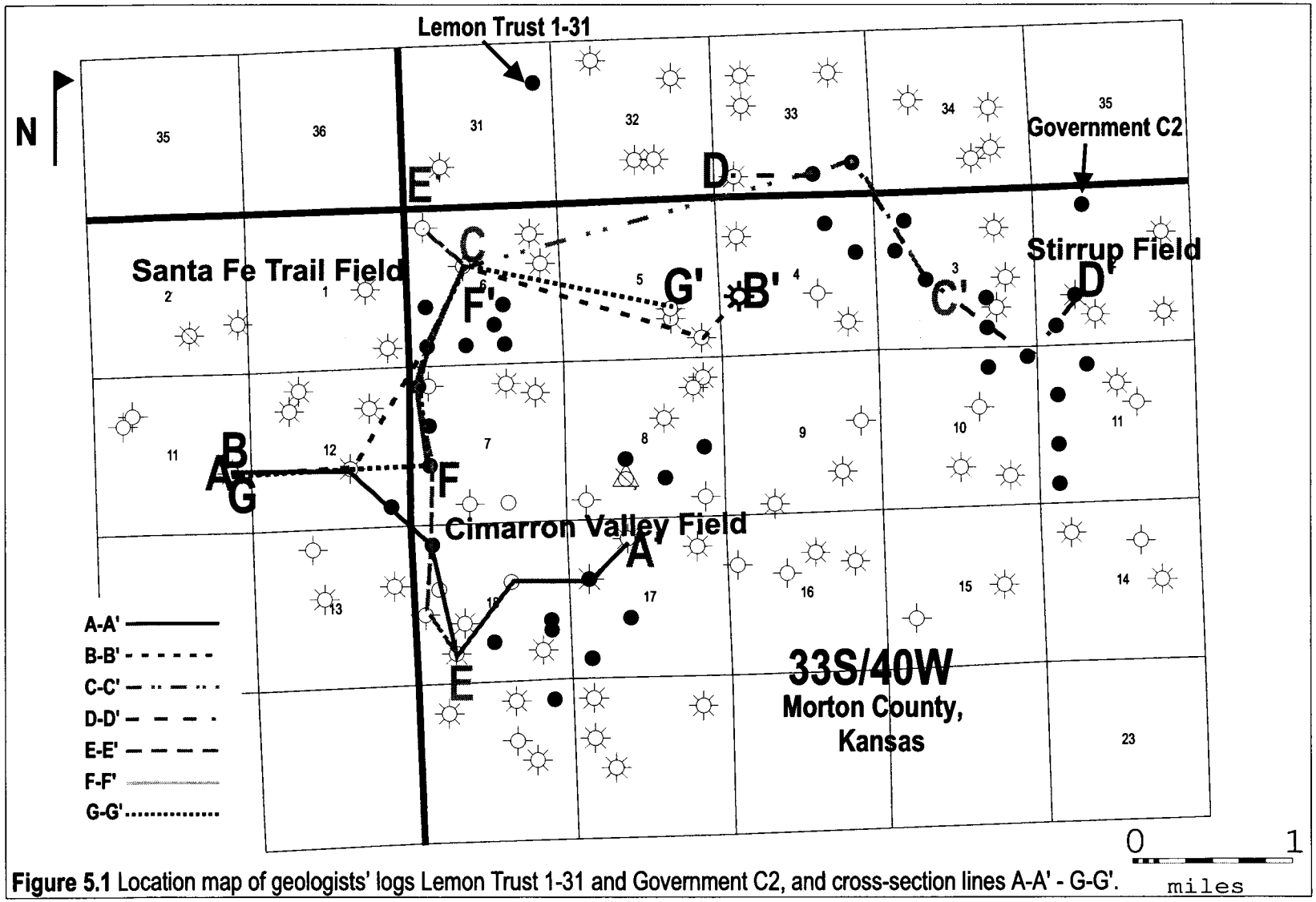

Figure 5.1 Location map of geologists' logs Lemon Trust 1-31 and Government C2, and cross-section lines A-A' - G-G'.

and incision of the shelf, whereas rises in sea-level resulted in the deposition of the upper Morrowan strata. The upper Morrowan successions are composed of two types of systems tracts: transgressive systems tracts (TST) and highstand systems tracts (HST). The TST is composed of fluvial and estuarine strata: the fluvial lithofacies (Lithofacies Two, Three, Four, and Five) are present throughout the entire study area, whereas the estuarine lithofacies (Lithofacies Six and Seven) are restricted to the western side. The HST consists of marine shales, mudstones, and limestones (Lithofacies One, One-B, and One-C). Systems tracts provide a high-degree of lithofacies predictability for reservoir evaluation.

Review of Sequence-Stratigraphic Concepts

Sequence-stratigraphic concepts were first developed in the mid-1970's by Exxon Production Research Company as a tool to aid in the regional interpretation of seismic data (Vail et al., 1977; 1981; 1984). Recent applications using sequence-stratigraphic concepts combine core descriptions, seismic sections, and wireline logs to interpret relatively small-size oil and gas fields (Stockholm Southwest Field, Colorado [Brown et al., 1990], Sorrento and Mt. Pearl fields, Colorado [Wheeler et al., 1990]).

Sequence stratigraphy is the study of genetically related facies within a framework of chronostratigraphically significant surfaces (Van Wagoner et al., 1987; 1988). The sequence is the main component of sequence stratigraphy and has been defined by Mitchum et al. (1977) as a stratigraphic unit composed of a relatively

conformable succession of genetically related strata bounded at its top and base by unconformities or their correlative conformities. A sequence is composed of systems tracts that are defined by key surfaces, including sequence boundary (SB), transgressive surface of erosion (TSE), maximum flooding surface (MFS), and transgressive surface (TS) or flooding surface (FS).

The sequence boundary is a surface that resulted from a significant fall in sea-level and separates younger (generally shallower-water) strata from older (generally deeper-water) strata (Mitchum et al., 1977; Van Wagoner et al., 1988; Emery and Myers, 1996). Sequence boundaries can be identified by a laterally continuous and correlative subaerial exposure (e.g., paleosols or the *Glossifungites* ichnofacies); a basinward shift in lithofacies, an onlapping relationship with older strata; or a vertical change in parasequence stacking patterns (Vail et al., 1977; 1984; Van Wagoner et al., 1987; 1988).

The downdip correlative conformity of a subaerial sequence boundary is a transgressive surface of erosion. A TSE, the shoreface unconformity surface, is a scour surface cut by wave action on the shoreface during transgression (Embry and Podruski, 1988). The TSE generally erodes basal nonmarine to brackish (estuarine) water deposits, as well as the subaerial unconformity, and forms the sequence boundary (Emery and Myers, 1996). The TSE is referred to as the ravinement surface and is generally recognized in core by transgressive lag deposits (pebbles or fossil fragments), hardgrounds (*Glossifungites* ichnofacies), glauconitic siltstones, or other erosive strata (Embry and Podruski, 1988).

The converse of a sequence boundary is the maximum flooding surface (MFS). The MFS is the result of an abrupt increase in water depth and separates older, shallow-water successions from younger, deeper-water successions (Van Wagoner et al., 1988; Emery and Myers, 1996). The MFS represents the time of maximum flooding and records a slow period of sedimentation within a stratal unit called a condensed section (Posamentier and James, 1993). The MFS is characteristically easy to identify because the condensed section occurs as highly radioactive shales on wireline logs (gamma-ray and resistivity), as organic-rich shales in core, and as downlap surfaces on seismic data (Posamentier and James, 1993). The MFS is laterally continuous and separates the transgressive systems tract from the highstand system tract (Vail et al., 1977; 1984; Van Wagoner, 1988; Zaitlin et al., 1994).

Cores and wireline logs can be used to subdivide sequences into stratal patterns based on position relative to key surfaces (SB, TSE, and MFS) and internal geometries (Emery and Myers, 1996). The stratal patterns, called systems tracts, include Lowstand Systems Tract (LST), TST, and HST. Systems tracts are controlled by fluctuations in relative sea-level and sediment supply. The LST occurs during a relative sea-level fall and is represented by a sequence boundary on the shelf (Zaitlin et al, 1994). The TST, a retrogradational systems tract, is deposited during a relative rise in sea-level when the rate of accommodation increases faster than the rate of sediment supply (Dalrymple et al., 1992; Zaitlin et al., 1994; Emery and Myers, 1996). The HST is established when the rate of accommodation development on the

shelf decreases to less than the sediment supply (Posamentier and James, 1993). The HST is characterized by a decelerating rate of relative sea-level rise through time, resulting in an initial aggradational and later progradational architecture (Zaitlin et al., 1994; Emery and Myers, 1996). Systems tracts represent fundamental mapping units as they contain a predictable set of depositional systems with a consistent paleogeography (Emery and Myers, 1996).

Review of an Incised Valley and Estuary

Incised Valley

Incised valleys are entrenched fluvial systems that have extended their valleys landward by headward migration and basinward by erosion of the underlying strata as a response to a relative fall in sea-level (Figure 5.2; Van Wagoner et al., 1988; Bowen et al., 1993). Depending on the coastal gradient and the magnitude and duration of a relative sea-level fall, incised valleys assume many paleotopographic geometries (Wood et al., 1993; Zaitlin et al., 1994; Emery and Myers, 1996). Incised valleys are commonly characterized by the following:

(a) Incised valleys are generally perpendicular to the coastlines and increase in width and depth down the valley.
(b) Incised valleys are larger and deeper than individual channels.
(c) Sequence boundaries have valley-like shapes.
(d) The bases and walls of the incised valleys are bounded by sequence boundaries that are correlated laterally to subaerial erosional surfaces (e.g., paleosols, hardgrounds).

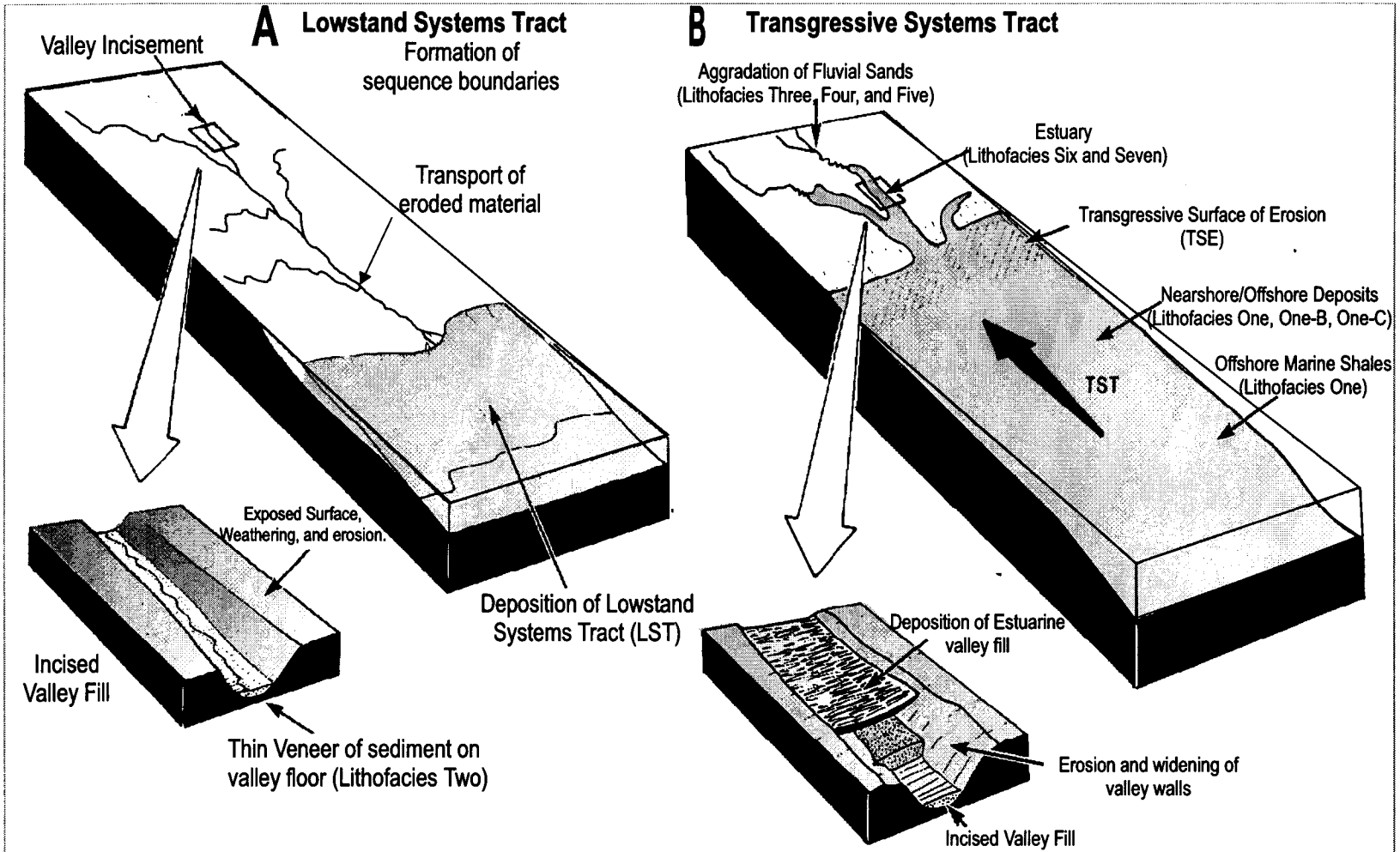

Figure 5.2 Schematic block diagram illustrating the evolution of the valley-fill deposits in terms of sequence stratigraphy. **(A)** sea-level fall (Lowstand Systems Tract [LST]) and **(B)** sea-level rise (Transgressive Systems Tract [TST]; modified from Wheeler et al., 1990).

(e) The fill of an incised valley displays a basinward shift in lithofacies and has an onlap relationship with the valley walls.

Incised-valley fills are interpreted to be the result of a relative rise in sea-level (transgression), and an increase in accommodation space (Van Wagoner et al., 1988; Sonnenberg et al., 1990; Dalrymple et al., 1992; Zaitlin et al., 1994; Al-Shaieb et al., 1995; Emery and Myers, 1996). With a relative rise in sea-level, an incised valley develops into a sediment trap (Zaitlin et al., 1994; Figure 5.2A). Sediment is supplied by two main sources: from the sea by waves, tides, storms, and longshore currents and from the land by rivers. An incised valley may be filled completely or partially with fluvial, estuarine, and marine sands and muds due to the variances in marine and fluvial processes, and the fluctuations in sediment supplies (Viking Formation, Canada; Krystinik and Blakeney, 1990; Blakeney et al., 1990; Allen and Posamentier, 1993; Alissa, 1999).

Van Wagoner et al. (1988) classified incised valleys as Type I unconformities representing incision into the shelf below the depositional shoreline break. Zaitlin et al. (1994) classified incised valleys into simple and compound valleys. Simple incised valleys are relatively small valleys that are commonly found in low-gradient coastal plain settings and are filled by one sequence during a continual sea-level rise. Compound incised valleys are commonly found in steeper gradient (piedmont) settings and consist of complex fills composed of numerous sequences that were deposited during multiple fluctuations of relative sea-level (Figure 5.3).

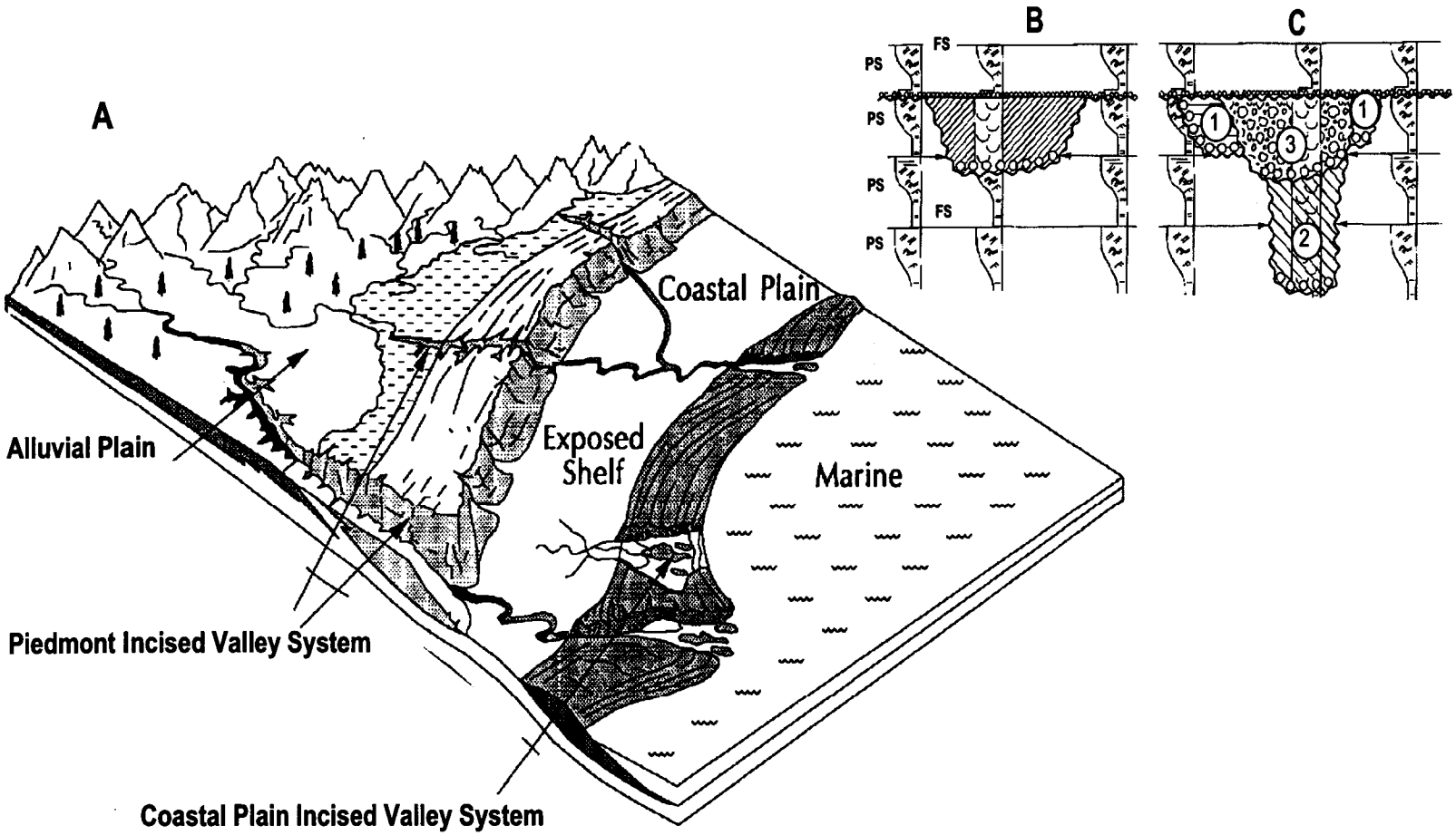

Figure 5.3 Schematic diagrams illustrating **(A)** the distinction between piedmont and coastal-plain incised valley systems, **(B)** simple and **(C)** compound incised-valley systems. Numbers 1-3 refer to successive episodes of erosion and deposition within the incised valley. PS = parasequence; FS = flooding surface (modified from Zaitlin et al.,1994).

Estuary

An estuary is defined as the seaward portion of a drowned river valley that receives sediments from both fluvial and marine sources and contains lithofacies that are influenced by tide, wave, and fluvial processes (Dalrymple et al., 1992). Estuarine environments are identified by fluctuations in salinity and current energy (tide or wave energy); sedimentary structures with wave or tidal influences; an increase in accommodation space; and a landward transgression of marine lithofacies. As the transgression continues there is a change from stressful to less stressful marine conditions and an increase of *in situ* bioclasts, bioturbation, and ichnofauna size, abundance, and diversity (Reinson, 1992). Fluctuations in current energy within an estuary result in a mixture of salinities from marine to brackish to fresh. Fluctuations in current energy are recognized by alternating intervals containing siderite and glauconite; shifting between high- and low-energy sedimentary structures (cross-bedding to ripple marks and mud drapes); bi-directional cross-bedding (herringbone cross-stratification); mud alternating with sand (heterolithic bedding); bioturbated and non-bioturbated intervals; high-energy ichnofauna (*Skolithos*) alternating with lower-energy ichnofauna (*Cruziana*); and reactivation surfaces (Reinson et al., 1988; Dalrymple et al., 1992; Reinson, 1992; Alissa, 1999).

An estuarine system can be composed of many types of environments, including shoreface; tidal channel complexes; tidal flats; lagoons and lakes; barrier islands; and swamps and marshes. Estuaries are classified as tide- or wave-dominated and influenced by sediment supply, energy level, and relative dominance

of fluvial and marine processes (Reinson et al., 1988; Dalrymple et al., 1992; Zaitlin et al., 1994). Wave-dominated estuaries are controlled by waves and longshore currents, and are associated with barrier islands that protect the estuary. As a result, wave-dominated estuaries are characterized by a tripartite division of sediments consisting of landward, high-energy fluvial sandstones; low-energy lagoonal muds; and seaward, high-energy marine sandstones (Figure 5.4; Dalrymple et al., 1992).

Tide-dominated estuaries are found in meso- (2–4 m) to macrotidal (4–6+ m) environments in which the controlling force is the tidal range. Tidal currents can carry onshore and shoreface sands landward into the estuary as far as 130 km from the estuary mouth (e.g., Holocene Gironde estuary, France; Allen, 1992). A tidal-dominated estuary shows a gradual transition (seaward to landward) from coarse-grained tidal bars, to intertidal fluvial mud flats with an abundance of tidally influenced structures, to coarse-grained fluvial sediments (Figure 5.5; Dalrymple et al., 1992; Zaitlin et al., 1994). The dominance of tidal currents blocks coarse fluvial sands and gravels from entering the estuary, whereas medium- and fine-grained fluvial sediments are introduced into the estuary and reworked (Allen, 1992; Dalrymple et al., 1992).

Chronostratigraphic Correlations

A chronostratigraphic cross-section is a correlation of time-related units rather than lithological units (Lemon, 1990). Maximum flooding surfaces are commonly used as the datum in a chronostratigraphic cross-section. The cross-sections for the study area used either MFS#2 or MFS#3 as the datum (Appendix A). MFS#2 and

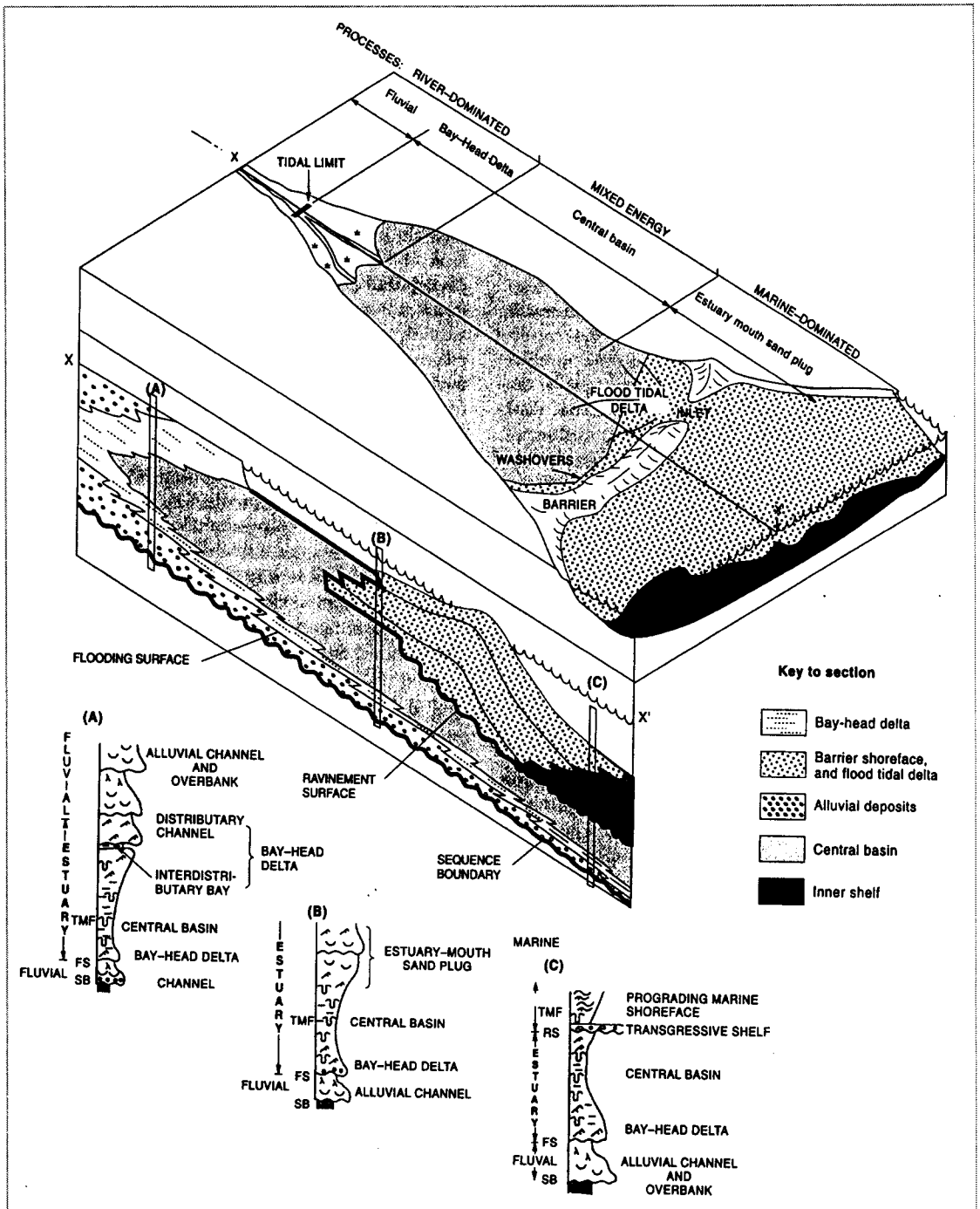

Figure 5.4 Schematic block diagram illustrating wave-dominated estuary (modified from Zaitlin et al., 1994).

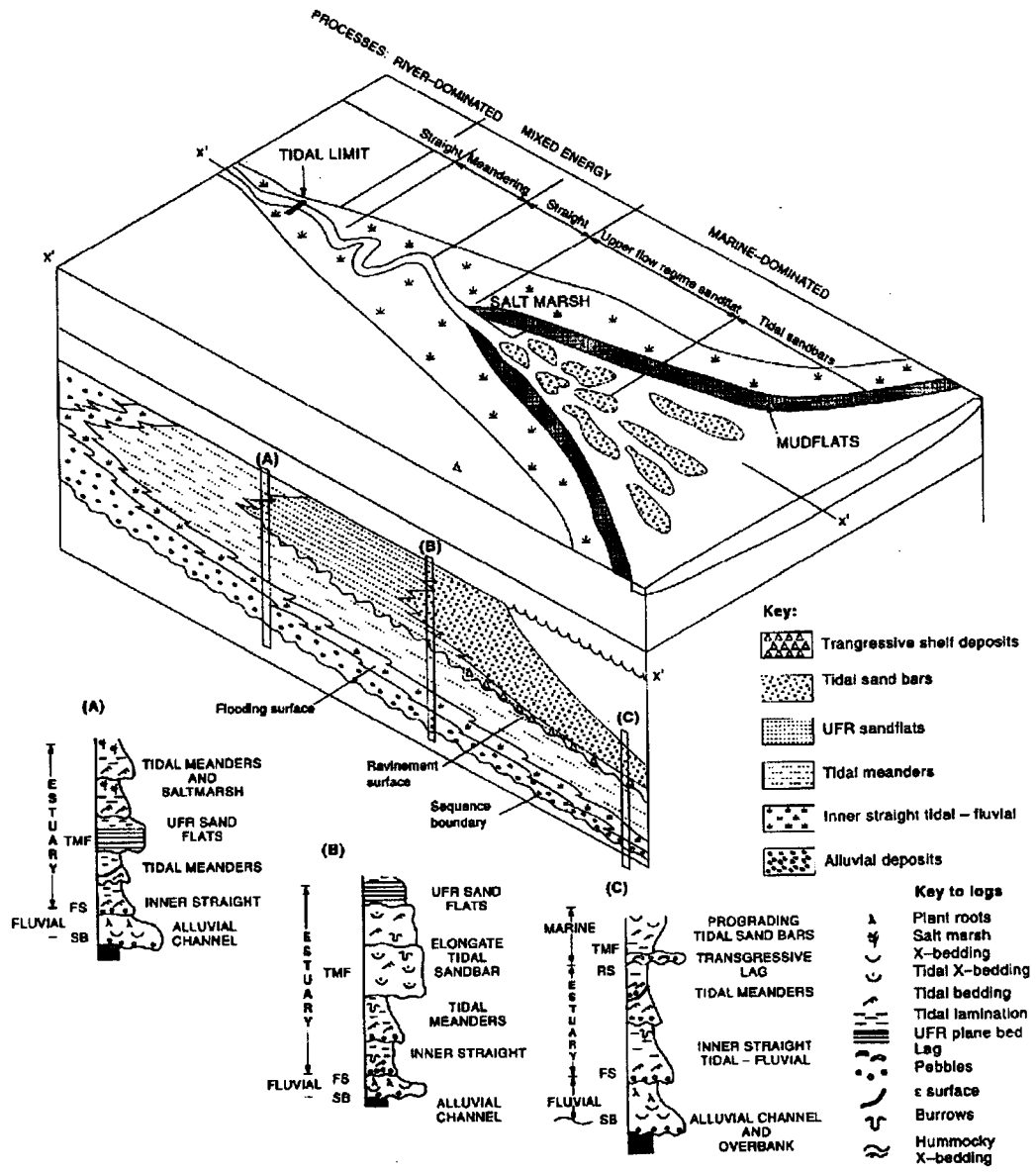

Figure 5.5 Schematic block diagram illustrating tide-dominated estuary (modified from Zaitlin et al., 1994).

MFS#3 are defined by sharp deflections and relatively high values (~115 API) on the gamma-ray logs, abrupt wide separation of the neutron and density porosity curves, low spontaneous potential log values, and low values on the resistivity logs. Seven chronostratigraphic cross-sections were constructed (Figure 5.1; Appendix A). Three MFS, two SB, and one TSE were recognized (Appendix A). The upper Morrowan strata were divided into two sequences, lower and upper. The sequences represent incised-valley fills.

The top of the lower Morrow strata was determined from scout tickets, completion reports, Low A5 core study (Rader, 1987), and Barrel Springs Field study, Colorado (Von Drehle, 1990). Maximum flooding surface #1 (MFS#1) is located above the top of the lower Morrow strata and below sequence boundary #1 (SB#1); (Appendix A). MFS#1 was traced laterally across the study area and separates more porous, limey sandstones from overlying marine shales and mudstones.

The lower sequence is bounded by sequence boundaries #1 and #2 (SB#1 and SB#2). Both sequence boundaries are laterally correlative, have valley-like shapes, and are incised into deep-water shales and mudstones of Lithofacies One (figures 3.2C, 3.2D, 4.3, and 4.4) and into nearshore to intertidal wackestones and packstones of Lithofacies One-B and One-C (Figure 4.4). Upper Morrowan strata have an onlap relationship with SB#1 and SB#2. SB#1 was observed in three cores (Tucker F3, Low G1, and Myers B2); however, SB#2 was not observed in core. In the cores, the lithofacies above and below SB#1 show a landward shift from marine shales,

mudstones, and limestones (Lithofacies One, One-B, and One-C) into fluvial sandstones (Lithofacies Two, Three, Four, and Five; figures 3.2C and 3.2D).

Within the incised valleys, sequence boundary #1 (SB#1) is overlain by fluvial and estuarine lithofacies assemblages (Lithofacies Two–Seven) representing a TST. Cross-section C-C' ties the four cored intervals and shows that the estuarine lithofacies assemblage is restricted to the western side of the study area (Appendix A). The fluvial lithofacies assemblage is separated from the overlying estuarine lithofacies assemblage by a TS (Appendix A, Figure C-C'). In the cross-sections, the TS is placed where there is a gradual increase in the shale indicator curves (gamma-ray, spontaneous potential, Nphi/Dphi, and resistivity; Table 4.1). The TST is bounded by a maximum flooding surface (MFS#2). MFS#2 immediately overlies SB#1 where the transgressive systems tract is very thin or absent at the valley walls and interfluve areas (Appendix A, figures A-A' and B-B'). The MFS#2 represents the termination of the TST and separates the TST from the subsequent HST as indicated by wireline-log responses. The HST is composed of marine shales, mudstones, and limestones assigned to Lithofacies One, One-B, and One-C (Table 4.1).

The geologists' log from the Lemon Trust 1-31 well (Figure 5.1), reports a 12 ft (3.64 m) interval containing upper Morrowan, fine- to medium-grained, subrounded to angular, slightly glauconitic sandstones that lie abruptly over the marine shales of the HST. The sandstones are restricted to the western side of the study area, have hydrocarbon production, and are recognized in wireline logs, scout tickets, and completion reports. The surface that separates the sandstones from the

underlying marine lithofacies is interpreted as sequence boundary #2 (SB#2). MFS#3 is the datum for cross-section G-G' which displays SB#2 having a valley-like shape (Appendix A). The sandstones located above the SB#2 are interpreted as TST deposits (Appendix A, Figure G-G'). The TST deposits of the upper sequence have similar wireline-log responses as the marine-influenced estuarine sandstones of the lower sequence (Table 4.1, Appendix A). Maximum flooding surface #3 (MFS#3) is located above SB#2 and is laterally correlated using gamma-ray and resistivity curves. MFS#3 immediately overlies SB#2 where the transgressive systems tract is very thin or absent at the valley walls and interfluve areas (Appendix A). The MFS#3 represents the termination of the TST of the upper sequence and separates the TST from the subsequent HST.

The geologists' log from the Lemon Trust 1-31 well (Figure 5.1) records a 4-ft interval of gray, fine-grained sandstone with scattered glauconite and pyrite that fines upward into a 10-ft interval of fossiliferous siltstone. The sandstones lie abruptly above the deep-water shales and mudstones of the underlying HST of the upper sequence (Appendix A). The surface that separates the fining-upward interval from the HST strata is interpreted as a TSE and represents the top boundary of the upper sequence. The TSE is correlatable across the study areas with sharp gamma-ray deflections, low resistivity values, and overlapping Nphi and Dphi curves (Appendix A).

Depositional Model for the Santa Fe Trail, Cimarron Valley, and Stirrup fields

The depositional model for the Santa Fe Trail, Cimarron Valley, and Stirrup fields is based on the integration of physical and biogenic sedimentary structures that were observed in cores, chronostratigraphic correlations, and upper Morrowan sandstone isopach maps (figures 5.6, 5.7, 5.8; Appendix A). Upper Morrowan strata within the study area consist of two sequences that were deposited within two incised valleys. The incisions occurred as a result of at least two major relative sea-level falls followed by subsequent sea-level rises. The upper Morrowan incised valleys of the Santa Fe Trail, Cimarron Valley, and Stirrup fields are each filled with one sequence, therefore, the incised valleys are classified as simple (Zaitlin et al., 1994). This interpretation is consistent with the low gradient of the Hugoton Embayment shelf and with the degree of maturity of the valley fill (Krystinik and Blakeney, 1990; Al-Shaieb et al., 1995).

The observed sequence boundaries (SB#1 and SB#2) at the base of each sequence have valley-like shapes; are incised into marine shales, mudstones, and limestones (Lithofacies One, One-B, and One-C); and show a landward shift in lithofacies. SB#1 demonstrates a landward shift from deep marine lithofacies (Lithofacies One, One-B, and One-C) into fluvial lithofacies (Lithofacies Two–Five; figures 4.3 and 4.4). The landward shift in lithofacies indicates a relative fall in sea-level and exposure of the shelf (figures 5.6A and B) during the upper Morrowan. The upper Morrowan sequence boundaries are classified as Type I unconformities by Van Wagoner et al. (1988) since the first topsets within the sequence have an onlap

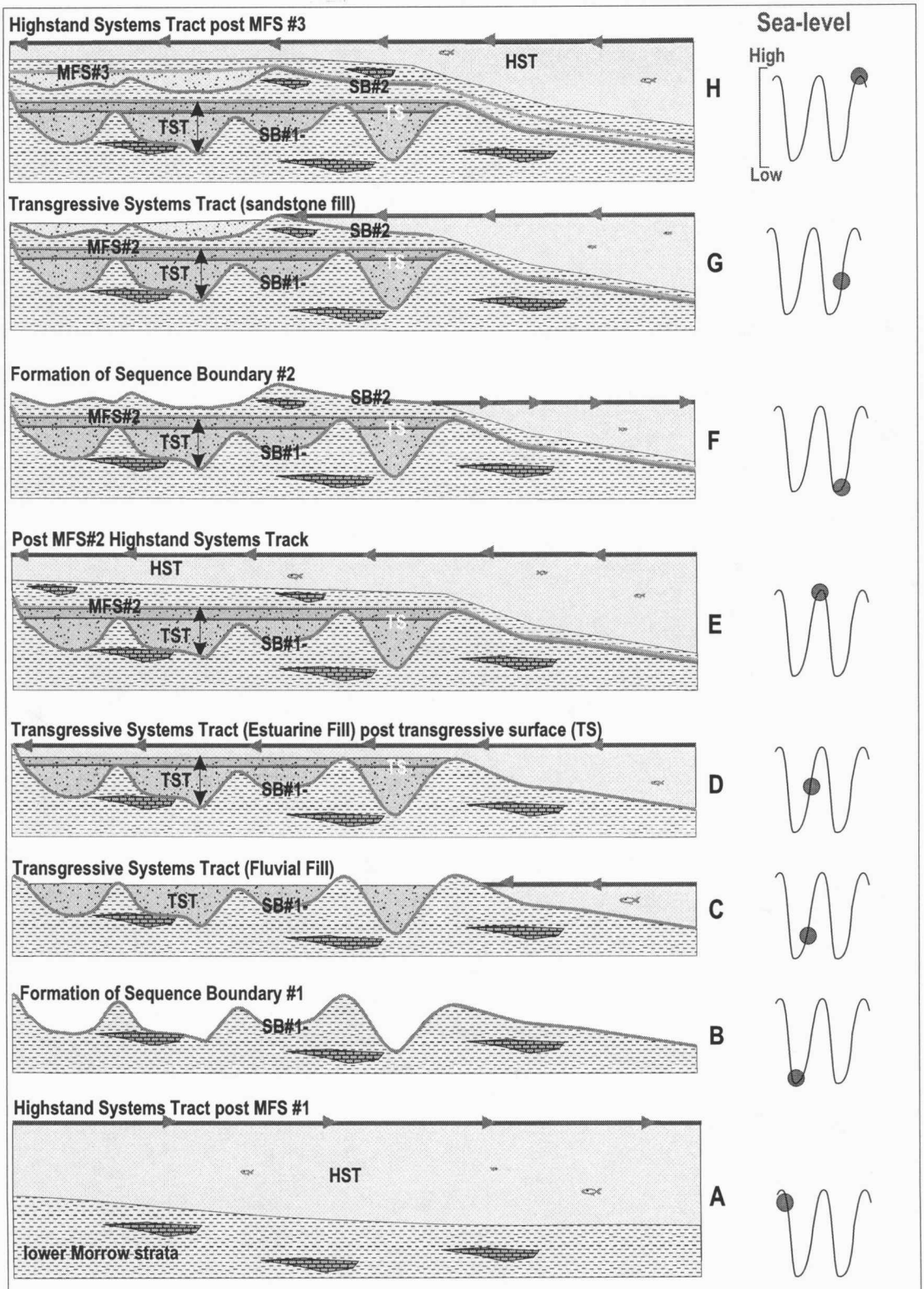

Figure 5.6 Evolution of upper Morrowan successions in study area.

relationship with the underlying older strata (Appendix A). During the relative fall in sea-level, the Hugoton Embayment became a bypass margin that was incised by paleochannels that flowed in a predominantly northwest to southeast direction. Figure 5.7 documents the trend of the paleochannels with an upper Morrowan gross sandstone (fluvial and esturaine) isopach map that has an overall northwest–southeast trend that bifurcates down-dip towards the south and the southeast. The estuarine sandstones (Lithofacies Six and Seven) are confined to the western side of the study area and trend south and southeast (Figure 5.8).

With a rise in sea-level, the Hugoton Embayment became a sediment trap that resulted in the deposition of the fluvial lithofacies assemblage (Figure 5.6C). Subsequent rises in sea-level resulted in a landward shift of source areas and the deposition of marine-influenced estuarine successions (Figure 5.6D). The marine intrusion into the study area is documented in core by the fluvial lithofacies having a sharp erosional contact (TS) with the overlying tidally influenced estuary deposits (figures 4.3 and 4.4; Appendix A, Figure C-C'). In core, a transition from fluvial conditions (lack of ichnofauna) to stressful estuarine conditions to more open marine conditions (high diversity in ichnofauna, mud drapes, and herringbone cross-stratification) records a gradual increase in accommodation space. The upper Morrowan successions (fluvial and estuarine lithofacies assemblages) are confined within the valley walls and have an onlap relationship with the underlying sequence boundaries (SB#1 and SB#2; figures 5.6C and D; Appendix A). The upper Morrow

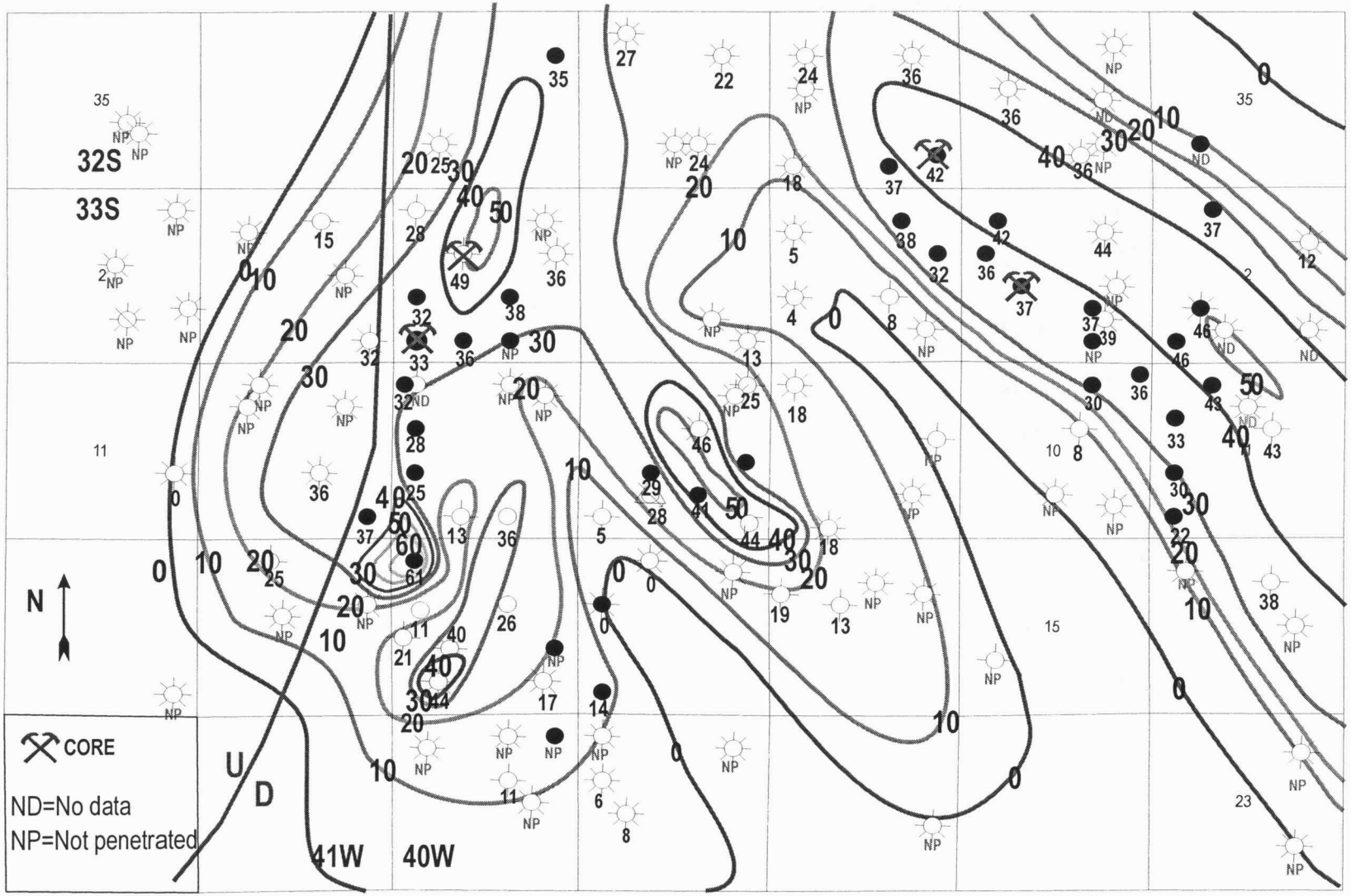

Figure 5.7 Gross isopach map of upper Morrowan sandstones (fluvial and estuarine lithofacies). Contour interval 10 ft

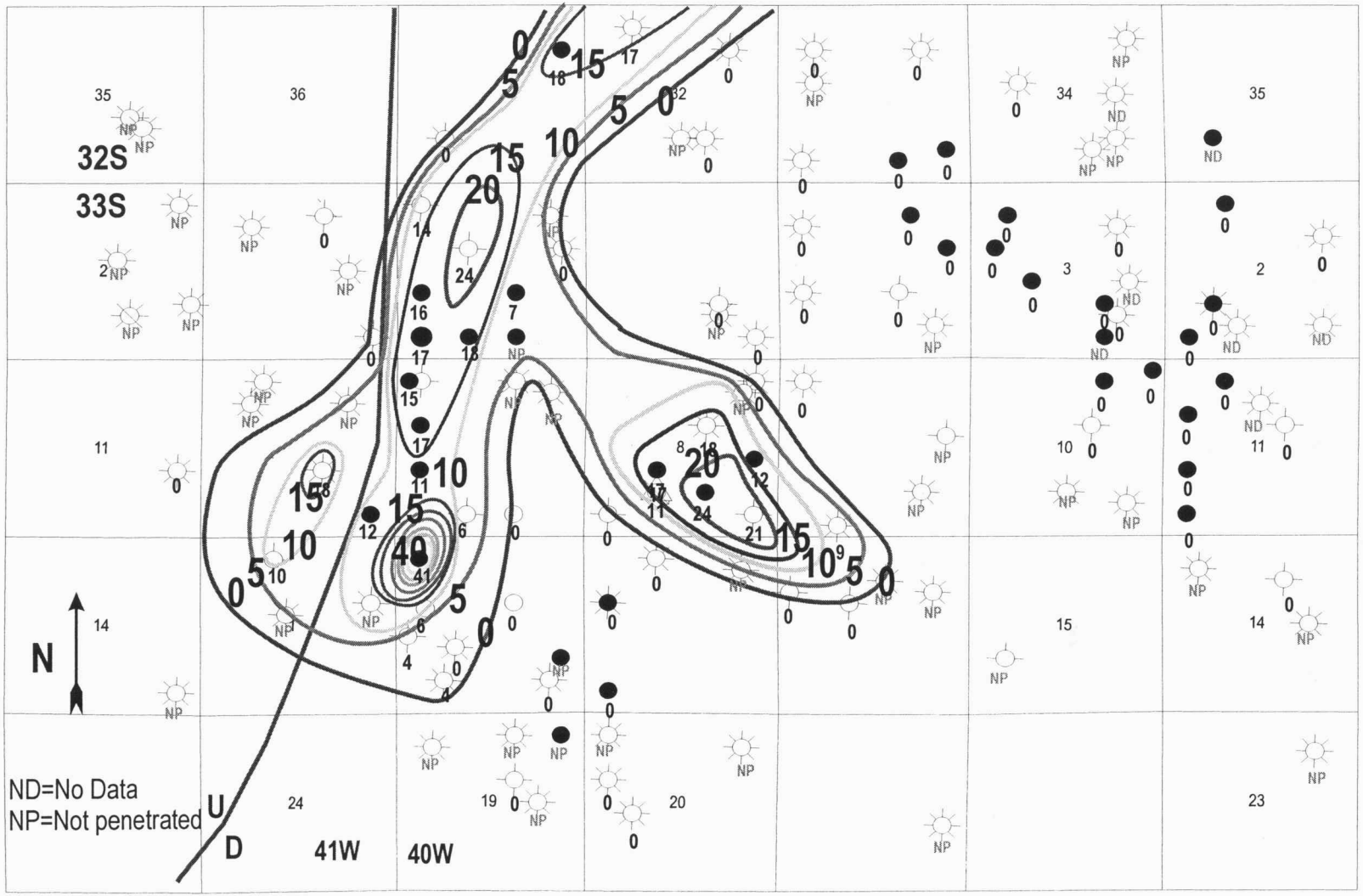

Figure 5.8 Upper Morrowan estuarine sandstone (Lithofacies Six and Seven) isopach map. contour interval 5 ft

deposits within the incised valleys represent the transgressive systems tracts (Figure 5.6; Appendix A, figures A-A' and G-G').

As the sea-level continued to rise, the siliciclastic source areas shifted further landward and the entire study area was completely covered by the sea (figures 5.6E and H). The marine intrusion into the study area signifies the termination of the TST and the initiation of the HST. The HST is separated from the underlying TST by a maximum flooding surface (MFS#2 and MFS#3; figures 5.6E–H; Appendix A). The HST consists predominantly of marine shales, mudstones, and limestones (Lithofacies One, One-B, and One-C; figures 3.2–3.4). The MFS coincides with the SB at the valley walls and the interfluves (figures 5.6E and F; Dalrymple et al., 1992; Zaitlin et al., 1994; Emery and Myers, 1996).

Sequence-stratigraphic concepts emphasize the importance of eustatic and relative sea-level fluctuations as well as tectonics and subsidence as the major controls on the sedimentary style in the nearshore environment (Reinson, 1992). The chronostratigraphic correlations and the upper Morrowan sandstone isopach maps demonstrate that the fluvial lithofacies assemblage are present across the study area, however, the estuarine lithofacies assemblage are restricted to the western side of the study area (figures 5.7 and 5.8; Appendix A). The restriction of the estuarine strata suggests that active river mouths were present exclusively in the western side of the study area during the deposition of the estuarine lithofacies. The observations from the cross-sections and the isopach maps led to the hypothesis that the deposition of upper Morrowan strata was not controlled only by glacial eustacy, but also by local

(e.g., fault reactivation) and regional (e.g., continental collision) tectonics. Local depositional effects due to the reactivation of the fault located on the western margin of the study area are shown by:

(a) The valley-like shape of SB#2 being developed and filled exclusively in the western side of the study area.

(b) The estuarine strata being restricted to the western side of the study area and parallel to the fault.

(c) The thickest sandstone accumulations occurring along the down-thrown side of the fault (figures 2.5, 5.7, and 5.8; Appendix A).

Lack of available seismic data made it difficult to map fault segments and to accurately document the magnitude and the timing of fault reactivation.

CHAPTER SIX

RESERVOIR CHARACTERIZATION

Introduction

The upper Morrowan sandstones of Cimarron Valley, Santa Fe Trail, and Stirrup fields are prominent oil and gas reservoirs (Gerhard et al., 1999; Figure 6.1). Within these fields, 45 wells produce hydrocarbons from the fluvial and estuarine lithofacies of the upper Morrowan reservoirs (Appendix B). The fluvial lithofacies assemblage has higher production rates and more lateral continuity compared with the estuarine lithofacies assemblage of the reservoirs (figures 5.7, 5.8, and 6.1). The fluvial and estuarine sandbodies are incised into and overlain by the offshore marine mudstones and shales of Lithofacies One, which serve as both lateral and vertical seals for the reservoirs (Bowen et al., 1993; Appendix A, Figure B-B').

The observed performance of upper Morrowan reservoirs in the fields studied are closely related to their depositional lithofacies and detrital composition. Five types of sandstones found within the incised valley fill are identified as potential reservoirs:

(a) fine- to coarse-grained sandstones (Lithofacies Three)

(b) conglomeratic, cross-bedded sandstones (Lithofacies Four)

(c) coarse- to medium-grained sandstones with mud drapes (Lithofacies Five)

(d) fine-grained sandstones (Lithofacies Six)

(e) fine-grained, mud-rich sandstones (Lithofacies Seven)

Field (Upper Morrow producers)		Year Discovered/ drilled	Oil Production Cumulative (As of October 1998)	Gas Production Cumulative (As of October 1998)
Stirrup		1987	1,404,179 bbls	15,746,918 mcf
	Core			
	Myers B2	1991	49,308 bbls	0
	USA I2	1992	99,430 bbls	0
Santa Fe Trail		1975	1,207,404 bbls	26,725,548 mcf
Cimarron Valley		1963	546,212 bbls	4,372,248 mcf
	Core			
	Low G1	1976	0 bbls	0
	Tucker F3	1981	85,593 bbls	1,195,834 mcf

Figure 6.1 Hydrocarbon production history for Santa Fe Trail, Cimarron Valley, and Stirrup oil and gas fields. Individual core production data is included (data provided by the Kansas Geological Survey, 1998).

Most of the production in the study area is associated with the coarser-grained cross-bedded sandstones of the fluvial lithofacies assemblage (Lithofacies Three, Four, and Five). Scout tickets indicate a series of small intervals of perforations (1–18 ft) into the reservoir sandstones. Lithofacies Three, Four, and Five were perforated in 48 wells and Lithofacies Six and Seven were perforated in 14 wells within the study area (Appendix B). Upper Morrowan sandstones are perforated below the gas–oil contact to prevent the depletion of the gas caps (Rader, 1990). Figures 4.3–4.6 show the variations between core intervals tied to log suites and perforation intervals. For example, the Low G1 core was perforated into estuarine Lithofacies Six and Seven as well as fluvial Lithofacies Four and Five (Figure 4.4; Appendix B, Figure B-2). In contrast, the Tucker F3 core (containing both estuarine and fluvial lithofacies) was perforated only into fluvial Lithofacies Three and Four (Figure 4.3; Appendix B, Figure B-2).

Petrography and Petrophysics

Twenty-five thin sections were examined from fluvial and estuarine lithofacies (Table 6.1). Thin sections were not stained for feldspar or carbonate cements, but were impregnated with blue epoxy to highlight porosity. Each thin section was examined for varieties of grains, grain sizes, grain sorting, cements, and porosity.

One-inch-diameter plugs were sampled at 1-ft intervals from the fluvial and estuarine lithofacies assemblages from three cores in the study area (Tucker F3,

Core	Sample depth	Lithofacies	Depositional Environment
Low G1	5358	7	Estuarine
	5360	7	
	5366	7	
	5370	5	Stacked Fluvial Channels
	5370.7	5	
	5371.5	5	
	5372.5	3	Migrating Fluvial Channel Bars
	5372.7	3	
	5372.78	3	
	5373.5	3	
	5373.6	3	
	5376	3	
	5376.1	3	
	5379	4	Stacked Fluvial Channels
	5380	4	
	5383.7	4	
	5386	4	
	5388.7	4	
Tucker F3	5353.1	7	Estuarine
	5357.9	7	
	5362.6	6	
	5363.2	5	Stacked Fluvial Channels
	5365.4	3	Migrating Fluvial Channel Bars
	5369.7	4	Stacked Fluvial Channels
	5376.8	4	

Table 6.1 Location of thin sections examined from fluvial and estuarine lithofacies.

Myers B2, and USA I2). The plugs were analyzed to determine rock porosity, permeability, and water saturation (Table 6.2; data provided by Core Laboratories, Dallas, Texas).

Methodology

Porosity (ϕ), permeability (K), water saturation (Sw), bulk volume water (BVW), and lateral continuity of the fluvial and estuarine lithofacies of the reservoirs are the primary petrophysical characteristics examined in this study. Lab analyses of three cores along with petrophysical analyses of wireline-logs in the study area were integrated to provide an overview of variations in reservoir characteristics among the upper Morrowan lithofacies.

Core Porosity and Permeability

Reservoir capacity and hydrocarbon production are controlled by the porosity of a reservoir (Phillips Petroleum, 1989). Porosity (%) is measured by comparing the total volume of the rock to the volume of void space in the rock (Doveton, 1994, 1998). Porosity (helium percentage) varies between 3.3 and 19.5% with a mean of 14.2% in the Tucker F3 core (Cimarron Valley Field), while in the Myers B2 and USA I2 cores (Stirrup Field), porosity varies between 3.6 and 18.6% with a mean of 12.8% (Table 6.2; Appendix C).

The rate of oil production is controlled by the permeability of a reservoir. Permeability in milidarcies (md) is a measure of the rate of flow of a fluid through a porous medium under specified conditions (Phillips Petroleum, 1989). Permeability

in the fluvial lithofacies ranges from 1.1 to 1,410 md with a mean of 286 md in the Tucker F3 core, from 1.3 to 125 md with a mean of 34.5 md in the Myers B2 core, and from 0.1 to 484 md with a mean of 88 md in the USA I2 core (Table 6.2).

Porosity and permeability measurements from three cores (Tucker F3, USA I2, and Myers B2) were plotted with porosity on the x-axis and the permeability on the y-axis (Figure 6.2). Upper Morrowan reservoirs display two distinct trends that distinguish fluvial from estuarine lithofacies (Figure 6.2). The assemblages of fluvial and estuarine lithofacies of the reservoirs have very similar porosity measurements (Figure 6.2). However, estuarine permeability of a given porosity is approximately one-order of magnitude lower than fluvial permeability.

Lithofacies of the reservoir	Porosity and permeability	Tucker F3 (Cimarron Valley Field)	Myers B2 (Stirrup Field)	USA I2 (Stirrup Field)
Fluvial	Porosity geometric mean	3.3–18.3% 13.17%	6.2–17.9% 13.07%	3.6–18.6% 12.83%
	Permeability geometric mean	1.1–1,410 md 286 md	1.3–125 md 34.5 md	0.1–484 md 88 md
Estuarine	Porosity geometric mean	10.2–19.5% 13.44%	— —	— —
	Permeability geometric mean	2.2–147 md 19.61 md	— —	— —

Table 6.2 Summary chart of porosity and permeability measurements from the Tucker F3, Myers B2, and USA I2 cores.

Porosity from Wireline-Log Data

In addition to measurements derived from the three core analyses, log porosity measurements were taken and mapped from the fluvial and estuarine lithofacies in 66 wells within the study area (figures 6.3 and 6.4). Porosity was determined by the use

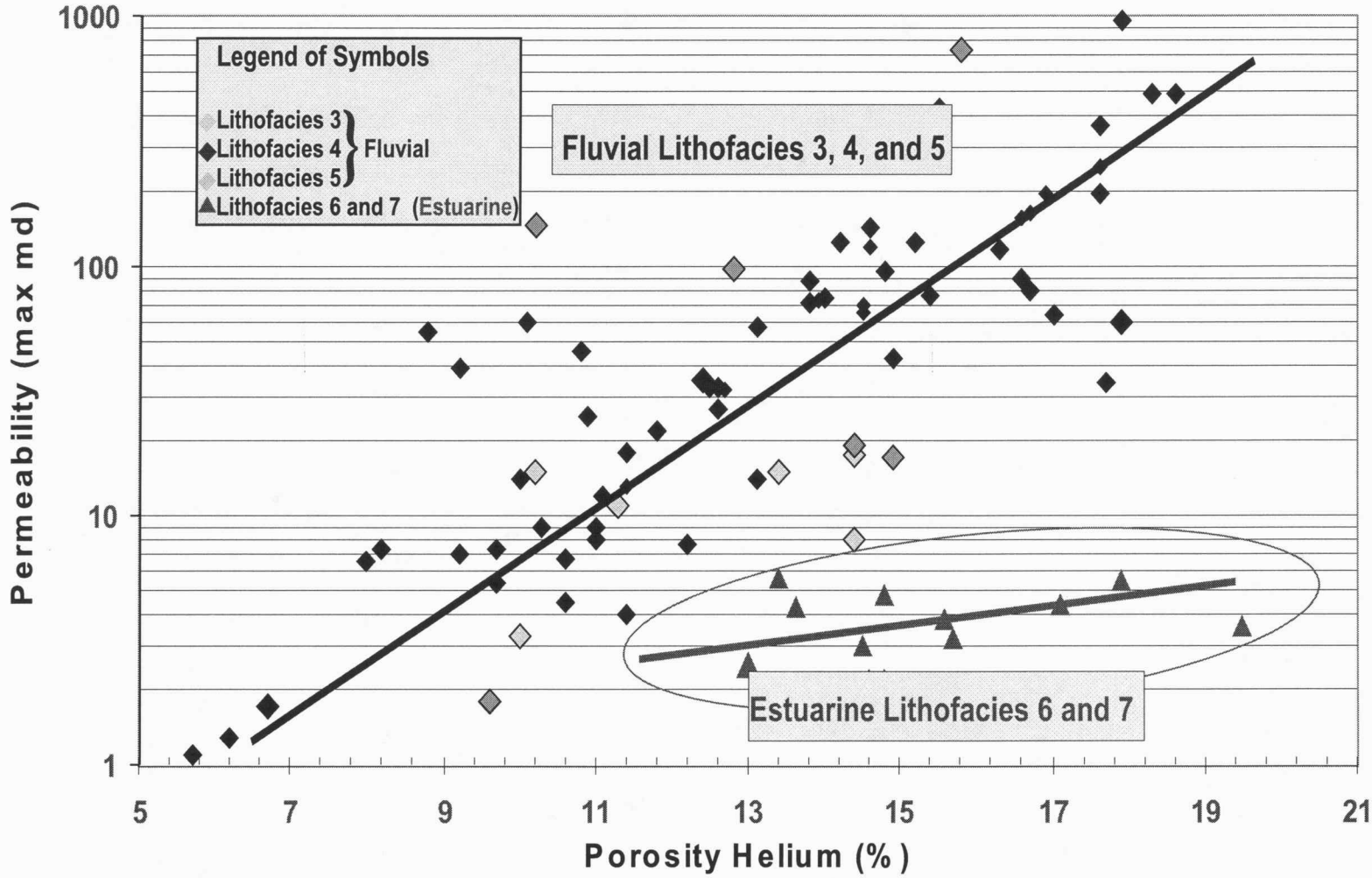

Figure 6.2 Permeability versus porosity cross-plot using measurements from the USA I2, Myers B2, and Tucker F3 core plugs. Estuarine and fluvial lithofacies have distinct permeability versus porosity tendlines.

of at least one of three different wireline porosity tools (i.e., litho-porosity [neutron and density porosity combination], bulk-density [Rhob], and sonic porosity [$\Delta\tau$]).

Litho-Porosity (neutron and density porosity overlay)

Neutron logs are used primarily to delineate porous formations and determine their porosity (Phillips Petroleum, 1989). The neutron log responds to the amount of hydrogen present in the formation (Doveton, 1994, 1998). The density log (g/cc) measures the electron density of the elements within the formation by recording the number of Compton-scattering collisions made after gamma rays have been injected into the formation (Schlumberger, 1989). The electron density of a formation depends on the density of the rock matrix, its porosity, and the density of its pore fluids (Doveton, 1994). When the neutron log is combined with the density log on the same log-track, they provide lithologic resolution, accurate porosity measurements, and gas indications. In this study, all of the neutron and density logs were calibrated to limestone-porosity-equivalent units.

The three basic rules used in deriving porosity measurements from the neutron (Nphi) and density (Dphi) porosity combination were as follows: (1) When Dphi and Nphi overlie each other, this indicates that the formation is limestone, allowing the porosity measurement to be taken directly from the log; (2) when Dphi is further to the left than Nphi, this indicates a sandstone lithology and the midpoint between the two log curves is taken as the porosity; (3) when the Dphi shows a large abrupt separation to the left of Nphi, this indicates a possible gas effect and the porosity is

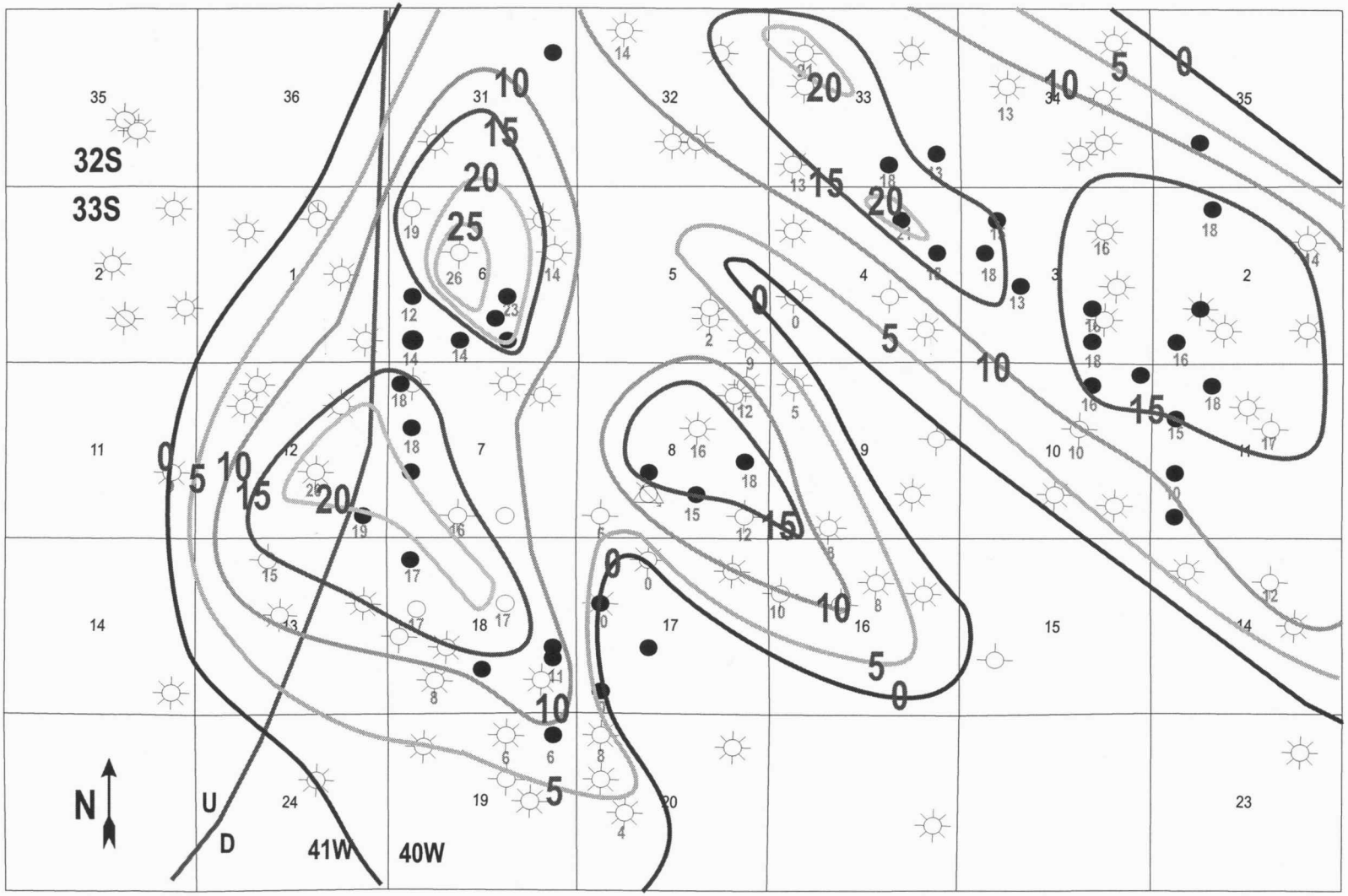

Figure 6.3 Isoporosity map of fluvial Lithofacies Three, Four, and Five. contour interval 5 porosity units (%

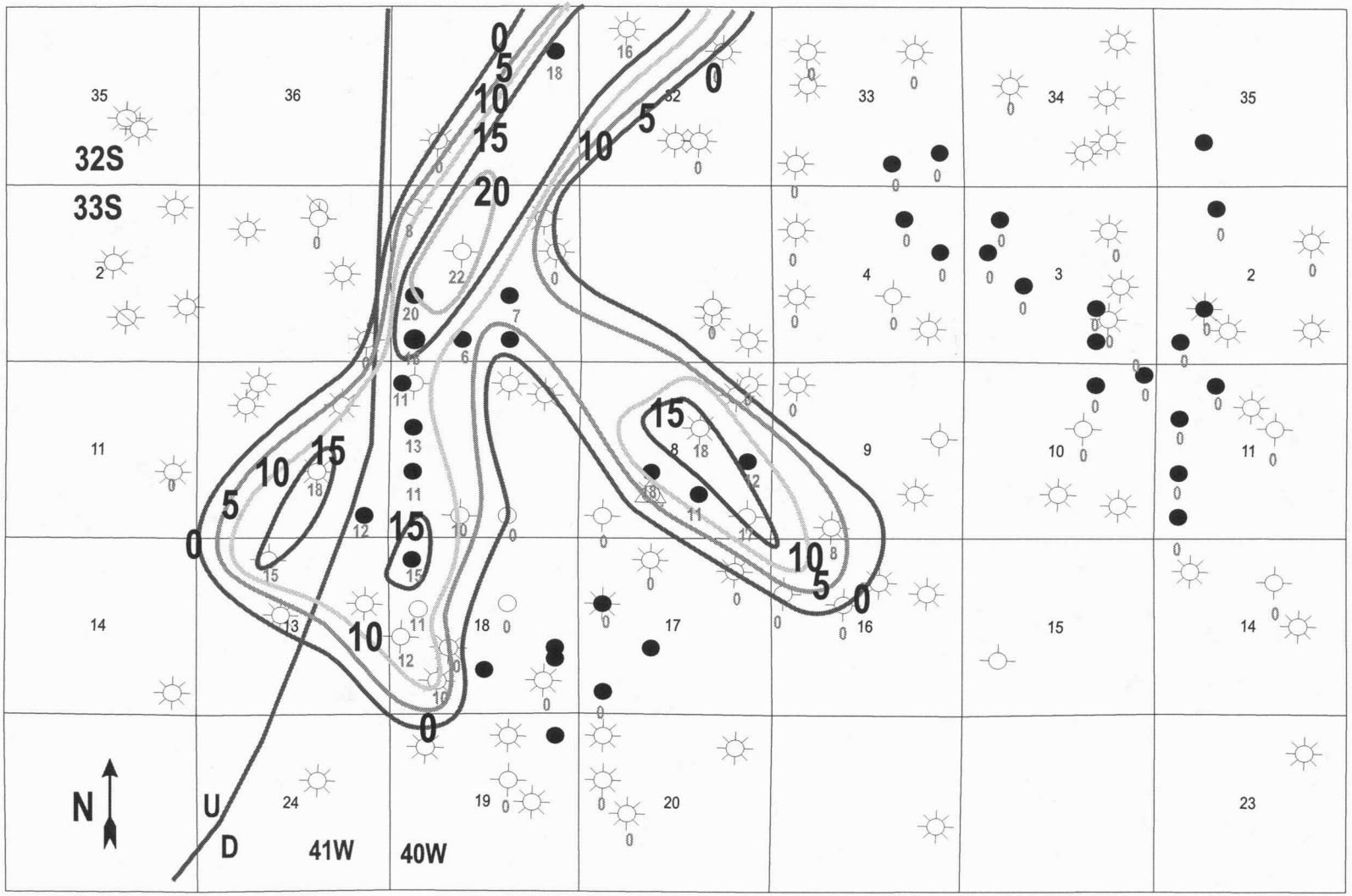

Figure 6.4 Isoporosity map of estuarine Lithofacies Six and Seven.

found by using the 2/3 empirical rule (i.e., read the porosity value from 1/3 the distance from the Dphi to the Nphi curve; Phillips Petroleum, 1989).

Bulk-density

Porosity was computed by taking values directly from the bulk-density (Rhob) log and placing those values on the x-axis of the Schlumberger formation density log porosity chart (Schlumberger, 1989). This procedure requires the knowledge of the average grain density (ρma) within the formation and the density of the fluid (ρf) as found on the y-axis. The ρma for the study area as derived from core analyses measurements was 2.68 g/cc. The ρf was assumed to be a salt mud that has a Rhob value of 1.1 g/cc.

Sonic porosity

The sonic log records the time required for a compressional elastic wave to traverse 1 ft of formation (Schlumberger, 1989). The interval transit time, $\Delta\tau$, corresponds to the shortest acoustic path (i.e., the path of lowest porosity). Porosity measurements were calculated by the use of the following equation:

$$\Phi = (\Delta\tau - \Delta\tau_{ma})/(\Delta\tau_f - \Delta\tau_{ma}).$$

The equation uses a previously computed rock matrix ($\Delta\tau_{ma}$) value for sandstones of 55.5 and a fluid ($\Delta\tau_f$) value for brine of 189 (Schlumberger, 1989).

Porosity Discussion

Porosity values were derived from both core and down-hole wireline-logs. Core porosity measurements can be erroneous due to core-handling procedures and the complexity of returning the cores back to *in situ* conditions (Phillips Petroleum, 1989). Porosity from log analysis is subject to the constraints imposed by the real world, the logging tools themselves (i.e., calibration), and certain assumptions that are made in order to convert the log-measured data to porosity (i.e., gas effects, matrix density; Doveton, 1994, 1998).

In the study, both log and core porosity measurements were taken over the same sampling interval (Figure 6.5). The core porosity values averaged 12.24% and the log porosity values averaged 13.08%. In general, when compared interval by interval, the wireline-log porosity values were higher than the core porosity values by 0.2 to ~7%, with an average of 3.43% (Figure 6.5). However, in approximately 35% of the samples, core porosity values were higher than log porosity values (e.g., core ϕ = 14.9% and log ϕ = 12.4%; core ϕ = 17.7% and log ϕ = 11.8%; Figure 6.5). The differences in porosity measurements taken from wireline-logs and cores are attributed to the sampling problems induced by the averaging of the porosity tool as compared to the focused sampling of the plugs.

The fluvial and estuarine isoporosity maps exhibit axial bifurcated closures (figures 6.3 and 6.4). The highest porosity values coincide with the thickest

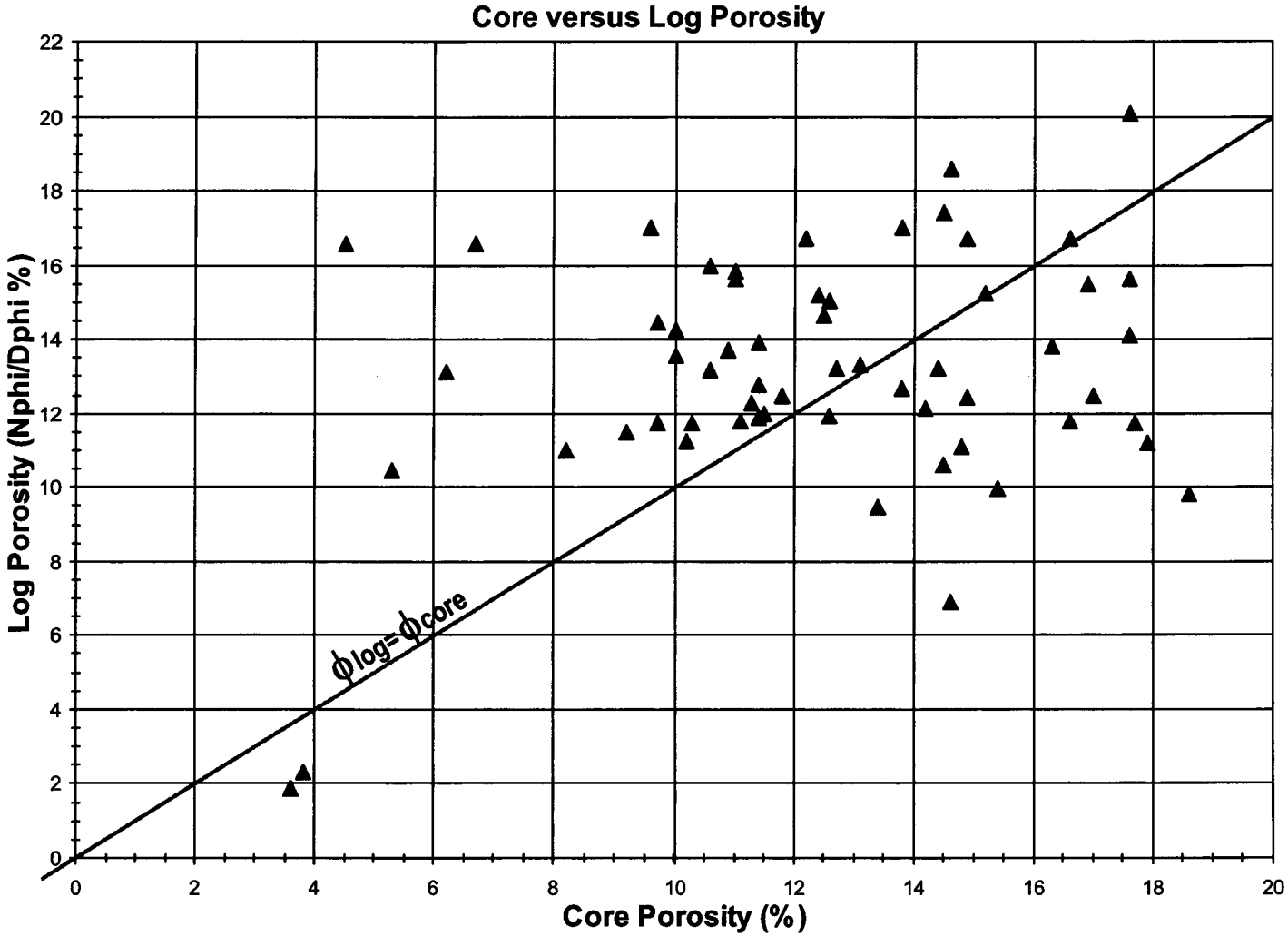

Figure 6.5 Log porosity plotted against core porosity from the same sampling interval of the USA I2 and Myers B2 cores. The wireline log porosity values were higher than the core porosity values by 0.2 to~ 7%.

sandstone accumulations and are adjacent to the fault in the western margin of the study area (figures 6.3 and 6.4). The fluvial isoporosity map shows that the fluvial lithofacies of the reservoirs follow the paleovalley walls and are present across the study area (figures 6.3 and 6.4). However, the estuarine isoporosity map demonstrates that the estuarine lithofacies of the reservoirs are restricted to the western half of the study area.

Petrography

Upper Morrowan sandstones in the study area are predominantly quartzarenites to subarkoses with quartz overgrowths, calcite, and dolomite cement. Secondary porosity is present in most of the fluvial and estuarine sandstones. The petrographic variations between the assemblages of fluvial and estuarine lithofacies are discussed individually.

Fluvial lithofacies assemblage

The sandstones interpreted as the fluvial lithofacies assemblage are subangular to subrounded quartzarenites to subarkoses (Folk, 1974) with 3–12% microcline and plagioclase feldspars and ~5% rock fragments (figures 6.6 and 6.7). The predominant quartz grain is monocrystalline quartz based on its undulose extinction. Quartz grains found in the Low G1 core are highly fractured, which increases the porosity (Figure 6.7A).

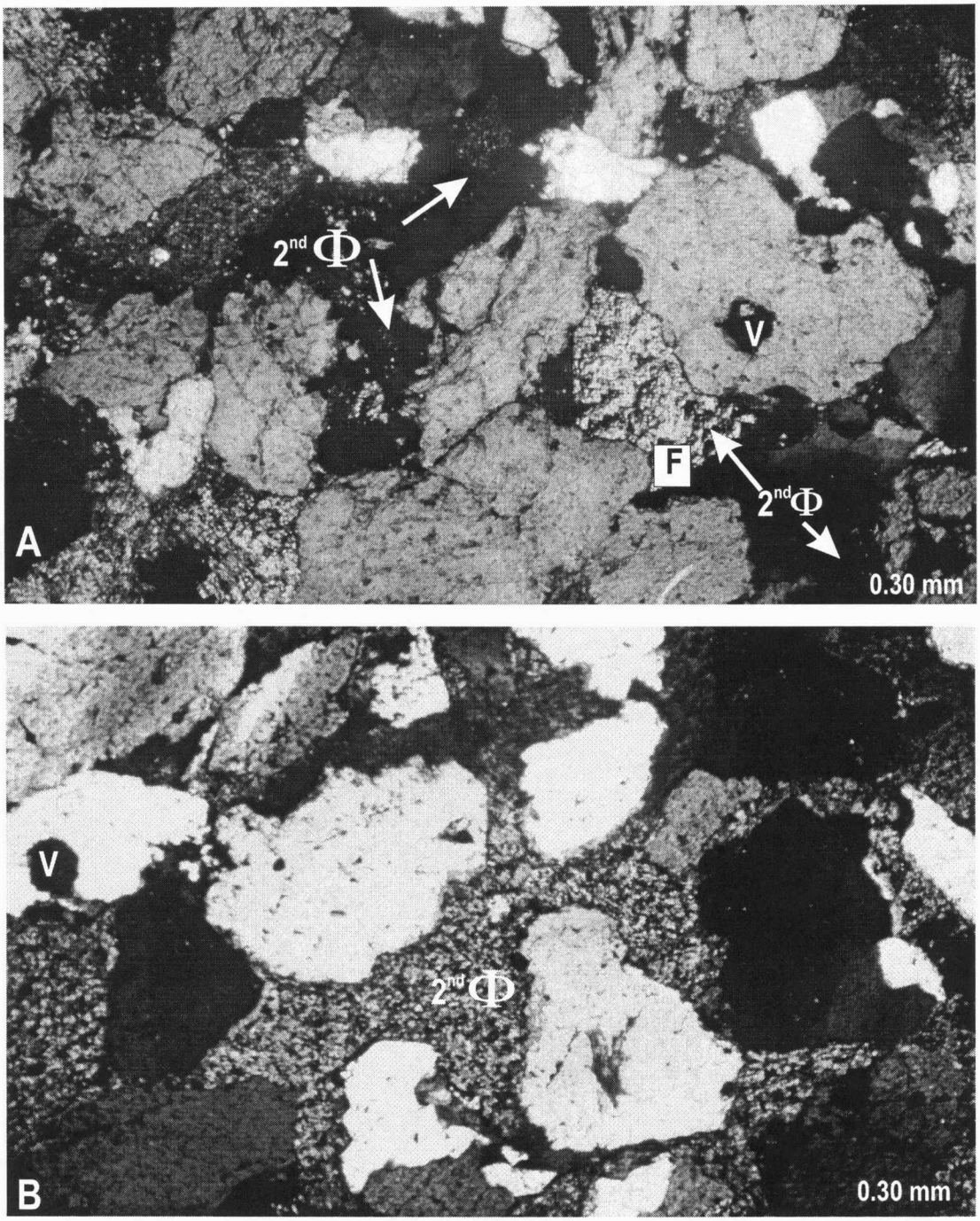

Figure 6.6 Photomicrographics of fluvial Lithofacies Four

(A) and (B) Lithofacies Four is very coarse-grained conglomeratic, subangular to angular, quartzarenite to subarkosic sandstones. The quartz grains in this sample have undulose extinction and vacuoles (V) that indicate a volcanic origin (Rader, 1990). Secondary porosity ($2^{nd}\Phi$) results from the dissolution of calcite and dolomite cement and feldspars, creating wide pore throats. There is calcite replacement of detrital feldspars (F) that is partially dissolved and forms intraparticle and microporosity.

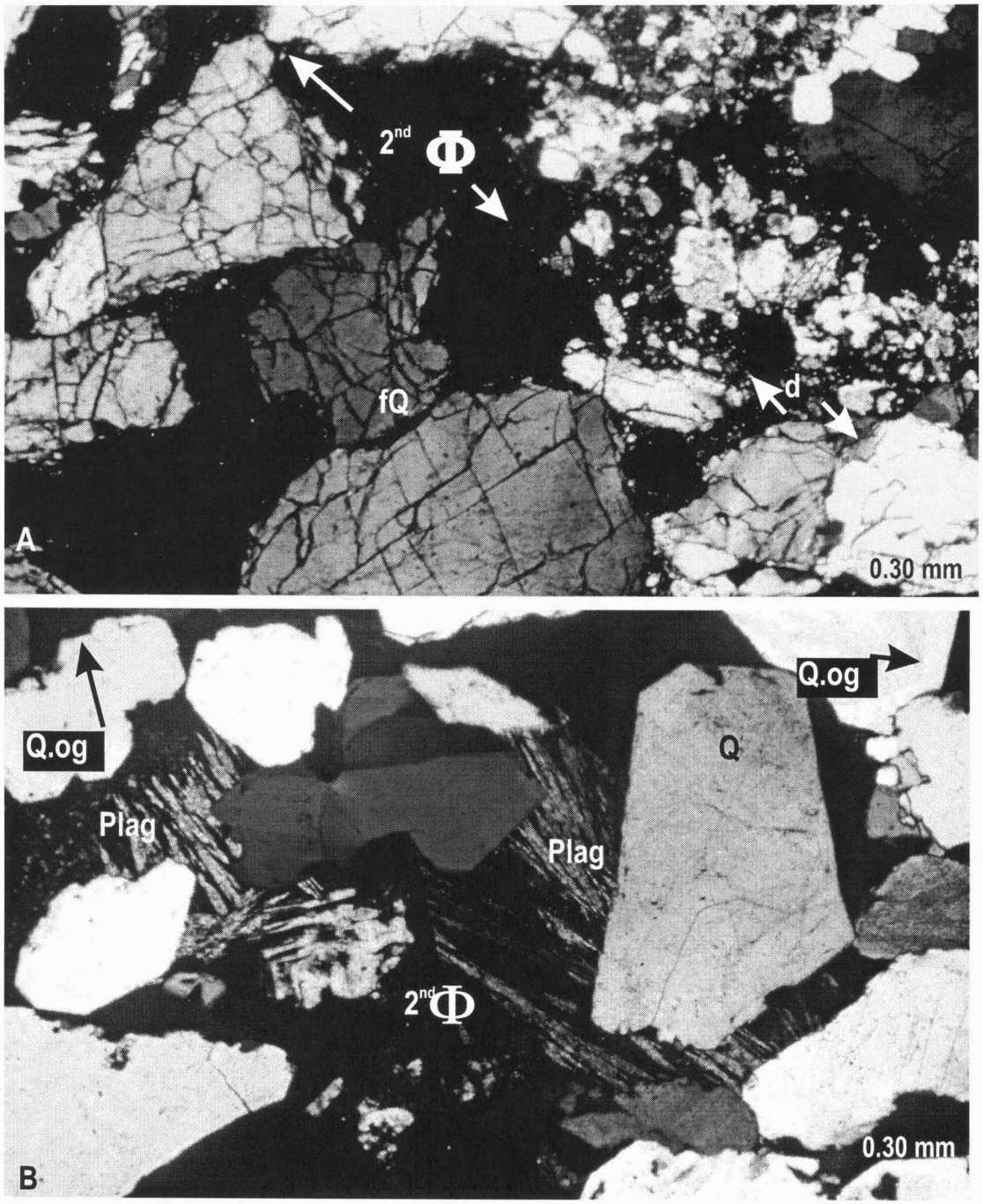

Figure 6.7 Photomicrographs of fluvial Lithofacies Four and Five
(A) Lithofacies Four is very coarse-grained, conglomeratic, subangular to angular, highly-fractured (fQ- fractures filled with blue epoxy) quartzarenite to subarkosic sandstones that have dissolution of quartz grains (d). **(B)** Lithofacies Five is medium- to coarse-grained, subangular subarkosic sandstones with dissolution of plagioclase (Plag), quartz (Q), and quartz overgrowths (Q.og). The quartz grains in these samples have undulose extinction. Secondary porosity (2^{nd} Φ) results from the dissolution of calcite and dolomite cement and feldspars.

Minor amounts of chert and volcanic rock fragments with vacuoles are found in several samples (Figure 6.6). These volcanic rock fragments are composed of chert-like rounded grains with phenocrysts of plagioclase. Volcanic grains have also been observed in the upper Morrowan in Texas County, Oklahoma (Swanson, 1979), and in Morton County, Kansas (Rader, 1987).

Plagioclase is found in the majority of the samples and is partially dissolved into honeycomb porosity structures (Figure 6.6A; Scholle, 1979). Plagioclase exhibits polysynthetic twinning that distinguishes it from orthoclase grains (Figure 6.7B).

Estuarine lithofacies assemblage

The upper Morrowan estuarine lithofacies assemblage contains subangular to subrounded, fine-grained subarkosic sandstones (figures 6.8 and 6.9). The dominant grains consist of quartz, plagioclase, chert, and rock fragments. The quartz grains have undoluse extinction. Stylolites are locally present. Glauconite is found as green to yellow pellets in the sandstone and displays parallel extinction (figures 6.8A and 6.9). Estuarine lithofacies generally contain plagioclase grains (6–14%) that have undergone less dissolution, compared with plagioclase in fluvial lithofacies (figures 6.7B and 6.9).

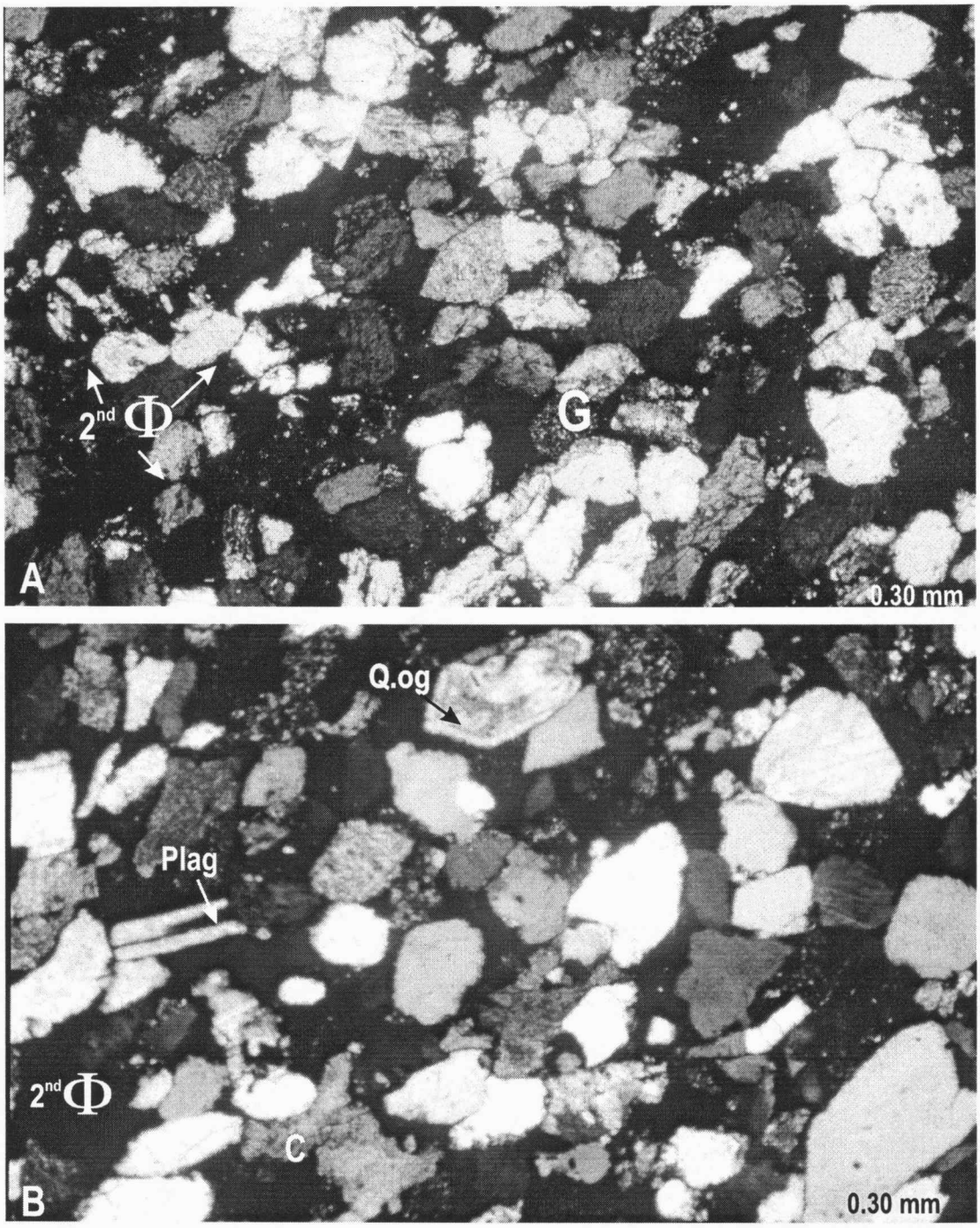

Figure 6.8 Estuarine Lithofacies Six and Seven
(A) Lithofacies Seven is fine-grained, subangular to subrounded, subarkosic sandstones that contain grains of glauconite (G). Dissolution of calcite/dolomite cement and feldspars results in secondary porosity ($2^{nd}\Phi$). **(B)** Lithofacies Six is fine-grained to very fine-grained, subangular to subrounded, subarkosic sandstones with calcite cement (C), plagioclase (Plag), and quartz overgrowths (Q.og).

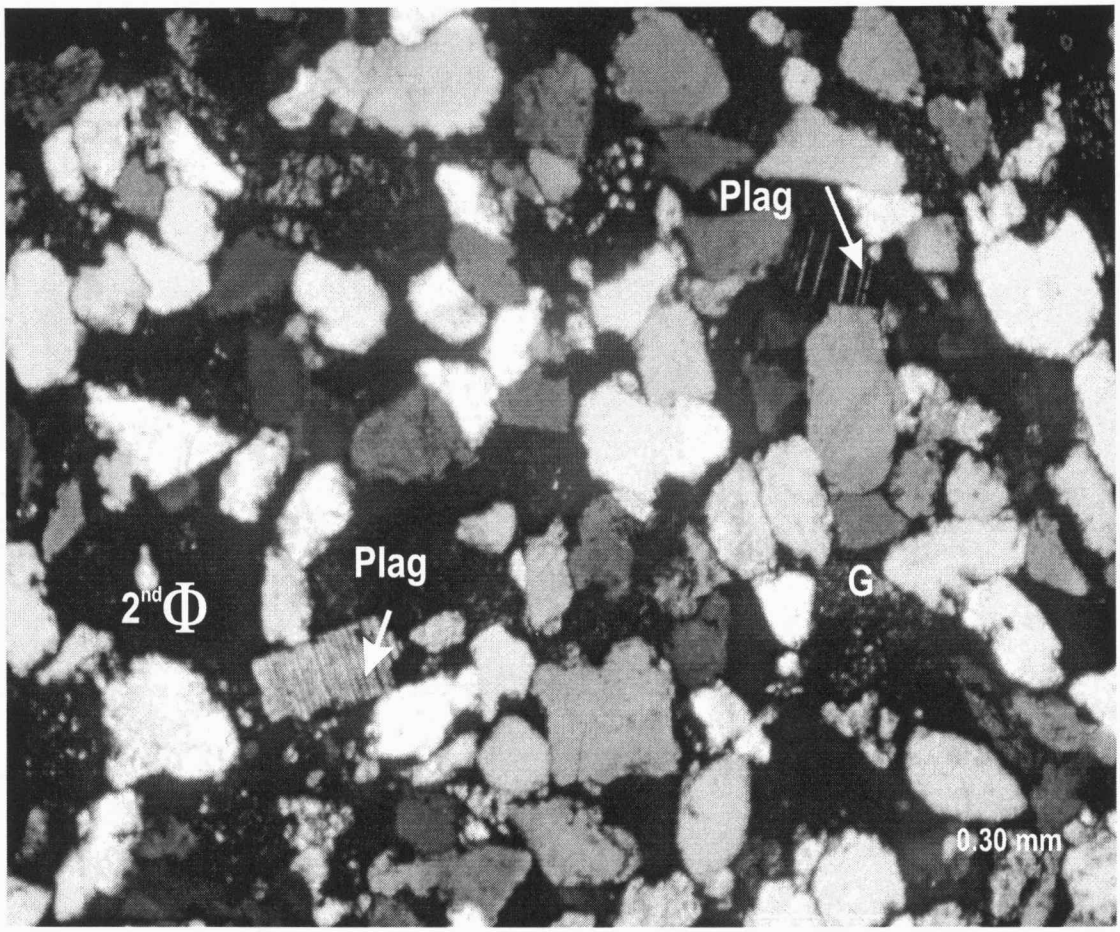

Figure 6.9 Estuarine Lithofacies Seven
Lithofacies Seven is fine-grained to very fine-grained, subangular to subrounded, subarkosic sandstones. Dissolution of calcite and dolomite cement and feldspars results in secondary porosity ($2^{nd}\Phi$). The estuarine lithofacies contain well-preserved grains of plagioclase (Plag) and glauconite (G).

Petrographic Discussion

The fluvial and estuarine lithofacies are cemented primarily by quartz overgrowths, ferroan dolomite, and calcite. This intensive cementation occludes most of the primary porosity. Therefore, pore types present in the sandstones include rare preserved primary porosity between quartz grains, secondary intergranular pores resulting from the dissolution of feldspars (microcline and plagioclase) and the carbonate cement, and microporosity within the clay and the feldspars.

Leaching of carbonate cements and feldspars are important factors in the development of secondary porosity in the upper Morrowan sandstones. Secondary porosity is dominant in both the fluvial and estuarine lithofacies (figures 6.6–6.9). The porosity in the estuarine lithofacies shows less dissolution or leaching compared with the fluvial lithofacies (figures 6.7B and 6.9). Secondary porosity is displayed by the honeycomb appearance of the feldspars and the blue epoxy shown in the carbonate cement (Figure 6.6A). The dissolution of carbonate cement is the dominant porosity in the upper Morrowan strata of Texas County, Oklahoma (Kasino and Davies, 1979).

Compared to the fluvial lithofacies, the estuarine lithofacies with the same porosity have poorer reservoir quality because of much lower permeability measurements (Figure 6.2). Estuarine permeability of a given porosity is approximately one order of magnitude lower than fluvial permeability. The decrease in estuarine permeability compared with the fluvial permeability is attributed to the estuarine lithofacies having much finer grain sizes, containing higher silt, shale, and

mud contents (e.g., heterolithic bedding), and consisting of higher amounts of feldspars.

Vertical fractures in the USA I2 core indicate extensive burial or tectonic stress. These vertical fractures add to the observed porosity. The fracturing of the quartz grains is interpreted as post-depositional (tectonic-induced) as evidenced by the continuity of the fracturing from one grain to the next; the abundance of fractured grains; the display of blue epoxy in fractures; and the assumption that such intensely fractured grains could not have survived transport (Figure 6.7; Scholle, 1979).

The angularity and the immaturity of the fluvial and estuarine lithofacies indicate that the grains were not transported long distances. The well-preserved plagioclase grains indicate relatively close proximity to the source areas. The presence of glauconite in the estuarine lithofacies suggests *in situ* deposition of fecal pellets and indicates a marine influence (figures 6.8A and 6.9; Scholle, 1979).

Archie Equations and Reservoir Water Characteristics

Water saturation (Sw) refers to the percent of water filling the pore space of a particular rock (Phillips Petroleum, 1989). Bulk volume water (BVW) is the product of porosity and water saturation. Variations in BVW are related to lithology, pore type, and grain size and can provide insight into the type of fluid a reservoir will produce (i.e., oil, water, or both; Doveton, 1994, 1998). The calculation of Sw is computed by using the Archie (1952) equation, i.e.,

$$Sw = (a/\phi^m \times Rw/Rt)^{1/n}$$

The Archie formula consists of two separate equations (Archie, 1952). The first equation compares the ratio between the resistivity of a water saturated rock (Ro) and the formation water resistivity (Rw) to the fractional porosity (ϕ); (Archie, 1952; Doveton, 1998). The resistivity ratio is sometimes referred to as the formation factor (F) and is expressed as:

$$F = Ro/Rw = a/\phi^m$$

The second equation relates the ratio of the observed formation resistivity (Rt) to its expected resistivity (Ro) if it were completely saturated with water to the fractional water saturation (Sw); (Archie, 1952; Doveton, 1994, 1998), i.e.,

$$Rt/Ro = 1/Sw^n$$

The basic Archie equation includes formation water factor (Rw) resistivity measurements (from wireline-logs), a cementation component (m), porosity measurement (ϕ), and constant values for a and n.

The Pickett plot was developed as a graphical solution to the Archie equation and the equation relating formation factor to ϕ (Pickett, 1973; Doveton, 1994, 1998). The Pickett plot shows a linear relationship between log (Rt) and log (ϕ). When Rt is plotted on the x-axis and porosity (%) on the y-axis of a log–log grid, points corresponding to an equal water saturation fall on a straight line (Doveton, 1998).

Calculating formation water resistivity

Formation water resistivity measurements (Rw) are required to analyze the variations in water saturation (Sw) between the fluvial and the estuarine lithofacies of

Calculating Rw

1.) Graph SP (spontaneous potential) against Rwa
2.) Calculate slope of the line to estimate true Rw

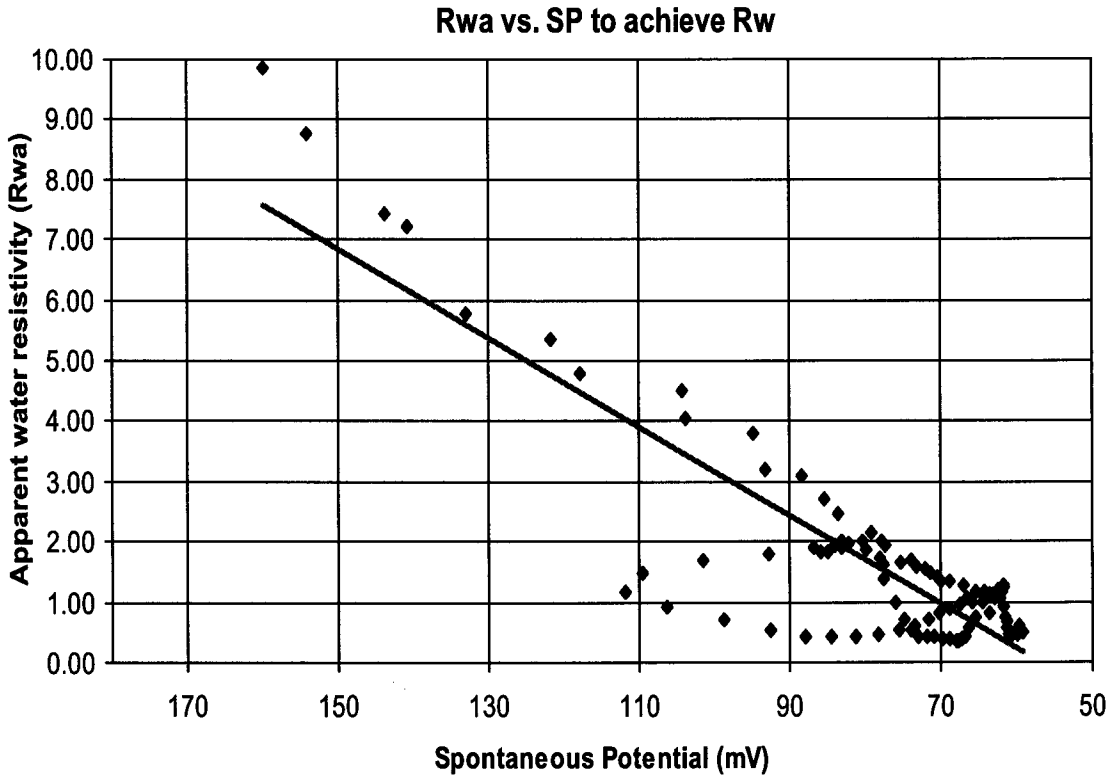

$$Rw = \frac{y2 - y1}{x2 - x1} \qquad Rw = \frac{(1.48 - 68)}{(1.06 - 88)} \qquad Rw = 0.044$$

Figure 6.10 Calculation of formation water resistivity (Rw) for the study area. The graph contains well data from the USA AC1, Stirrup Field.

the reservoirs. Digitized log suites in the Log Ascii Standard (LAS) format were entered into the PfEFFER 2.0 program (Bohling et al., 1998). The PfEFFER 2.0 program was used to generate an apparent Rw (Rwa) for each depth interval (Bohling et al., 1998). The Rwa values were plotted on the y-axis against the spontaneous potential log (SP) values on the x-axis (Figure 6.10). The slope of the Rwa versus SP graph is the calculated Rw (Figure 6.10). The Rwa versus SP technique was applied to several wells within the study area and a true Rw value of 0.044 was produced. The estimated true Rw value for the study area is consistent with computed values using water analyses data (Haliburton Energy Service, 1994; Bill Guy, Kansas Geological Survey, pers. comm., 1999).

Fluvial and Estuarine Water Saturations and Bulk Volume Water

After computing a value for Rw, Pickett plots were generated for several wells within the study area, including the cored intervals. The Pickett plots (using the Archie [1952] equation) display the differences in water saturation (Sw) and bulk volume water (BVW) for the fluvial and estuarine lithofacies of the reservoirs (figures 6.11–6.13).

The Pickett plots of the Myers B2 and the USA I2 wells show the average Sw and BVW values within the fluvial lithofacies (figures 6.12 and 6.13). The Sw values for the two cored intervals range from 25 to 65%. Upper Morrowan production occurs predominantly in the upper depth intervals of the fluvial lithofacies, which have an average BVW of 0.045–0.06 (figures 6.12 and 6.13).

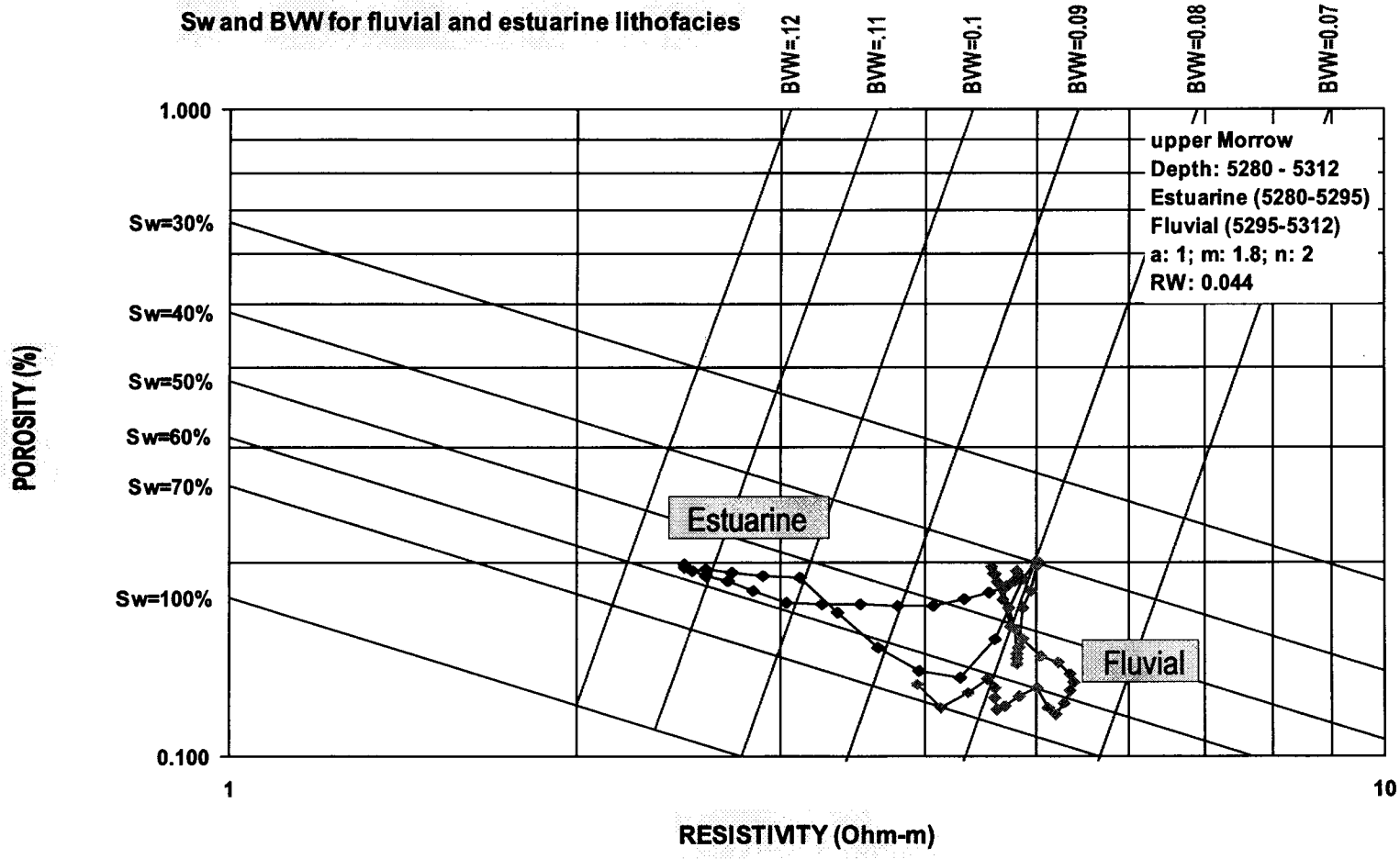

Figure 6.11 Pickett plot displaying water saturation (Sw) and bulk volume water (BVW) ranges for fluvial and estuarine lithofacies in upper Morrowan reservoirs in the Lemon Trust A1 well. Fluvial lithofacies are represented by the light-colored dots and the estuarine lithofacies are represented by the dark-colored dots.

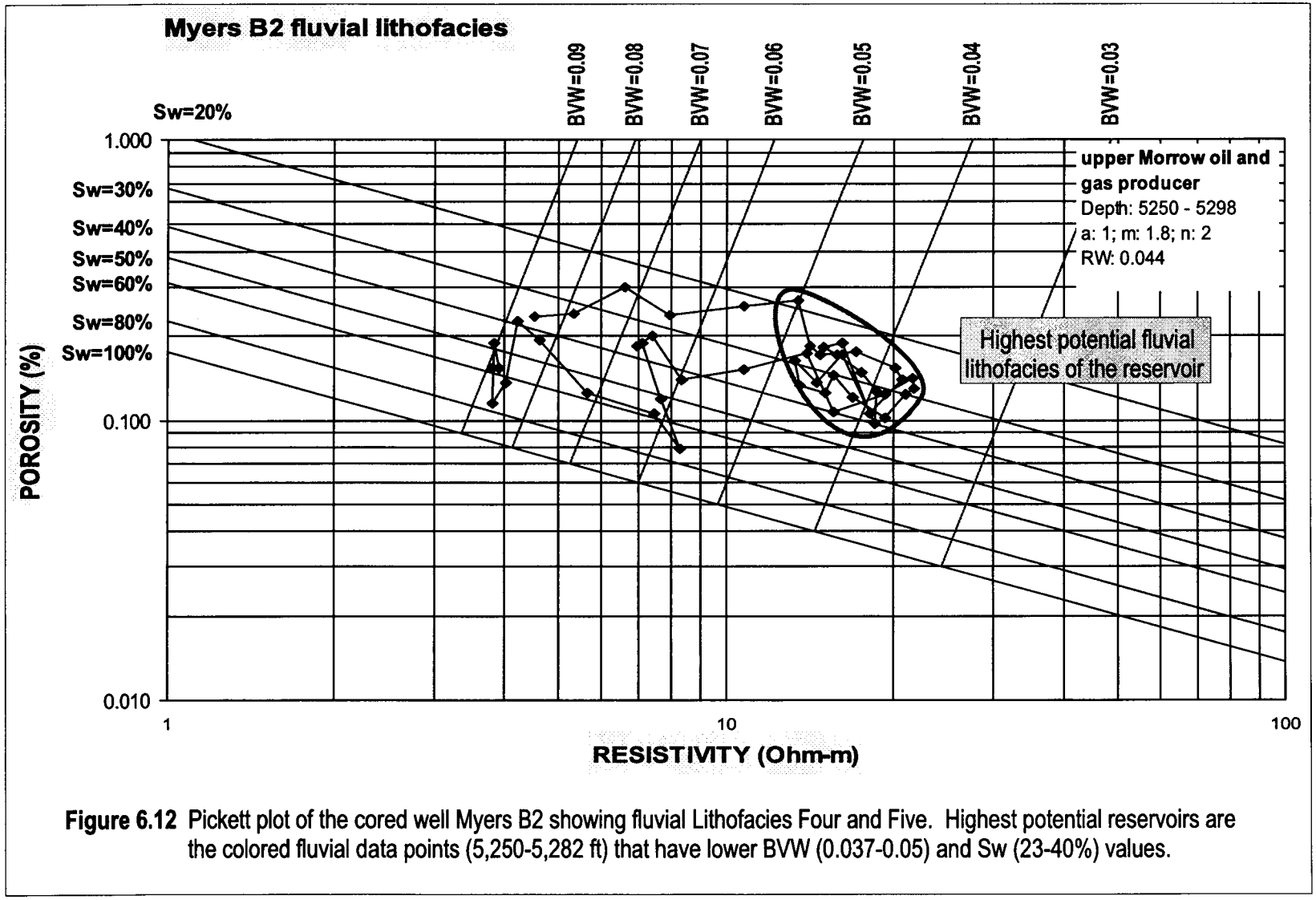

Figure 6.12 Pickett plot of the cored well Myers B2 showing fluvial Lithofacies Four and Five. Highest potential reservoirs are the colored fluvial data points (5,250-5,282 ft) that have lower BVW (0.037-0.05) and Sw (23-40%) values.

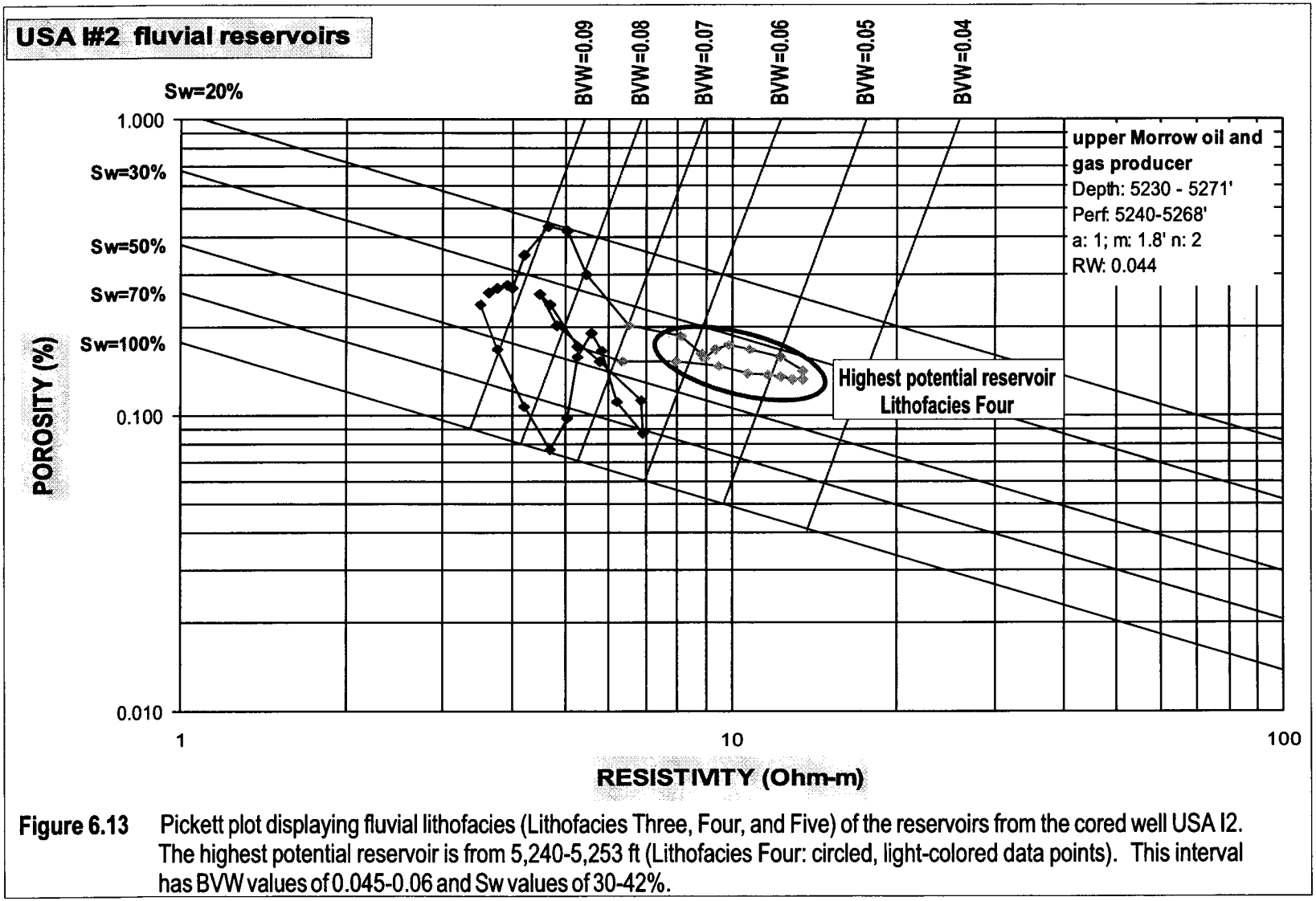

Figure 6.13 Pickett plot displaying fluvial lithofacies (Lithofacies Three, Four, and Five) of the reservoirs from the cored well USA I2. The highest potential reservoir is from 5,240-5,253 ft (Lithofacies Four: circled, light-colored data points). This interval has BVW values of 0.045-0.06 and Sw values of 30-42%.

Water saturations (Sw) were calculated for the study area using wireline-log data to derive the porosity values needed for the Archie equation (Archie, 1952; Schlumberger, 1989; Doveton, 1994, 1998; Figure 6.14). The porosity techniques were previously described in this chapter and included litho-porosity (neutron and density porosity combination), bulk-density (Rhob), and sonic porosity ($\Delta\tau$). Values for variables within the Archie equation include: a = 1, Rw = 0.044, m = 1.8 (sandstone), and formation resistivity (Rt) = the values from the ILD resistivity log (Figure 6.14).

Discussion of Water Saturation and Bulk Volume Water

In the Lemon Trust A1, the fluvial and estuarine lithofacies of the reservoirs show distinct separation on the Pickett plot (Figure 6.11). The data points of the fluvial lithofacies assemblage form a cluster that has water saturation (Sw) values in the range of 40 to 70% and bulk volume water (BVW) values in the range from 0.075 to 0.085 (Figure 6.11). Core Labs calculated the average water saturation for the fluvial lithofacies within the Tucker F3 (Cimarron Valley Field) core as ~40% and within the Myers B2 and USA I2 cores (Stirrup Field) as 37–47% (Appendix C).

Estuarine lithofacies have a distinct linear trend along the 60% water saturation line (Figure 6.11). The shallowest depths have water saturations near ~40%, and with an increase in depth, the water saturations gradually increase to 60%. Core Labs calculated water saturations of the estuarine lithofacies as an average of 66% in the Tucker F3 core (Cimarron Valley Field). The estuarine lithofacies have

Calculating Sw for logs in study

$$Sw = \sqrt{\frac{(1*Rw)}{\phi^{m} * Rt}}$$

Rw = 0.044 (calculated)
m = 1.8 (sandstone)
Rt = ILD wireline-log value

Calculating Sw using NPHI and DPHI wireline-log values

$$Sw = \sqrt{\frac{(1*.044)}{\left(\sqrt{\frac{NPHI^2 + DPHI^2}{2}}\right)^{1.8} * ILD}}$$

Calculating Sw using RHOB wireline-log values

$$Sw = \sqrt{\frac{(1*.044)}{\left(\frac{2.68\ (\text{core data}) - \text{RHOB log value}}{2.68\ (\text{core data}) - 1.1\ (\text{salt mud fluid})}\right) * ILD}}$$

Calculating Sw using Delta T (sonic) wireline-log values

$$Sw = \sqrt{\frac{(1*.044)}{\left(\frac{\Delta t(\text{log value}) - 55.5\ (\text{quartz})}{189\ (\Delta t\ \text{brine}) - 55.5\ (\text{quartz})}\right)^{1.8} * ILD}}$$

Figure 6.14 Calculation of water saturation (Sw) in percent (%) from wireline-log data.

higher BVW values (0.08–0.12) than the fluvial lithofacies of the reservoirs (Figure 6.11).

Water saturations (Sw) vary across the fields and are not laterally correlatable. The wide variability of water saturations is attributed to several oil/water and oil/gas contacts throughout the fields. In general, the upper 5–20 ft of the fluvial lithofacies assemblage of each reservoir has the lowest Sw and the lowest BVW values (figures 6.12 and 6.13). These intervals are also the most productive for hydrocarbons.

Conclusions

In the upper Morrowan sandstones of the study area, secondary porosity is the major pore type. The secondary porosity is the result of the dissolution of carbonate cements and feldspars. The removal of carbonate cement has been attributed to petroleum maturation and migration processes and the emplacement of hydrocarbons into the reservoirs (Rader, 1990).

The higher quality upper Morrowan reservoirs are the coarse-grained, cross-bedded fluvial sandstones of Lithofacies Three, Four, and Five. The coarse-grained fluvial lithofacies (Lithofacies Three, Four, and Five), as compared with the fine-grained estuarine lithofacies (Lithofacies Six and Seven), form reservoir intervals that are more laterally continuous; contain less detrital mud and clay; retain more primary and secondary porosity; have lower BVW and Sw; and have higher permeabilities. Reservoir quality within the study area is strongly influenced by depositional lithofacies.

CHAPTER SEVEN

CONCLUSIONS

Upper Morrowan sandstones are oil and gas productive over a large area in southwestern Kansas, southeastern Colorado, and northwestern Oklahoma (Emery, 1985; Wheeler et al., 1990; Al-Shaieb et al., 1995; Andrews, 1997; Schoeling and Fox, 1998). Continued exploration and development and the potential for application of enhanced oil-recovery techniques (e.g., carbon-dioxide flooding) require a better understanding of upper Morrowan stratigraphy and facies relationships to improve success rates and the efficiency of hydrocarbon recovery. The depositional environments, sequence stratigraphy, and reservoir characterization of the upper Kearny Formation (Morrowan Series, Pennsylvanian System) were examined within the Santa Fe Trail, Cimarron Valley, and Stirrup fields, Morton County, southwestern Kansas. The case study demonstrates the application of sequence-stratigraphic concepts and incised-valley depositional models in the prediction of lithologic successions occurring in response to fluctuations of relative sea-level as well as sediment supply.

Four cores containing 176 ft (52.80 m) of upper Morrowan reservoir rock were subdivided into nine lithofacies and three lithofacies assemblages. The marine lithofacies assemblage consists of Lithofacies One, One-B, and One-C representing strata deposited in deep anoxic water conditions to high-energy shoreface environments. Lithofacies Two, Three, Four, and Five contain conglomerates, medium- to very coarse-grained subarkoses, and quartzarenites deposited within

migrating channel bars and stacked fluvial channels and are assigned to the fluvial lithofacies assemblage. Lithofacies Six and Seven consist of fine-grained subarkoses with tidally influenced sedimentary structures deposited in mid- to upper estuary settings and are assigned to the estuarine lithofacies assemblage.

The lithofacies assemblages were correlated with wireline-log responses to extend the lithofacies interpretations beyond the limited core control. Seven stratigraphic cross-sections show the result of the integrated core and wireline-log interpretations. The cross-sections were combined with upper Morrowan sandstone isopach and isoporosity maps, sedimentary structures (core), geologists' reports and logs, and wireline-log data to develop a sequence-stratigraphic framework and to construct a depositional model for the study area.

Upper Morrowan successions within the study area consist of two sequences that were deposited within two incised valleys. Two sequence boundaries (SB#1 and SB#2), one transgressive surface of erosion (TSE), and three maximum flooding surfaces (MFS#1, MFS#2, and MFS#3) were observed (Appendix A). The incised valleys occurred as a result of at least two major relative sea-level falls followed by subsequent sea-level rises. The observed sequence boundaries (SB#1 and SB#2) at the base of each sequence have valley-like shapes and are incised into marine shales, mudstones, and limestones (Lithofacies One, One-B, and One-C). The sequence boundaries show a landward shift from marine into fluvial and estuarine lithofacies. As sea-level rose, the Hugoton Embayment became a sediment trap resulting in the deposition of the fluvial and estuarine lithofacies assemblages.

Seven chronostratigraphic cross-sections and upper Morrowan sandstone isopach maps demonstrate that the estuarine lithofacies assemblage and the thickest sandstones are confined to the western side of the study area. Restriction of the estuarine strata suggests that during deposition of estuarine lithofacies, active river mouths were present exclusively in the western side of the study area. The western margin of the study area is bounded by a fault that may have influenced the deposition of the upper Morrowan strata. Cross-section and isopach map observations led to the hypothesis that relative sea-level in the study area may have been controlled by local (e.g., fault reactivation) and regional tectonics in addition to glacial eustacy.

Five types of sandstones found within the incised valley fill (fluvial and estuarine) are identified as potential reservoirs. Secondary porosity is the predominate type of porosity in the sandstones and results from multistage dissolution of carbonate cements and feldspars. Reservoir quality is influenced by the grain-sizes and the mud content of the depositional lithofacies. In the study area, the coarse-grained, cross-bedded fluvial sandstones of Lithofacies Three, Four, and Five form the higher quality upper Morrowan reservoirs. However, the fine-grained estuarine Lithofacies Six and Seven from lower quality reservoir intervals. The coarse-grained fluvial lithofacies as compared with the fine-grained estuarine lithofacies have higher production rates; are more laterally continuous; contain less detrital mud and clay; retain more primary and secondary porosity; have lower bulk volume water (BVW) and water saturations (Sw); and have higher permeabilities.

REFERENCES CITED

Abegg, F. E., 1994, Lithostratigraphy of the Shore Airport Formation (Chesterian), southwestern Kansas, *in* D. L. Baars, ed., Revision of stratigraphic nomenclature in Kansas: Kansas Geological Survey Bulletin, v. 230, p. 21–38.

Adams, G. I., 1904, Zinc and lead deposits of northern Arkansas, with a section by Ulrich, E. O., Determination and correlation of formations: United States Geological Survey Professional Paper 24, p. 1–118.

Alberta, P. L., 1987, Depositional facies analysis and porosity development of the (Pennsylvanian) upper Morrow chert-conglomerate Puryear member, Roger Mills and Beckham counties, Oklahoma: Oklahoma State University, unpublished M.S. thesis, p. 60–140.

Alissa, A. M. I., 1999, Electrofacies model and sequence stratigraphic framework of the lower Morrow rocks, case study, Arroyo and Gentzler oil fields, Hugoton Embayment southwestern Kansas: Kansas Geological Survey and University of Kansas, unpublished M.S. thesis, p. 1–95.

Allen, G. P., 1992, Sedimentary processes and facies in the Gironde estuary: a recent model for macrotidal estuarine systems, *in* D. G. Smith, G. E. Reinson, B. A. Zaitlin, and R. A. Rahmani, eds., Canadian Society of Petroleum Geologists Memoir 16, p. 29–40.

Allen, G. P., and H. W. Posamentier, 1993, Sequence stratigraphy and facies model of incised valley-fill: The Gironde Estuary, France: SEPM Special Publication, v. 63, n. 3, p. 378–391.

Al-Shaieb, Z., J. Puckette, and A. Abdalla, 1995, Influence of sea-level fluctuation on reservoir quality of the upper Morrowan sandstones, northwestern shelf of the Anadarko Basin, *in* N. J. Hyne, ed., Sequence stratigraphy of the midcontinent: Tulsa Geological Society Special Publication, n. 4, p. 249–268.

Andrews, R. D., 1997, Upper and lower Morrow core descriptions from three wells in Dewey and Texas counties, Oklahoma: Oklahoma Geological Survey, Open-File Report 9-97, p. 1–9.

Archie, G. E., 1952, Classification of reservoir rocks and petrophysical considerations: American Association of Petroleum Geologists Bulletin, v. 36, n. 2, p. 278–298.

Arro, E., 1965, Morrowan sandstones in the subsurface of the Hough area, Texas, County, Oklahoma: Shale Shaker, v. 1, no. 16, p. 2–16.

Barclay, J. E., 1988, The lower Carboniferous Golata Formation of the Western Canada Basin, in the context of sequence stratigraphy, *in* D. P. James and D. A. Leckie, eds., Sequences, stratigraphy, sedimentology: surface and subsurface: Canadian Society of Petroleum Geologists Memoir 15, p. 6–10.

Barnes, R. S. K., 1984, Estuarine Biology (2nd ed.): London, Edward Arnold Ltd., p. 73–76.

Benton, J. W., 1971, Subsurface stratigraphic analysis, Morrow (Pennsylvanian), north central Texas County, Oklahoma: University of Oklahoma, unpublished M.S. thesis, 60 p.

Beynon, B. M., S. G. Pemberton, D. D. Bell, and C. A. Logan, 1988, Environmental implications of ichnofossils from the lower Cretaceous Grand Rapids Formation, Cold Lake Oil Sands Deposits, *in* D. P. James and D. A. Leckie, eds., Sequences, stratigraphy, sedimentology: surface and subsurface: Canadian Society of Petroleum Geologists Memoir 15, p. 275–290.

Blakeney, B. A., L. F. Krystinik, and A. A. Downey, 1990, Reservoir heterogeneity in Morrow valley fills, Stateline trend—implications for reservoir management and field expansion, *in* S. A. Sonnenberg, L. T. Shannon, K. Rader, W. F. von Drehle, and G. W. Martin, eds., Morrowan sandstones of southeast Colorado and adjacent areas: Rocky Mountain Association of Geologists, p. 191–206.

Bohling, G., J. Doveton, B. Guy, L. Watney, and S. Bhattacharya, 1998, PfEFFER 2.0 manual, Development and demonstration of an enhanced spreadsheet-based well log analysis software: Kansas Geological Survey, p. 1–164.

Bolyard, D. W., 1990, Upper Morrow "B" sandstone reservoir, Flank Field, Baca County, Colorado, *in* S. A. Sonnenberg, L.T. Shannon, K. Rader, W. F. von Drehle, and G. W. Martin, eds., Morrowan sandstones of southeast Colorado and adjacent areas: Rocky Mountain Association of Geologists, p. 191–206.

Bowen, D. W., P. Weimer, and A. J. Scott, 1993, The relative success of siliciclastic sequence stratigraphic concepts in exploration: examples from incised valley fill and turbidite systems reservoirs, *in* P. Weimer and H. W. Posamentier, eds., Siliciclastic sequence stratigraphy: recent developments and applications: AAPG Memoir 58, p. 15–42.

Brown, L. G., W. A. Miller, E. M. Goff-Hundley, and S. L. Veal, 1990, Stockholm Southwest Field, *in* S. A. Sonnenberg, L. T. Shannon, K. Rader, W. F. von Drehle, and G. W. Martin, eds., Morrowan sandstones of southeast Colorado and adjacent areas: Rocky Mountain Association of Geologists, p. 117–130.

Brown, R. L., 1995, Ablative subduction and its structural effects upon the midcontinent during the Pennsylvanian, *in* K. S. Johnson, ed., Structural styles in the southern midcontinent: Oklahoma Geological Survey, v. 97, p. 83–98.

Canadian Well Logging Society's LAS Committee, 1993, New features of LAS 2.0, the floppy disk standard for log data: The Log Analyst, March–April, p. 60–68.

Cant, D. J., and R. G. Walker, 1976, Development of a braided-fluvial facies model for the Devonian Battery Point Sandstone, Quebec: Canadian Journal of Earth Sciences, v. 13, p. 102–119.

Cant, D. J., and R. G. Walker, 1978, Fluvial processes and facies sequences in the sandy, braided South Saskatchewan River: Sedimentology, v. 25, p. 625–648.

Clark, S. L., 1987, Seismic stratigraphy of Early Pennsylvanian Morrowan sandstones, Minneola Complex, Ford and Clark counties, Kansas: American Association of Petroleum Geologists Bulletin, v. 71, n. 11, p. 1329–1341.

Collinson, J. D., 1996, Alluvial sediments, *in* H. G. Reading, ed., Sedimentary environments: processes, facies and stratigraphy: Cambridge, United Kingdom, Blackwell Science, University Press, p. 37–82.

Craig, L. C., and K. L. Varnes, 1979, History of the Mississippian System—an interpretative summary: USGS Professional Paper 1010-R, p. 371–406.

Dalrymple, R. W, 1992, Tidal depositional systems, *in* R. G. Walker and N. P. James, eds., Facies models: response to sea level: Stittsville, Ontario, Geological Association of Canada, Love Printing Service Ltd., p. 195–233.

Dalrymple, R. W., B. A. Zaitlin, R. Boyd, 1992, Estuarine facies model: conceptual basis and stratigraphic implication: Journal of Sedimentary Petrology, v. 62, p. 1130–1146.

Davis, H. G., 1963, Kinsler Morrowan gas field, Morton County, Kansas: Shale Shaker Digest, v. 14, n. 2, p. 10.

DeVoto, R. H., 1980, Pennsylvanian stratigraphy and history: Colorado geology: Rocky Mountain Association of Geologists Symposium, p. 71–101.

Diessal, C. F. K., 1992, The nature of inertinite and its effect on hydrogenation, carbonization and combustion, *in* S. A. Stout, ed., Ninth Annual Meeting of the Society for Organic Petrology, abstracts and program, p. 3–6.

Digital Petroleum Atlas, 1997, Kansas Geological Survey web site pages, http:\\www.kgs.ukans.edu\DPA.

Doveton, J. H., 1986, Log analysis of subsurface geology, concepts and computer methods: New York, John Wiley and Sons, p. 271–275.

Doveton, J. H., 1994, Geological interpretation, SEPM short course, n. 29, 169 p.

Doveton, J. H., 1998, Petrophysical well log analysis: Handouts for PE531.

Dunham, R. J., 1962, Classification of carbonate rocks according to texture, *in* W. E. Ham, ed., Classification of carbonate rocks: Tulsa, Oklahoma, American Association of Petroleum Geologists Memoir 1, p. 108–121.

Ekdale, A. A., R. G. Bromley, and S. G. Pemberton, 1987, Ichnology: Society of Economic Paleontology and Mineralogists, short course n. 15, 317 p.

Embry, A. F., and J. A. Podruski, 1988, Third-order depositional sequences of the Mesozoic succession of Sverdrup Basin, *in* D. P. James and D. A. Leckie, eds., Sequences, stratigraphy, sedimentology: surface and subsurface: Canadian Society of Petroleum Geologists Memoir 15, p. 79–83.

Emery, D., and K. J. Myers, eds., 1996, Sequence stratigraphy: Great Britain, Blackwell Science, p. 3–269.

Emery, D., and P. G. Sutterlin, 1986, Characterization of a Morrowan sandstone reservoir, Lexington Field, Clark County, Kansas: Shale Shaker Digest, v. 22, p. 18–33.

Emery, M., 1985, A detailed investigation of Morrowan sandstone reservoir, Lexington Field, Clark County, Kansas: Wichita State University, unpublished M.S. thesis, p. 35–190.

Franz, R. H., 1985a, Distribution of petrophysical properties in a lower Morrowan sandstone (Keyes), southwest Kansas, *in* W. L. Watney, A. W. Walton, and J. H. Doveton, eds., Core studies in Kansas, sedimentology and diagenesis of economically important rock strata in Kansas: p. 48–55.

Franz, R. H., 1985b, Lithofacies, diagenesis, and petrophysical properties of selected sandstones from the Morrowan Kearny Formation of southwestern Kansas: Department of Geology, University of Kansas, unpublished M.S. thesis, 177 p. (Available as Kansas Geological Survey open-file report 87-31.)

Frey, R. W., and J. D., Howard, 1975, Endobenthic adaptations of juvenile thalassinidean shrimp: Bulletin of the Geological Society of Denmark, v. 24, p. 225–301.

Frey, R. W., and J. D. Howard, 1980, Physical and biogenic processes in Georgia estuaries. II. Intertidal facies, *in* S. B. McCann, ed., Sedimentary processes and animal–sedimentary relationships in tidal environments: Geological Association of Canada, short course notes, v. 1, p. 183–220.

Frey, R. W., and J. D. Howard, 1985, Trace fossils from the Panther Member, Star Point Formation (upper Cretaceous, Coal Creek Canyon, Utah): Journal of Paleontology, v. 59, p. 370–404.

Frezon, S. E., and J. H. Dixon, 1975, Texas Panhandle and Oklahoma: Pennsylvanian Systems: USGS Professional Paper 853, part 1, p. 177–194.

Folk, R. L., 1951, Stages of textural maturity in sedimentary rocks: Journal of Sedimentary Petrology, v. 21, p. 127–130.

Folk, R. L., 1974, Petrology of sedimentary rocks: Austin, Texas, Hemphills, p. 170–175.

Gerhard, L. C., T. R. Carr, D. Adkins-Heligeson, S. Bhattacharya, P. Gerlach, W. Guy, R. O'Dell, K. Stalder, and W. L. Watney, 1999, Digital petroleum atlas annual report: KGS open-file report 99-19,URL=http://www.kgs.ukans.edu/PRS/publication/99_19/9919exec.html

Haliburton Energy Service, 1994, Water flood study, Morrow, Pattin no. 1-3, Clark County, Kansas, p. 1–9.

Hammuda, O., 1973, Influence of the pre-Pennsylvanian unconformity on deposition of Morrow sandstone in Kiowa, Bent, and Prower counties, southeast Colorado: Mountain Geology, v. 11, p. 33–40.

Heckel, P. H., 1972, Recognition of ancient shallow marine environments, *in* J. K. Rigby and W. K. Hamblin, eds., Recognition of ancient sedimentary environments: Tulsa, Oklahoma, Society of Economic Paleontologists and Mineralogists Special Publications 18, p. 90–154.

Jopling, A. V., and R. G. Walker, 1968, Morphology and origin of ripple-drift cross lamination, with examples from the Pleistocene of Massachusetts: Journal of Sedimentary Petrology, v. 38, p. 971–984.

Kasino, R. E., and D. K. Davies, 1979, Environments and diagenesis, Morrow sands, Cimarron County (Oklahoma), and significance to regional exploration, production, and well completion practices, *in* H. J. Hyne, ed., Pennsylvanian sandstones of the mid-continent: Tulsa, Oklahoma, Tulsa Geological Society, p. 169–194.

Krystinik, L. F., D. W. Bowen, and H. G. Swanson, 1987, Depositional systematics and exploitation of Morrow valley-fill complexes in Cheyenne County, Colorado (abstract): American Association of Petroleum Geologists Bulletin, v. 71, p. 579.

Krystinik, L. F., and B. A. Blakeney, 1990, Sedimentary of the upper Morrowan Formation in Eastern Colorado and Western Kansas, *in* S. A. Sonnenberg, L. T. Shannon, K. Rader, W. F. von Drehle, and G. W. Martin, eds., Morrowan sandstones of southeast Colorado and adjacent areas: Rocky Mountain Association of Geologists, p. 37–50.

Lemon, R. R., 1990, Principles of Stratigraphy: Toronto, Merrill Publishing, p. 17–27.

McKee, E. D., 1965, Experiment in ripple lamination, *in* G. V. Middleton, ed., Primary sedimentary structures and their hydrodynamic interpretation: Tulsa, Oklahoma, Society of Economic Mineralogists and Paleontologists Special Publications 12, p. 66–83.

Merriam, D. F., 1963, The geologic history of Kansas: Kansas Geological Survey Bulletin 162, p. 135–144, 185–192.

Miall, A. D., 1992, Alluvial deposits, *in* R. G. Walker and N. P. James, eds., Facies models; response to sea level change; Ontario, Geological Association of Canada, Love Printing Service Ltd., p. 119–142.

Miall, A. D., 1996, The geology of fluvial deposits: Berlin, Springer, p. 99–249.

Mitchum, R. M., Jr., and P. R. Vail, 1977, Seismic stratigraphy and global changes of sea-level, part 7: stratigraphic interpretation of seismic reflection patterns in depositional sequences, *in* C. E. Payton, ed., Seismic stratigraphy—applications to hydrocarbon exploration: Tulsa, Oklahoma, Memoir of the American Association of Petroleum Geologists, p. 26, 135–144.

Montgomery, S. L., and E. Morrison, 1999, South Eubank Field, Haskell County, Kansas; a case of field redevelopment using subsurface mapping and 3-D seismic data: American Association of Petroleum Geologists Bulletin, v. 83, n. 3, p. 393–409.

Nemec, W., 1992, Depositional controls on plant growth and peat accumulation in a braidplain delta environment: Helvetiafjellet Formation (Barremian-Aptian), Svalbard, *in* P. J. McCabe and J. T. Parrish, eds., Controls on the distribution and quality of Cretaceous coals: Geological Society of America Special Papers, n. 267, p. 209–226.

Nichols, M. M., G. H. Johnson, and P. C. Peebles, 1991, Modern sediments and facies model for a microtidal coastal plain estuary, James Estuary, Virginia: SEPM Special Publication, v. 61, n. 6, p. 883–889.

Pemberton, S. G., and R. W. Frey, 1982, Trace fossil nomenclature and the *Planolites-Palaeophycus* dilemma: Journal of Paleontology, v. 56, p. 843–881.

Pemberton, S. G., and J. A. MacEachern, 1992, Trace fossil facies models: environmental and allostratigraphic significance, *in* R. G. Walker and N. P. James, eds., Facies models: response to sea level: Stittsville, Ontario, Geological Association of Canada, Love Printing Service Ltd., p. 47–72.

Pettijohn, F. J., P. E. Potter, and R. Siever, 1973, Sand and sandstone: New York, Springer-Verlag, p. 618.

Phillips Petroleum Company, 1989, Open hole log evaluation short course text book.

Pickett, G. R., 1973, Pattern recognition as a means of formation evaluation: The Log Analyst, v. 14, n. 4, p. 3–11.

Posamentier, H. W., and D. P. James, 1993, An overview of sequence-stratigraphic concepts; uses and abuses, *in* H. W. Posamentier, C. P. Summerhayes, B. U. Haq, and G. P. Allen, eds., Sequence stratigraphy and facies associations: p. 5–22.

Puckette, J., A. Abdalla, A. Rice, and Z. Al-Shaieb, 1996, The upper Morrow reservoirs: complex fluvio-deltaic depositional systems, *in* K. S. Johnson, ed., Deltaic reservoirs in the southern midcontinent, 1993 symposium: Oklahoma Geological Survey Circular, n. 98, p. 47–84.

Raddysh, H. K., 1988, Sedimentology and "geometry" of the lower Cretaceous Viking Formation, Gilby A and B fields, Alberta, *in* D. P. James and D. A. Leckie, eds., Sequences, stratigraphy, sedimentology: surface and subsurface: Canadian Society of Petroleum Geologists Memoir 15, p. 417–430.

Rader, K., 1987, Petrographic and subsurface analysis of Pennsylvanian Morrowan sandstone of southwest Kansas: Department of Geological Sciences, University of Colorado, unpublished M.S. thesis, 106 p. (Available as Kansas Geological Survey open-file report 87-31).

Rader, K., 1990, Petrography of Morrowan sandstones in southeast Colorado, southwest Kansas, and northwest Oklahoma, *in* S. A. Sonnenberg, L. T. Shannon, K. Rader, W. F. von Drehle, and G. W. Martin, eds., Morrowan sandstones of southeast Colorado and adjacent areas: Rocky Mountain Association of Geologists, p. 51–58.

Rascoe, B., Jr., and F. J. Adler, 1983, Permo-carboniferous hydrocarbon accumulations, midcontinent, U.S.A.: American Association of Petroleum Geologists Bulletin, v. 67, p. 979–1001.

Reading, H. G., and J. D. Collinson, 1996, Clastic coasts, *in* H. G. Reading, ed., Sedimentary environments: processes, facies and stratigraphy: Cambridge, United Kingdom, Blackwell Science Ltd., p. 154–231.

Reinson, G. E., J. E. Clark, and A. E. Foscolos, 1988, Reservoir geology of Crystal Viking Field, lower Cretaceous estuarine tidal channel-bay complex. South central Alberta: American Association of Petroleum Geologists Bulletin, v. 72, p. 1270–1294.

Reinson, G. E., 1992, Transgressive barrier island and estuarine systems. Tidal depositional systems, *in* R. G. Walker and N. P. James, eds., Facies models: response to sea level: Stittsville, Ontario, Geological Association of Canada, Love Printing Service Ltd., p. 179–194.

Ross, C. A., and J. R. P. Ross, 1985, Late Paleozoic depositional sequences are synchronous and worldwide: Geology, v. 13, p. 194–197.

Schlumberger, 1989, Log interpretation principles/applications: Houston, Schlumberger Educational Surfaces, p. 3.1–3.11, 5.1–5.23, 6.1–6.13.

Schoeling, L., and C. E. Fox, 1998, CO_2 floods look good in midcontinent: The American Oil and Gas Reporter, p. 120–123.

Scholle, P., 1979, A color illustrated guide to constituents, textures, cements, and porosities of sandstones and associated rocks: AAPG Memoir 28, p. 16–181.

Schopf, J. M., 1975, Pennsylvanian climate in the United State, *in* E. D. McKee and E. J. Crosby, coordinators, Paleotectonic investigations of the Pennsylvanian System in the United States, Part II: USGS Professional Paper 853, p. 23–31.

Shirley, K., 1985, Point bars spur Las Animas activity: American Association of Petroleum Geologists Bulletin, v. 5, n. 15, p. 40, 42, 43.

Shultz, A. W., 1984, Subaerial debris-flow deposition in the upper Paleozoic Cutler Formation, Western Colorado: Journal of Sedimentary Petrology, v. 54, p. 759–772.

Sonnenberg, S. A., 1985, Tectonic and sedimentation model for Morrow sandstone deposition, Sorrento Field area, Denver basin, Colorado: Mountain Geologist, v. 22, p. 180–191.

Sonnenberg, S. A., 1990, Upper Morrowan Purdy Sandstone, Interstate Field, Morton County, Kansas, *in* S. A. Sonnenberg, L. T. Shannon, K. Rader, W. F. von Drehle, and G. W. Martin, eds., Morrowan sandstones of southeast Colorado and adjacent areas: Rocky Mountain Association of Geologists, p. 207–225.

Sonnenberg, S. A., L. T. Shannon, R. Kathleen, W. F. von Drehle, 1990, Regional structure and stratigraphy of the Morrowan series, southeast Colorado and adjacent areas, *in* S. A. Sonnenberg, L. T. Shannon, K. Rader, W. F. Von Drehle, and G. W. Martin, eds., Morrow sandstones of southeast Colorado and adjacent areas: Rocky Mountain Association of Geologists, p. 1–8.

Stear, W. M., 1985, Comparison of the bedform distribution and dynamics of modern and ancient sandy ephemeral flood deposits in the southwestern Karoo region, South Africa: Sedimentary Geology, v. 45, p. 209–230.

Steel, R. J., and D. B. Thompson, 1983, Structures and textures in Triassic braided stream conglomerates ('Bunter' Pebble Beds) in the Sherwood Sandstone Group, North Staffordshire, England: Sedimentology, v. 30, p. 341–367.

Strobl, R. S., 1988, The effects of sea level fluctuations on prograding shorelines and estuarine valley-fill sequences in the Glauconitic Member, Medicine River Field and adjacent areas, *in* D. P. James and D. A. Leckie, eds., Sequences, stratigraphy, sedimentology: surface and subsurface: Canadian Society of Petroleum Geologists Memoir 15, p. 221–236.

Sutterlin, P. G., and J. P. Hastings, 1986, Trend-surface analysis revisited; a case history, *in* D. F. Merriam (ed.), Computer applications in petroleum exploration and development, v. 12, n. 4B, special issue, p. 537–562.

Swanson, D. C., 1979, Deltaic deposits in the Pennsylvanian upper Morrow Formation of the Anadarko Basin in Pennsylvanian sandstones of the midcontinent: Tulsa Geological Society, n. 1, p. 115–168.

Tarbuck, E. J., and F. K. Lutgens, 1990, Sedimentary rocks, *in* The earth, an introduction to physical geology (3rd ed.): Toronto, Merrill Publishing, p. 132–136.

Thomas, R. G., D. G. Smith, J. M. Wood, J. Visser, E. A. Calverley-Range, and E. H. Koster, 1987, Inclined heterolithicstratification—terminology, description, interpretation and significance: Sedimentary Geology, v. 53, p. 123–179.

Tillman, R. W., and R. M. Martinson, 1984, The Shannon shelf-ridge sandstone complex, Salt Creek Anticline area, Powder River Basin, Wyoming, *in* R. W. Tillman and C. T. Siemers, eds., Siliciclastic shelf sediments: Tulsa, Oklahoma, Society of Economic Paleontologists and Mineralogists, Special Publication n. 34, p. 85–142.

Tornqvist, T. E., 1993, Holocene alternation of meandering and anastomosing fluvial systems in the Rhine-Meuse Delta (central Netherlands) controlled by sea-level rise and subsoil erodibility: Journal of Sedimentary Petrology, v. 63, n. 4, p. 683–693.

Vail, P. R., R. M. Mitchum, Jr., and S. Thompson III, 1977, Seismic stratigraphy and global changes of sea-level, part 3: relative changes of sea level from coastal onlap, *in* C. E. Payton, ed., Seismic stratigraphy—Applications to hydrocarbon exploration: Memoir of the American Association of Petroleum Geologists, Tulsa, Oklahoma, p. 26, 63–82.

Vail, P. R., and R. G. Todd, 1981, North Sea Jurassic unconformities, chronostratigraphy and global sea level changes from seismic stratigraphy: Petroleum Geology of the NW Continental Shelf, Proceedings, p. 216–235.

Vail, P. R., J. Hardenbol, and R. G. Todd, 1984, Jurassic unconformities, chronostratigraphy and sea level changes from seismic stratigraphy, *in* J. S. Schlee, ed., Interregional unconformities and hydrocarbon exploration: Memoir of the American Association of Petroleum Geologists, Tulsa, Oklahoma, p. 33, 129–144.

Van Wagoner, J. C., R. M. Mitchum, J. W. Posamentier, and P. R. Vail, 1987, Key definitions of sequence stratigraphy, *in* A. W. Bally, ed., Atlas of seismic stratigraphy: American Association of Petroleum Geologists Bulletin, v. 1, p. 11–14.

Van Wagoner, J. C., H. W. Posamentier, R. M. Mitchum, P. R. Vail, J. F. Sarg, T. S. Loutit, and J. Hardenbol, 1988, An overview of sequence stratigraphy and key definitions, *in* C. W Wilgus et al., eds., Sea level changes: an integrated approach: Society of Economic Paleontologists and Mineralogists Special Publication 42, p.39–45.

Von Drehle, W. F., 1990, Barrel Springs Field, Prowers County, Colorado, *in* S. A. Sonnenberg, L. T. Shannon, K. Rader, W. F. Von Drehle, and G. W. Martin, eds., Morrow sandstones of southeast Colorado and adjacent areas: Rocky Mountain Association of Geologists, p. 183–191.

Walker, R. G., 1992, Facies, facies models and modern stratigraphic concepts, *in* R. G. Walker and N. P. James, eds., Facies models: response to sea level: Stittsville, Ontario, Geological Association of Canada, Love Printing Service Ltd., p. 1–14.

Weimer, R. J., S. A. Sonnenberg, and L. T. Shannon, 1988, Production from valley-fill deposits, Morrow sandstone, southeast Colorado: New exploration challenges and rewards (abstract): American Association of Petroleum Geologists Bulletin, v. 72, p. 884.

Wheeler, D. M., A. J. Scott, V. J. Coringrato, and P. E. Devine, 1990, Stratigraphy and depositional history of the Morrowan Formation, southeast Colorado and southwest Kansas, *in* S. A. Sonnenberg, L. T. Shannon, K. Rader, W. F. von Drehle, and G. W. Martin, eds., Morrowan sandstones of southeast Colorado and adjacent areas: Rocky Mountain Association of Geologists, p. 9–35.

Wightman, D. M, S. G. Pemberton, and C. Singh, 1987, Depositional modeling of the upper Mannville (lower Cretaceous), east central Alberta: implications for the recognition of brackish water deposits, *in* Reservoir sedimentology: Society of Economic Mineralogists and Paleontologists Special Publication 40, p. 189–220.

Wilson, J. L., and C. Jordan, 1983, Middle shelf environment, *in* P. A. Scholle, D. G. Bebout, and C. H. Moore, eds., Carbonate depositional environments: American Association of Petroleum Geologists Memoir 33, p. 299–302.

Wood, L. J., F. G. Ethridge, and S. A. Schumm, 1993, The effects of rate of base-level fluctuation on coastal-plain, shelf and slope depositional systems, an experimental approach, *in* H. W. Posamentier, C. P. Summerhayes, B. U. Haq, G. P. Allen, eds., Sequence stratigraphy and facies associations: Special Publication of the International Association of Sedimentologists 18, p. 43–53.

Youle, J. C., 1992, Sequence stratigraphy of the Lower Middle Pennsylvanian and distribution of selected sandstone, Eastern Hugoton Embayment, southwestern Kansas: University of Kansas, unpublished M.S. thesis. (Available as Kansas Geological Survey open-file report 92-55), p. 157–166.

Zaitlin, B. A., R. W. Dalrymple, and R. Boyd, 1994, The stratigraphic organization of incised-valley system associated with relative sea level change, *in* Incised valley systems origin and sedimentary sequences: SEPM Special Publication n. 51, p. 48–60.

Zeller, D. E., ed., 1968, The stratigraphic succession in Kansas: Kansas Geological Survey Bulletin 189, p. 17–34.

APPENDIX A

Wireline-log Correlations

Chronostratigraphic Cross-Sections

STRATIGRAPHIC CROSS-SECTION: EQUAL SPACE

Datum = MAXIMUM FLOODING SURFACE (MFS#2)

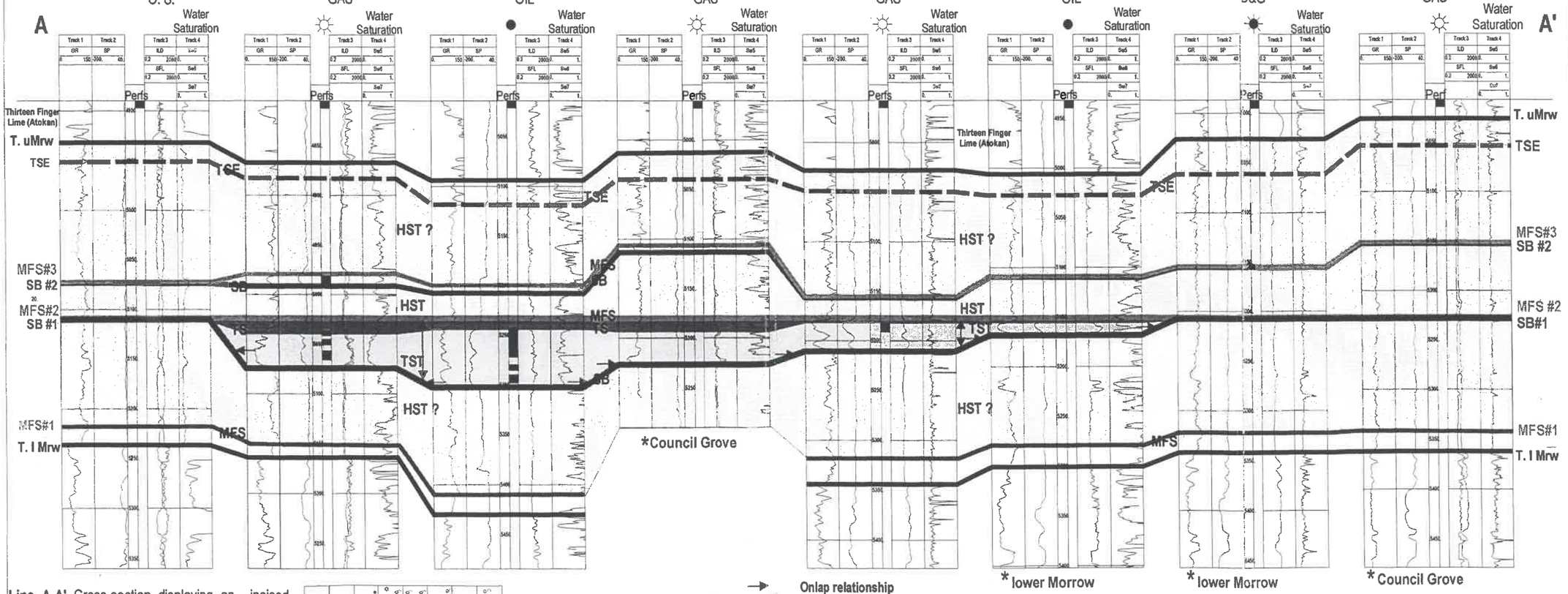

Line A-A' Cross-section displaying an incised valley associated with SB#1 and the fill of the incision (TST) that is capped by the datum MFS#2. The incised valley has an onlap relationship with the underlying shale (HST).

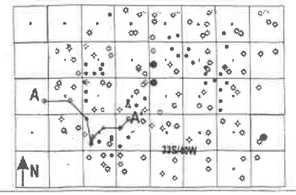

Water Saturation (Sw)

Sw5-- calculated with NPHI

Sw6-- calculated with RHOB

Sw7-- calculated with Delta T

Onlap relationship

(T. u-Mrw) Top of the upper Morrow

(TSE) Transgressive Surface of Erosion

(MFS) Maximum Flooding Surface

(SB #1) Sequence Boundary of upper Morrow sandstone

(SB #2) Sequence Boundary of upper Morrow sandstone

TS Transgressive Surface

(T. I-Mrw) Top of the lower Morrow

(HST) Highstand Systems Tract

(TST) Transgressive Systems Tract

Estuarine

Fluvial

Sandstone

Incised Valley

STRATIGRAPHIC CROSS-SECTION: EQUAL SPACE

Datum = MAXIMUM FLOODING SURFACE (MFS#2)

15129205410000	15129203130000	15129205660000	15129201790000	15129204340000	15129203220000
PANOMA GAS AREA	SANTA FE TRAIL	SANTA FE TRAIL	SANTA FE TRAIL	CIMARRON VALLEY	SANTA FE TRAIL
MCDOUGAL /A/	CHEROKEE /B/	TUCKER /F/	LOW /G/	JONES /C/	LOW /H/
1	1	3	1	3	1
6/33.S/41.W/11	6/33.S/41.W/12	6/33.S/40.W/6	6/33.S/40.W/6	6/33.S/40.W/5	6/33.S/40.W/4
B		CORE	CORE		B'

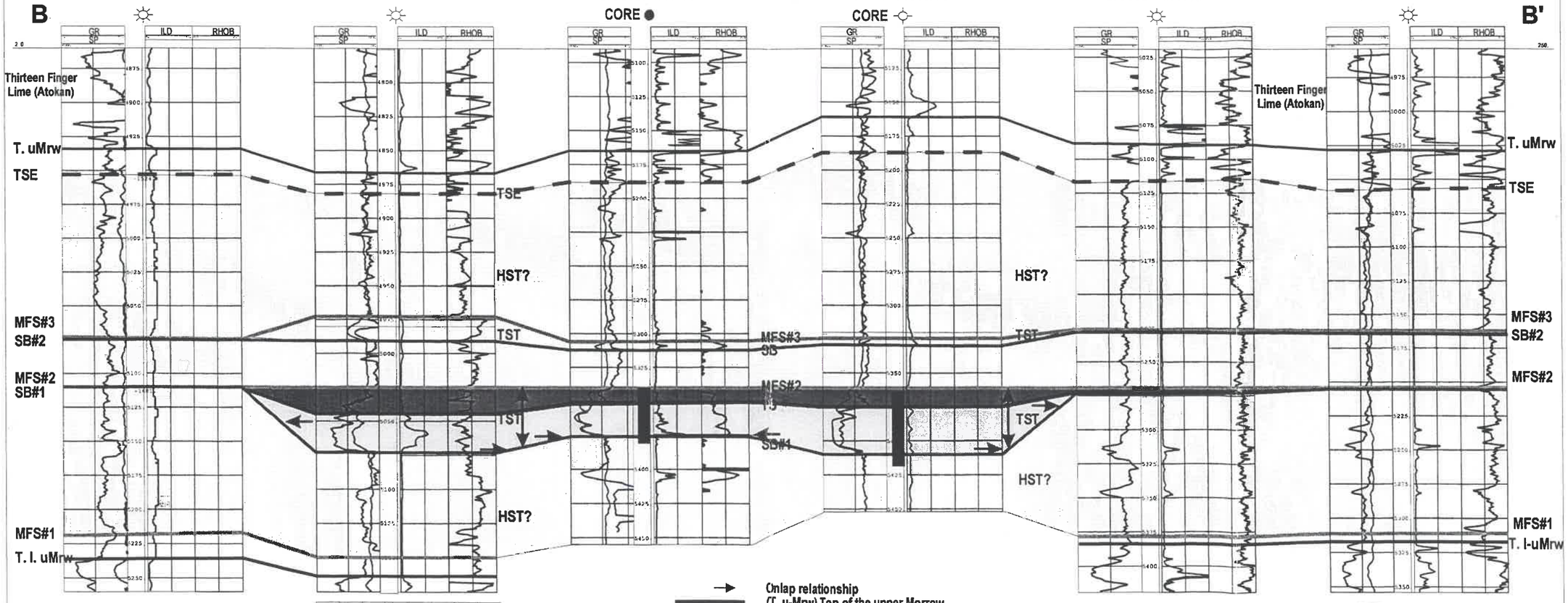

Line B-B' Cross-section along the upper part of the study area displaying two incised valley's on SB#1 and SB#2, and a transgressive surface of erosion (TSE).

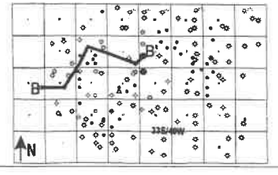

- Onlap relationship
- (T. u-Mrw) Top of the upper Morrow
- (TSE) Transgressive Surface of Erosion
- (MFS) Maximum Flooding Surface
- (SB #1) Sequence Boundary of upper Morrow sandstone
- (SB #2) Sequence Boundary of upper Morrow sandstone
- TS Transgressive Surface
- (T. l-Mrw) Top of the lower Morrow

- (HST) Highstand Systems Tract
- (TST) Transgressive Systems Tract
- CORE
- Estuarine
- Fluvial
- Sandstone
- Incised Valley

Stratigraphic Cross-Section of Cored Intervals: Equal Space

Datum = Maximum Flooding Surface (MFS#2)

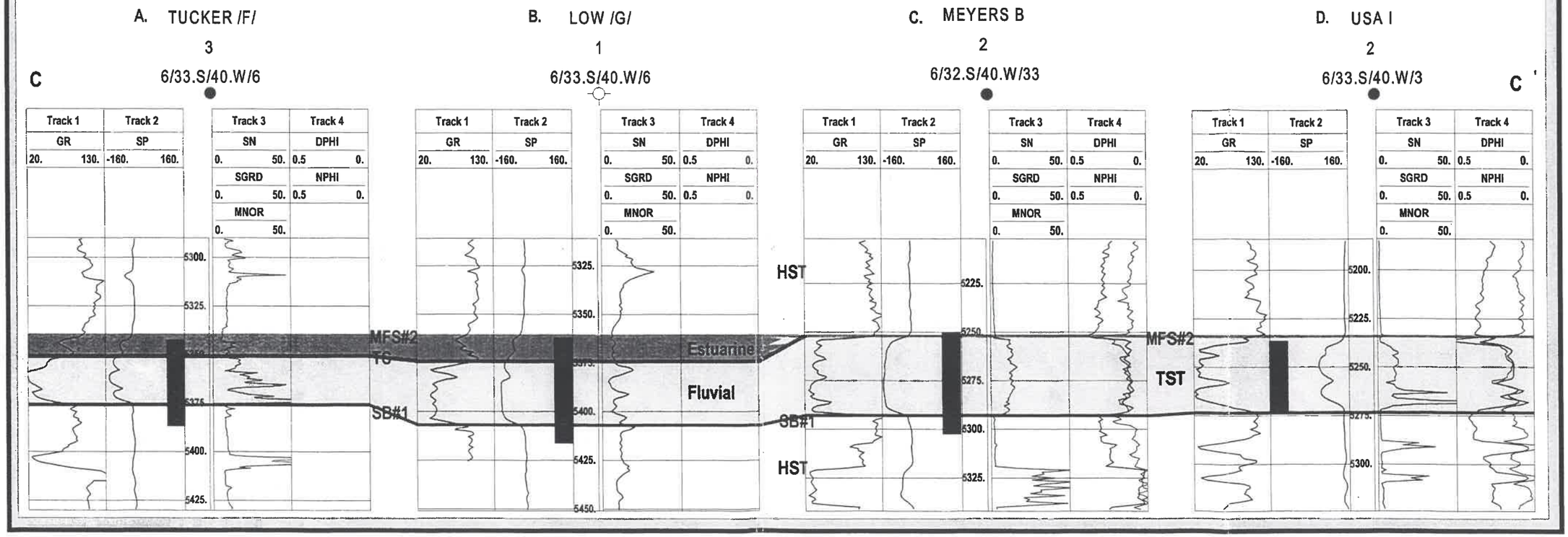

LINE C-C' Cross-section C-C', constructed using the cored wells, displays a fluvial incised valley fill. A sharp transgressive surface (TS) separates the fluvial from the estuarine lithofacies. This incised valley fill, a transgressive systems tract (TST), is capped by a Maximum Flooding Surface (MFS#2), marking the termination of the TST and the beginning of the highstand systems tract (HST).

Maximum Flooding Surface #2 (MFS#2)
Sequence Boundary #1 (SB#1)
Transgressive Surface (TS)

Cored intervals

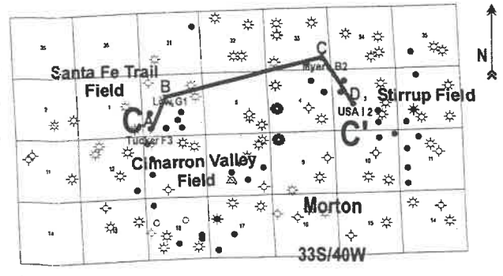

Core and Cross-section C-C' location map. Cores labeled: A) Tucker F3; B) Low G1; C) Myers B2 ; D) USA I 2. 0 1 miles

STRATIGRAPHIC CROSS-SECTION: EQUAL SPACE

Datum = **Maximum Flooding Surface (MFS #2)**

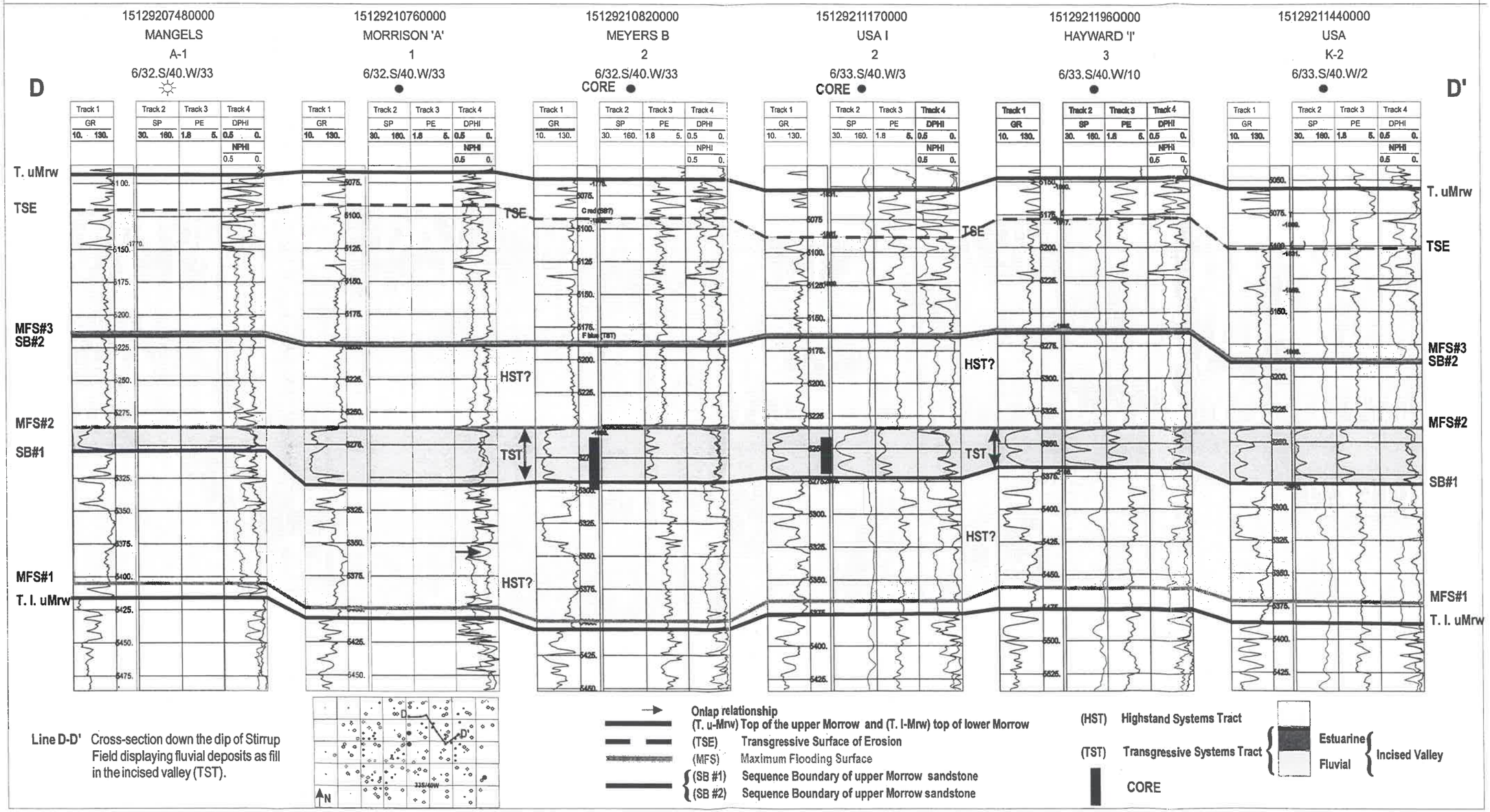

STRATIGRAPHIC CROSS-SECTION: EQUAL SPACE

Datum=Maximum Flooding Surface (MFS #2)

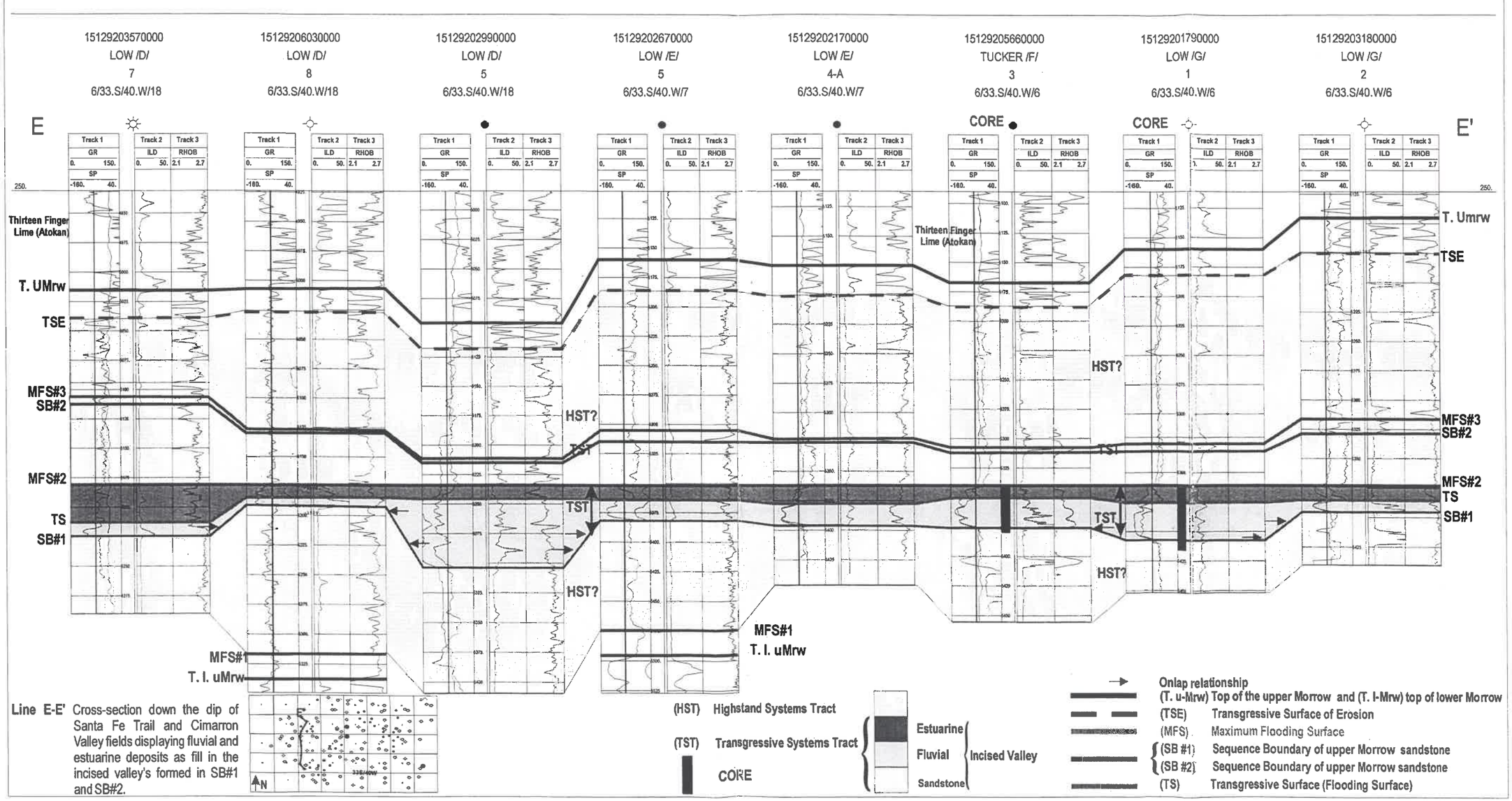

STRATIGRAPHIC CROSS-SECTION: EQUAL SPACE

Datum =**Maximum Flooding Surface (MFS #2)**

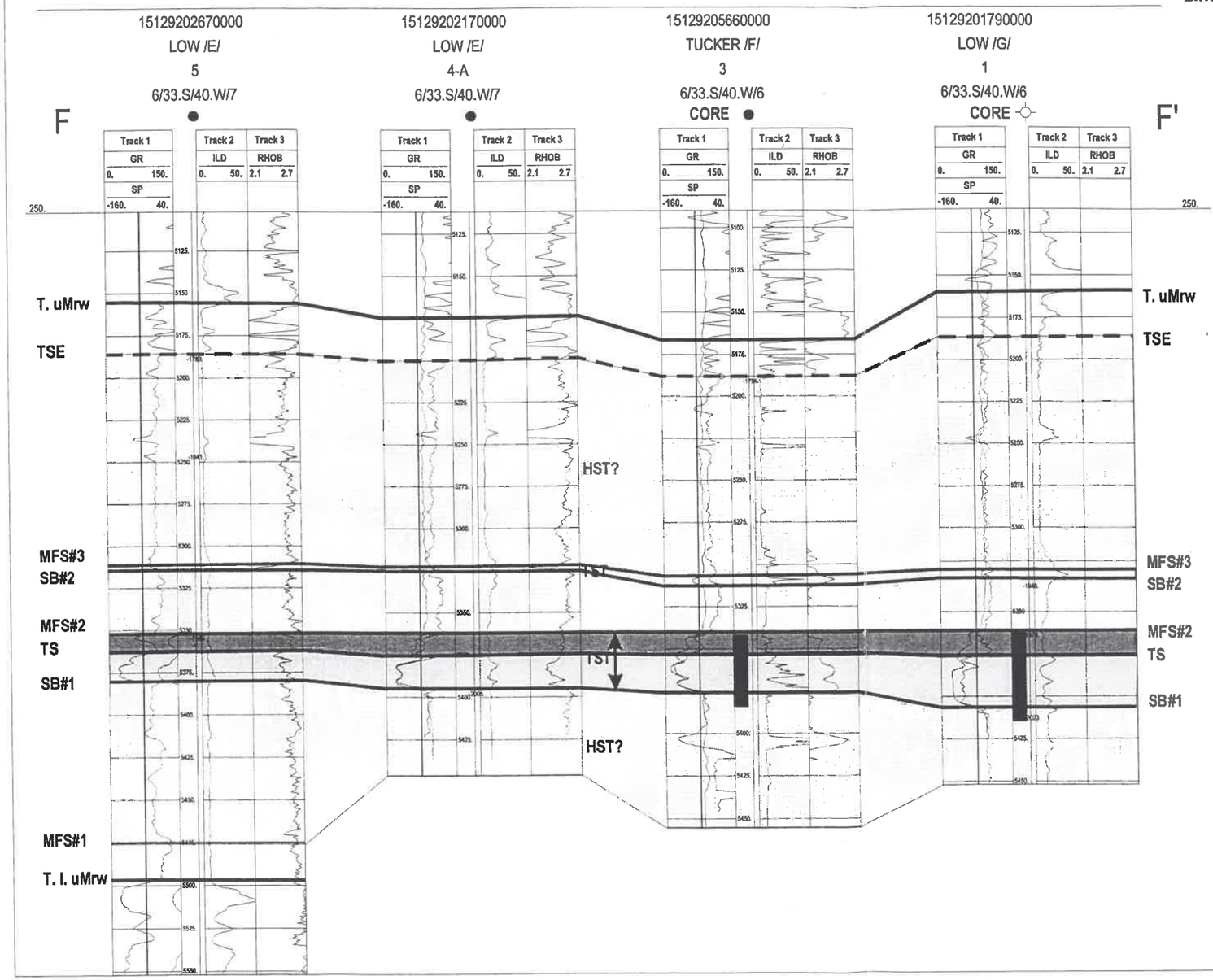

Line F-F' Cross-section showing a general decrease in fluvial thickness towards the south and an increase in estuarine thickness towards the north.

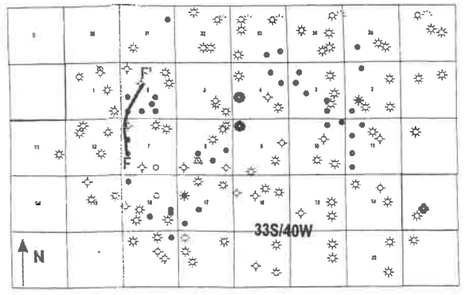

(HST) Highstand Systems Tract

(TST) Transgressive Systems Tract

CORE

Estuarine
Fluvial
Sandstone
Incised Valley

Onlap relationship

(T. u-Mrw) Top of the upper Morrow and (T. l-Mrw) top of lower Morrow

(TSE) Transgressive Surface of Erosion

(MFS) Maximum Flooding Surface

(SB #1) Sequence Boundary of upper Morrow sandstone

(SB #2) Sequence Boundary of upper Morrow sandstone

(TS) Transgressive Surface (Flooding Surface)

STRATIGRAPHIC CROSS-SECTION: EQUAL SPACE

Datum=Maximum Flooding Surface MFS#3

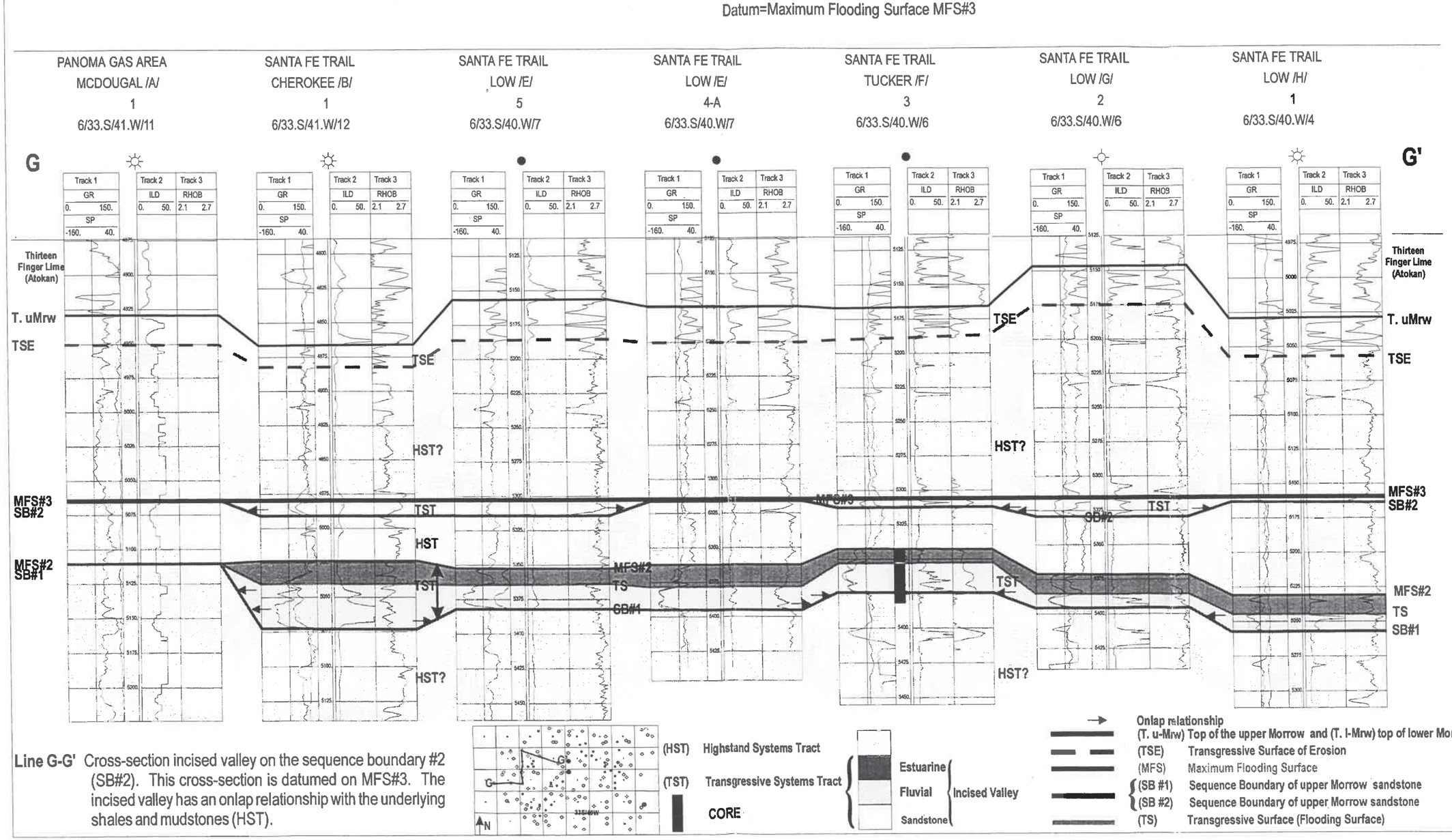

Line G-G' Cross-section incised valley on the sequence boundary #2 (SB#2). This cross-section is datumed on MFS#3. The incised valley has an onlap relationship with the underlying shales and mudstones (HST).

APPENDIX B

Reservoir Characterization Data

Stirrup Field								Lithofacies of Production				
Well Name	No.	API (15-129)	T(S)	R(W)	Sec	Perforation interval	Production	Fluvial Three	Fluvial Four	Fluvial Five	Estuarine Six	Estuarine Seven
Blucher A	2	20883	32	40	34	5166-5169 (gross)	gas	X	X	X		
Bowker	1--32	21121	32	40	32	5296-5313	gas	X	X	X		
Callahan A	1	21276	32	40	33	5232-5248	gas	X	X	X		
Forward A	3	21194	33	40	3	5228-5234/ 5196-5234	oil	X	X	X		
Hayward I	2	20594	33	40	10	5362-5366	D&A	X	X	X		
Hayward I	3	21196	33	40	10	5340-5350/5364-5368	oil	X	X	X		
Kraber A	1	21280	32	40	34	5233-5266 (gross)	gas	X	X	X		
Lemon Trust A	1	21143	32	40	32	5284-5302/5284-5313	gas	X	X	X	X	X
Morrison A	1	21076	32	40	33	5300-5304	oil		X	X	X	X
Myers B	2	21082	32	40	33	5286-5292	oil		X	X		
Ratzlaff E	1 or 5	21103	33	40	3	5288-5303	oil	X	X	X		
US Government C	2	21116	33	40	2	5248-5256/ 5256-5262/ 5268-5280	oil	X	X	X		
USA AA	1	21108	33	40	11	5354-5368/ 5368-5380	oil	X	X	X		
USA AC	1	21148	33	40	11	5357-5370/ 5387-5400	oil	X	X	X		
USA AD	1	21141	33	40	11	5392-5408/ 5408-5412	oil	X	X	X		
USA AD	2	21230	33	40	11	5468-5485/ 5485-5490	oil	X	X	X		
USA I	1	20931	33	40	3	5134-5152/ 5154-5174	gas	X	X	X		
USA I	2	21117	33	40	3	5240-5268	oil	X	X	X		
USA I	3	21118	33	40	3	5264-5278/ 5284-5296	oil	X	X	X		
USA I	4	21167	33	40	3	5258-5272	oil	X	X	X		
USA K	1	20949	33	40	2	5074-5076/5212-5246	oil&gas	X	X	X		
USA K	2	21144	33	40	2	5276-5281	oil	X	X	X		
USA L	1	21000	33	40	4	5334-5362	oil	X	X	X		
USA L	2	21119	33	40	4	5296-5314/ 5316-5314/ 5324-5318	oil	X	X	X		
USA P	1	20999	33	40	2	5475-5492/ 5635-5640	gas	X	X	X		
USA R	1	21017	32	40	35	5254-5266	oil	X	X	X		
USA X	1	21086	33	40	10	5340-5348	oil	X	X	X		

Figure B-1 Perforation intervals within the fluvial and estuarine lithofacies of the hydrocarbon reservoirs of the Stirrup Field.

Cimarron Valley								Lithofacies of Production				
								Fluvial			Estuarine	
Well Name	No.	API (15-129)	T(S)	R(W)	Sec	Perforation interval	Production	Three	Four	Five	Six	Seven
Low B	1	pre-1967	33	40	19	5182-5194	gas	X	X	X		
Mangels A	1	20748	32	40	33	5288-5301	oil&gas	X	X	X	X	X
Republic B	1	00515/62766	33	40	18	5181-5189/ 5186-5206	oil	X	X	X	X	X
Santa Fe Trail								**Lithofacies of Production**				
								Fluvial			Estuarine	
Well Name	No.	API (15-129)	T(S)	R(W)	Sec	Perforation interval	Production	Three	Four	Five	Six	Seven
B.R.U	22-3	20658	33	41	9	5000-5005	oil	X	X	X		
Cherokee B	1	20313	33	41	12	4976-4988	SIGW	X	X	X		
Cherokee B	2	20308	33	41	12	5307-5314	oil&gas	X	X	X	X	X
Government A	1	20012	33	41	9	5036-5038/ 5036-5040/ 5049-5050	oil&gas	X	X	X		
Jones B	1	45.138	33	41	9	5036-5050	oil	X	X	X		
Jones -Government	2	50131	33	41	9	5049-5054	oil	X	X	X		
Low E	5	20267	33	40	7	5373-5377	oil&gas	X	X	X	X	X
Low E	7	20354	33	40	7	5393-5395	oil&gas				X	X
Low E	4-A	20217	33	40	7	5380-5381	oil		X			
Low G	1	20179	33	40	6	5364-5368/ 5373-5376/ 5394-5400	D&A		X	X	X	X
Low G	2	20318	33	40	6	5319-5327	D&A	X	X	X	X	X
Low H	1	20322	33	40	4	5370-5380	gas	X	X	X	X	X
Santa Fe Trail B	1--9	20730	33	40	18	5215-5225	inj	X	X	X	X	X
Synder C	1	20167	33	40	6	5356-5364	oil	X	X	X		
Synder C	2	20167	33	40	6	5354-5378	oil	X	X	X	X	X
Synder C	3	20577	33	40	6	5338-5349	oil&gas	X	X	X		
Tucker F	1	20181	33	40	6	5358-5368	oil&gas	X	X	X	X	X
Tucker F	2	20218	33	40	6	5367-5372	oil&gas	X	X	X	X	X
Tucker F	3	20566	33	40	6	5369-5372	oil&gas	X	X			

Figure B-2 Perforation intervals within the fluvial and estuarine lithofacies of the hydrocarbon reservoirs of the Cimarron Valley and Santa Fe Trail fields.

APPENDIX C

Core Porosity and Permeability Data

CORE			Fluid	Saturation			
Depth	Perm to Maximum	Porosity Helium	Oil	Water	Grain Density	Lithofacies	
5352	**	15.7	0	72.3	2.67	7	
5353	3	14.5	1	66.2	2.7	7	
5354	2.2	14.6	0	69.4	2.67	7	
5355	*	14.8	0.5	69.1	2.69	7	
5356	2.6	13	0	72.4	2.68	7	
5357	3.8	15.6	0	67.2	2.71	6	Estuarine
5358	5.1	13.7	1.2	65.5	2.67	6	
5359	4.4	17.1	0.9	61.9	2.81	6	
5360	4.8	14.8	0.6	66.1	2.68	6	
5361	3.6	19.5	0.5	61.5	2.67	6	
5362	147	10.2	0.6	65.2	2.67	6	
5363	101	12.8	0.9	66.2	2.66	5	
5364	74	14	6.4	55.1	2.63	4	
5365	80	16.7	3.1	57.8	2.63	4	
5366	304	13.6	4.1	54.9	2.65	4	
5367	46	10.8	6.3	52.1	2.67	4	
5368	425	15.5	13.7	46.2	2.63	4	
5369	1410	16.9	12.2	38.2	2.63	4	
5370	60	10.1	5.5	56.4	2.67	4	
5371	1.2	3.3	4.2	54.2	2.74	4	
5372	39	9.2	11.7	44.9	2.7	4	Fluvial
5373	5.5	17.9	10.5	49.9	2.66	4	
5374	55	8.8	4.3	53.6	2.7	3	
5375	960	17.9	6.8	44.4	2.64	4	
5376	489	18.3	6.3	54.7	2.63	4	
5377	725	15.8	9.7	36.6	2.63	5	
5378	164	16.7	8	50.8	2.63	4	
5379	6.6	8	8.6	36.9	2.72	4	
5380	489	18.3	3.3	13.3	2.64	4	
5381	1.1	5.7	5.1	47.3	2.73	4	
Mean	200	13.8	4.7	57	2.67		

Figure C-1 Core analyses data for Tucker F3 core.

[redacted]

CORE			Fluid	Saturation			
Depth	Perm to Maximum	Porosity Helium	Oil	Water	Grain Density	Lithofacies	
5261	9	11	18.8	25.7	2.7	4	Fluvial
5262	7.3	9.7	22	30.4	2.71	4	
5263	13	11.4	18.9	39.1	2.71	4	
5264	43	14.9	22	38.1	2.65	4	
5265	87	13.8	24.1	42.8	2.66	4	
5266	90	16.6	20.3	37.7	2.66	4	
5267	8	11	20.9	32.1	2.7	4	
5268	6.7	10.6	19.3	24.1	2.73	4	
5269	3.3	10	21	24.2	2.73	3	
5270	11	11.3	20.1	24.4	2.73	3	
5271	4	11.4	27	32.7	2.65	4	
5272	no data						
5273	no data						
5274	14	13.1	23	38.1	2.69	4	
5275	4.5	10.6	20.7	41.8	2.68	4	
5276	5.4	9.7	18.9	50	2.69	4	
5277	27	12.6	23.7	31.5	2.68	4	
5278	125	14.2	22.2	34	2.68	4	
5279	66	14.5	23.1	30.4	2.69	4	
5280	12	11.1	21.4	25.5	2.72	4	
5281	9	10.3	23.4	26.4	2.71	4	
5282	7	9.2	22.8	27.7	2.72	4	
5283	95	14.8	23.8	49.8	2.67	4	
5284	79	15.4	25.6	51.5	2.66	4	
5285	22	11.8	24	36.8	2.71	4	
5286	117	16.3	21.8	52.4	2.67	4	
5287	64	17	29.3	46.6	2.65	4	
5288	20	14.4	30.2	40.3	2.7	5	
5289	17	14.9	26.1	37.3	2.73	5	
5290	1.8	9.6	23.3	39.9	2.71	5	
5291	7.6	12.2	21.3	33.8	2.75	4	
5292	1.3	6.2	8.9	56.8	2.66	4	
5293	60	17.9	22.3	50.8	2.66	4	
5294	34	17.7	23.9	45.3	2.66	4	
Mean	33.5	12.7	22.3	37.4	2.69		

Figure C-2 Core analyses data for Myers B2 core.

USA I#2
Sunnyhurst

CORE			Fluid	Saturation		
Depth	Perm to Maximum	Porosity Helium	Oil	Water	Grain Density	Lithofacies
5244	70	14.5	26.5	26.1	2.69	4
5245	155	16.6	26.8	37.2	2.66	4
5246	196	17.6	24.8	44.9	2.67	4
5247	251	17.6	25.5	39.4	2.65	4
5248	57	13.1	29	36.1	2.71	4
5249	32	12.7	28.8	35.6	2.7	4
5250	14	10	27.2	36.8	2.73	4
5251	25	10.9	27.6	33.3	2.72	4
5252	18	11.4	30.8	37.2	2.67	4
5253	32	12.5	28.5	27.8	2.68	4
5254	33	12.6	23.5	28.7	2.72	4
5255	35	12.4	24.4	32.8	2.7	4
5256	72	13.8	27.8	43.6	2.68	4
5257	73	13.9	28.9	42.5	2.68	4
5258	119	14.6	27.6	44.4	2.64	4
5259	368	17.6	25.1	46.8	2.65	4
5260	124	15.2	28.6	48.5	2.66	3
5261	15	10.2	20.1	66.2	2.67	3
5262	15	13.4	25.3	58.3	2.65	4
5263	7.3	8.2	33	60.8	2.7	4
5264	1.7	6.7	49.8	41.2	2.7	4
5265	0.1	3.6	50	40	2.74	4
5266	196	16.9	24	52.6	2.69	4
5267	484	18.6	21.3	52.3	2.67	4
5268	142	14.6	11.6	53.6	2.7	4
5269	0.91	5.3	32.7	55.7	2.74	4
5270		4.5	1.1	68.1	2.74	4
5271	4.4	3.8	40.7	55.8	2.76	5
5272	18	14.4	28.4	60.3	2.72	3
5273	5.6	13.4	18.5	71.4	2.71	3
5274	8	14.4	25.3	73.9	2.74	3
Mean	85.7	12.4	27.2	46.8	2.69	

Fluvial

Figure C-3 Core analyses data for USA I#2 core.